Patterning of the *Ciona intestinalis* Motor Ganglion

by

Alberto Sunao Stolfi

A dissertation submitted in partial satisfaction of the

requirements for the degree of

Doctor in Philosophy

in

Molecular and Cell Biology

in the

Graduate Division

of the

University of California, Berkeley

Committee in charge:

Professor Michael S. Levine, Chair

Professor Sharon Amacher

Professor John Gerhart

Professor Lewis Feldman

Spring 2011

Abstract

Patterning of the *Ciona intestinalis* Motor Ganglion
by
Alberto Sunao Stolfi
Doctor of Philosophy in Molecular and Cell Biology
University of California, Berkeley
Professor Michael S. Levine, Chair

Sea squirts are the closest living relatives to the vertebrates. The Motor Ganglion (MG) of the sea squirt *Ciona intestinalis* provides the basic excitatory drive of the central pattern generator (CPG) underlying swimming behavior of the tadpole. Despite its cellular simplicity, the MG shows molecular and physiological parallels to the spinal cord of vertebrates. Here I uncover the morphological diversity of MG neuronal subtypes, and show that this diversity is generated by sequential Ephrin/FGF/MAPK and Delta/Notch signaling events. Despite the divergent signaling requirements for patterning of this motor pool, I believe that the conserved downstream transcription factors might be operating to specify neuronal subtypes that are similar to those in the vertebrate spinal cord. Taking advantage of the experimental tractability of the *Ciona* embryo, I can generate a series of tadpoles with differing composition of moto- and interneuron subtypes, which could serve as the basis for elucidating the development and connectivity of a chordate locomotor CPG.

Dedicado à minha querida Batian, Miyako.

This dissertation is dedicated to my grandmother, Miyako.

Acknowledgements

I would like to thank everybody who has helped me along this long, winding, often blurry, path to where I am today. Chronologically I would have to begin thanking my first boss, Dr. José Alberto Caram de Souza Dias ("Caram", for short) at the IAC, the Agronomical Institute of Campinas, for taking a chance on a punk straight out of high school who had never worked a day in his life. For that I am eternally grateful.

I would next have to thank all the professors and researchers who believed in me and inspired me to keep slogging away at this thing called science, through college and beyond. Again, in chronological order, I thank Anil Ranwala, Bill Miller, Ajay Garg, Adán Colón-Carmona, Kristophe Diaz, Lisa Earle, Jun Cao, Christine Smart, Mary Topa, David Burke, Carlos Lois, Ben Scott, and Shiro Tochitani. Your support and camaraderie was critical in keeping me on this focused path.

For my time in grad school, I have to thank all the beasts in the jungle that is the Levine Lab- thanks for bringing me up to speed *real* quick, and thanks for not immediately chewing me up and spitting me out, allowing me find my unique ecological niche in the lab. Thanks goes especially to *Team Ciona*: Brad Davidson, Weiyang Shi, Jeni Beh, Eileen Wagner, and Alex Mori. A special thanks goes out to my original mentor Lionel "Frenchy" Christiaen, a role model for me as I tried to master the sea squirts. Then there are those who I have had the pleasure of seeing arrive after me and who have helped me out tremendously not only with material goods (data) but also by teaching me the art of teaching others. Thus a shout-out goes to my former (yet forever) rotons Rich Price, Phil Cleves, Justin Bosch, Blair Gainous, Phil Abitua, and Nick Ellis, as well as my former undergrad assistant Andy Cooc. Whether you were able to escape the Levine Lab or not, I hope you have learned something from me (probably cloning). Whenever I am in doubt about my direct contributions to science and society, I comfort myself thinking about the exponential nature of my *indirect* contributions through *your* future achievements. No pressure guys, really!

I also have so many other people to thank in this awesome department that is Berkeley MCB. I would like to thank those who mentored me during my "other" rotations, namely Professors Dan Rokhsar and David Weisblat, and more senior graduate students Mansi Srivastava, Stephanie Gline, and Dede Lyons. I would also like to thank my qualifying exam committee, especially my chair Professor Don "The Duck" Rio, for humbling me so thoroughly and instilling in me the drive to prove myself in grad school. I thank my fellow graduate students in different labs who have collaborated and co-authored with me: John Young, Seemay Chou, and Matt Taliaferro. Thanks for showing me how to reach beyond the walls of the lab. Additional thanks goes to those classmates graduating with me who have kept me up to date with dissertation filing requirements: Kate Monroe and Saori Haigo; without you I am sure I would find a way to mess this whole process up.

I want to thank my thesis committee members, professors Sharon Amacher, John Gerhart, Lew Feldman, and Rich Kramer. Sharon, although the unfortunate timing of my committee meetings meant that we weren't able to discuss my project as often as I'd have liked, I have learned so much from you from taking the 1st year development class, as well as your "biological clocks and oscillators" 290 course. John, I thank you for coming on board late yet providing me with much insight into the question of chordate origins; it was due to my stint as GSI for your portion of the undergraduate development course that the parallels between the pharyngeal mesoderm of amphibians and that of *Ciona* came to my attention in the first place. Lew, I thank you for your irrepressible enthusiasm and encouragement. I dreaded having to bother an outside committee member with "A9.30 this, A13.474 that", but you made me feel that my research still retains some interest to the general audience. Lastly, I thank you Rich for coming to me with an keen interest in *Ciona* neurobiology, and I regret that a collaboration never came to fruition.

This brings me of course to my PhD advisor, The Boss, The Man, Mike Levine. I thank you for your unending enthusiasm and support, on good days and bad, for *Ciona* development and biology in general. Your unbridled, unapologetic passion for science has strongly motivated me during my PhD and will continue to do so for the rest of my career, even more so than the countless "weekend blowoff" and "left too early" inspirational notes.

I must also thank my classmates as well as my non-MCB friends (yes, I still have some). You are too numerous to mention each by name, though a special place is reserved for my roommates during grad school, the inhabitants of the Life Sciences Addition Addition: Roman Barbalat. Steve Bird, and Daniel "Danimal" Richter.

Finally I would like to thank my family for loving and supporting me throughout this time. Thanks Mami, Papi, and Eiji. I love you all.

Table of contents

Chapter 1:

Introduction

Ascidians belong to the urochordates, or tunicates, which comprise the sister group to the vertebrates within the chordate phylum (Delsuc et al., 2006). Thus, ascidians (or sea squirts) are the extant invertebrates most closely related to vertebrates. The sea squirt *Ciona intestinalis* (to which I will now refer in this text as simply *Ciona*) has emerged as a model system for studying the regulation of chordate developmental processes (Satoh, 2003). Their small size, rapid development, and deterministic cell lineages have long been appreciated by classical embryologists (Chabry, 1887; Conklin, 1905), while their compact genome and suitability to molecular perturbation and imaging have propelled them into the post-genome era (Dehal et al., 2002).

Although adult sea squirts feature numerous morphological adaptations to a life of sessile filter-feeding, their free-swimming tadpole larvae possess a typical chordate body plan. This includes a dorsally located central nervous system (CNS) derived from a neural plate which rolls up to form a hollow neural tube (Nicol and Meinertzhagen, 1988). The *Ciona* larval CNS is composed of ~335 cells, of which roughly a third are neurons (Nicol and Meinertzhagen, 1991). They arise through evolutionarily conserved, invariant cell lineages that have been described in detail (Cole and Meinertzhagen, 2004). The CNS is divided along the anterior-posterior axis into distinct anatomical regions. At its most anterior lies a sensory vesicle containing melanized pigment cells and associated sensory cells that sense light and gravity (Dilly, 1964; Dilly, 1962; Sato and Yamamoto, 2001).The majority of neurons of the CNS are located in a tight cluster associated with this sensory vesicle. Just posterior to the sensory vesicle and associated neurons lies the 'neck', which consists of a few quiescent precursors in larvae (Nicol and Meinertzhagen, 1991). After metamorphosis, these precursors differentiate into the branchial basket motoneurons of the adult that are thought to be homologous to the cranial motoneurons of the vertebrate hindbrain (Dufour et al., 2006).

Further posterior is a 'Motor Ganglion' (MG), which is alternately called the 'Visceral Ganglion' despite being situated dorsal to the notochord and not in contact with any viscera (Fig. 1A). The MG consists of cholinergic neurons innervating the longitudinal muscle bands on either side of the tail. These muscles contract in left/right alternation to produce the vigorous swimming behavior that aids in the dispersal of the larvae (Brown et al., 2005; Horie et al., 2010; Ohmori and Sasaki, 1977; Takamura et al., 2002). These neurons are thought to receive inputs from the sensory vesicle as well as from the peripheral nervous system (Horie et al., 2008a; Takamura, 1998). It has been shown that swimming behavior is modulated by light and gravity (Horie et al., 2008b; Jiang et al., 2005; Tsuda et al., 2003), and that the response of the larvae to these stimuli can change over time (Kajiwara and Yoshida, 1985).

Together with commissural inhibitory interneurons in the nerve cord, MG neurons drive the alternating left-right contractions of the tail that propel the tadpole forward. This is true even in dissected preparations consisting only of the MG, nerve cord, and tail (Nishino et al., 2010). Thus, the MG of the ascidian larva can be seen as the principal excitatory driver for the 'central pattern generator' (CPG) that controls swimming in *Ciona.* The term 'central pattern generator' refers to a discrete neuronal network that drives rhythmic motor behavior independently of sensory inputs (Marder and Bucher, 2001; Wilson and Wyman, 1965). CPGs thus provide a model in which to study how neurons assemble into a network and interact in order to produce a specific neural output. In vertebrates, spinal cord motoneurons and interneurons are assembled into 'motor pools', which innervate specific muscles (Goulding, 2009). Groups of motor pools that control body flexion during swimming or limb movement during walking can thus be considered CPGs. In recent years, developmental genetics and neuroscience have converged to study how the myriad neuronal subtypes of the spinal cord arise and subsequently interconnect within a motor pool to control locomotion (Goulding, 2009). This synthesis has the potential to bridge the gap in our understanding of how animal behavior can be encoded by the genome.

Gene expression studies suggest that many of the molecular mechanisms underlying the patterning of the ascidian larval CNS are shared with vertebrates (Meinertzhagen et al., 2004; Meinertzhagen and Okamura, 2001). Some of these conserved mechanisms, such as dorsoventral patterning involving *Pax3/7* (Wada et al., 1997), anteroposterior patterning by retinoic acid (Nagatomo and Fujiwara, 2003), and organizer activity of FGF8/17/18 (Imai et al., 2009), have so far been observed only in chordates. As such, *Ciona* has the potential to serve as a model system for studying chordate-specific gene regulatory networks underlying the development of the CNS. Furthermore, the phylogenetic position of sea squirts and the cellular simplicity underlying their swimming CPG make the *Ciona* tadpole a potential model for the development and function of chordate-specific neuronal networks.

Recently, preliminary gene regulatory networks have been described at single-cell resolution for each cell in the developing MG up to the tailbud stage (Imai et al., 2006; Imai et al., 2009). However, there is a gap in information between the cell lineages and gene regulatory networks in the embryo, and the final morphology of the differentiated neurons of the tadpole. For my dissertation work, I used fusion genes containing *cis*-regulatory elements ('enhancers') from several regulatory genes to reproducibly label unique pairs of cells in the developing MG and visualize them in their final differentiated state in swimming larvae. Included in this analysis are enhancers from *Ciona* orthlogues of transcription factors known to play a role in neuronal specification and differentiation in the spinal cord of vertebrates, such as *Dmbx1, Vsx2/Chx10, Islet1, Nkx6.1/Nkx6.2,* and *Pitx2.* These fusion genes (hereafter termed 'reporter constructs') revealed morphological traits that are specific to single pairs of MG neurons.

Furthermore, I present evidence that the morphology of distinct MG neuronal subtypes is regulated by these transcription factors, and that the FGF and Notch signaling pathways pattern the developing neural tube into giving rise to the invariant configuration of MG neuronal subtypes that we see. Thus, I have not only revealed a hitherto unappreciated specialization of MG neurons, but also which regulatory genes are controlling their specification and differentiation. The ultimate goal is to explain how a self-contained CPG network can arise from unspecified precursors according to an invariant pre-programmed genomic code. The mechanisms uncovered by studying this simple network could be used to understand the development and evolution of the seemingly infinite innate behaviors observed throughout the animal kingdom.

Chapter 2:

Materials and methods

Molecular cloning

Cis-regulatory regions were obtained by PCR off genomic DNA template isolated from California *C. intestinalis* adults and cloned into reporter expression plasmids. In the cases of isolated upstream or exonic/intronic fragments, these were cloned upstream of the basal promoter from the *Friend of GATA* gene (Rothbächer et al., 2007), fused in frame to the reporter gene. Previously published drivers used in this study include *FGF8/17/18* (Imai et al., 2009), *Islet* (Stolfi et al., 2010), and *Pitx* proximal fragment (Christiaen et al., 2005). The reporter genes used for lineage visualization were *lacZ* with a nuclear localization signal or Histone2B-tagged fluorescent proteins. For visualization of axons, unc-76-tagged fluorescent proteins were used (Dynes and Ngai, 1998).

Protein-coding cDNA sequences were amplified by PCR off full-length gene collection plasmids, or by RT-PCR. For RT-PCR, first-strand cDNA synthesis was performed off mixed-stage embryo whole mRNA preparations using oligo-dT primer. All primers were designed based on widely available mRNA, EST, and genomic sequence data. Some gene prediction models were incomplete, and thus the 5' and 3' transcription limits were determined with the SMART RACE cDNA amplification kit (Clontech).

Su(H)DBM (Hudson and Yasuo, 2006), caFGFR (Shi and Levine, 2008), Eph3ΔC (Picco et al., 2007) and *dnFGFR* (Davidson et al., 2006b) have been previously described and were cloned downstream of the *FGF8/17/18* and/or *Engrailed* drivers.

In situ hybridization

All ribonucleotide probe template plasmids were from the *Ciona intestinalis* gene collection (Nori Satoh, unpublished) or prepared by cloning coding sequence into pBSKM, the plasmid backbone of gene collection library clones. Plasmids were linearized NotI or SpeI and Digoxigenin-UTP-labeled anti-sense riboprobe was synthesized *in vitro* using T7 polymerase (Roche), cleaned up with RNAse-free DNAse I (Roche) and purified using RNeasy Mini Kit columns (Qiagen). Fluorescent *in situ* hybridization coupled to β-galactosidase immunodetection was performed using a TSA-plus tyramide signal amplification kit (Perkin-Elmer) and monoclonal mouse anti-β-galactosidase antibody (Promega #Z378A) as previously described (Beh et al. 2007). For double *in situ* hybridizations, Digoxigenin-UTP- and Fluorescein-UTP-labeled probes were prepared and co-hybridized. Each probe was detected by separate incubations of POD-conjugated fab fragments against Digoxigenin or Fluorescein, with a 0.01N HCl inactivation step between them. Each probe was revealed by a different color TSA-plus kit (Cy3 or Fluorescein).

Embryo handling, manipulation, and analysis

Adult *Ciona intestinalis* were obtained from Pillar Point marina (Half Moon Bay, CA) or purchased from M-Rep (San Diego, CA). Fertilization, dechorionation, electroporation, fixation, counterstaining, and mounting of embryos was carried out as established (Christiaen et al., 2009b). 50-100 ug of each plasmid was used per electroporation. Histone2B-fluorescent protein fusions are very stable and very bright, and thus only 5-10 ug of these plasmids were needed per electroporation. The technique of "consecutive electroporation" consisted of electroporating embryos with one plasmid mix, rinsing in sea water a couple of times by transferring to a new dish and gentle swirling, then electroporation with a second plasmid mix. For drug treaments, U0126 (Promega) was dissolved in DMSO and administered at 10 μm, while DAPT (Enzo Life Sciences) was dissolved in DMSO and administered at 100 μm. Embryos were imaged using Nikon or Zeiss AxioImager A.2 upright compound microscopes, or Leica SP2 upright or Zeiss700 inverted confocal microscopes.

Live confocal imaging of embryos and larvae

For live imaging, electroporated larvae were anaesthetized with 0.01% (w/v) benzocaine dissolved in buffered artificial sea water and placed on a 90mm plastic Petri dish to which they adhere. Image acquisition was performed on a Leica SP2 confocal microscope with a water-immersion 20x objective, using the time-lapse function of the Leica software. Twenty to forty micrometer-thick stacks were acquired by bi-directional scanning, with a 0.4 to 0.5μm/pixel resolution in x and y, one to two μm steps in z, every two or five minutes. Raw 512x512 image stacks were imported in Image J for time-lapse assembly and projections.

***Xenopus tropicalis in situ* hybridizations**

Xebf2 (Image clone# 5383656) *Xebf3* (Image clone# 7604756) *Nkx2.5* (Accession# DN012877) and *Islet1* (Accession# AL803057) probes were prepared by T7 polymerase in vitro transcription from linearized template using EcoRV, SalI, BamHI, ClaI restriction digests, respectively. All steps were performed as previously described (Harland, 1991). Brightfield images of hybridized embryos were taken using a Leica MZFLIII stereo-dissection microscope. Embryos for optical sections were cleared in 1:2 benzyl alcohol : benzyl benzoate and imaged on a Zeiss Axio Imager 2 using a 10x objective.

Some images and text are reproduced courtesy of Company of Biologists and AAAS.

Chapter 3:

Morphological diversity and gene expression in the *Ciona* Motor Ganglion

Rationale

In previous studies, the morphological diversity of CNS neurons in swimming larvae has been described using fluorescence microscopy (Imai and Meinertzhagen, 2007; Okada et al., 2001; Takamura et al., 2010; Yoshida et al., 2004). However, because pan-neural or neurotransmitter-related fusion genes were used to visualize the neurons, as opposed to individually labeling them, the identities and lineages of these cells remain uncertain.

Detailed descriptions of the mitotic history of the neural tube of *Ciona* have identified the precise lineages of the 5 pairs of cholinergic neurons comprising the MG (Cole and Meinertzhagen, 2004). Hereafter I will refer to them as single cells on either side of the embryo: the 4 anterior-most neurons are descended from the A9.30 blastomere (in order, from anterior to posterior: A12.239, A13.474, A11.118, A11.117), while the posterior-most 5th neuron (A10.57) is the posterior daughter cell of the A9.29 blastomere (summarized in Fig. 1D). I had previously shown that electroporation of 4.8kb of genomic DNA located immediately upstream of the *FGF8/17/18* transcription start site fused to a reporter gene preferentially labels cells descended from the A9.30 blastomere, as *FGF8/17/18* is strongly expressed in A9.30 at the late gastrula stage (Fig. 1B,C) (Imai et al. 2009). I therefore employed the same strategy in labeling individual MG neurons, identifying genes expressed in single MG precursors and then searching their upstream regulatory sequences for cell-specific enhancers.

Results

Identification of cell-specific enhancers

By coupling fluorescent *in situ* hybridization to immunofluorescence-based detection of β-galactosidase driven by the *FGF8/17/18* enhancer, I visualized, with single-cell resolution, the expression patterns of three homeodomain-containing transcription factors (TFs): *Dmbx, Vsx* (also known *Chx10*), and *Islet* (Fig. 2 A-C). These were described in previous studies as being exclusively expressed in a single pair of cells in the developing MG. Double *in situ* hybridization/antibody stains confirmed previous reports that, at the tailbud stage, *Dmbx* is expressed only in the A12.239 pair (Ikuta and Saiga, 2007; Takahashi and Holland, 2004), and Islet is expressed only in the A10.57 pair, in addition to being expressed in other tissues such as notochord, palps, pharyngeal mesoderm, and bipolar tail neurons (Giuliano et al., 1998a; Stolfi et al., 2010). In the distantly related ascidian *Halocynthia roretzi, Islet* has been shown to be transiently expressed in the A9.30 lineage, but maintained late only in A10.57 (Katsuyama et al., 2005). Similarly, I confirmed that *Islet* expression in the MG is eventually restricted to A10.57 (Imai et al., 2009). *Vsx* was found to be expressed by two pairs of neurons, initially being expressed in A11.117, and later in A13.474. This difference in the onset of *Vsx* expression is consistent with the difference in specification of these two pairs of neurons: A11.117 ceases mitotic activity at a time when A13.474 has not yet been born.

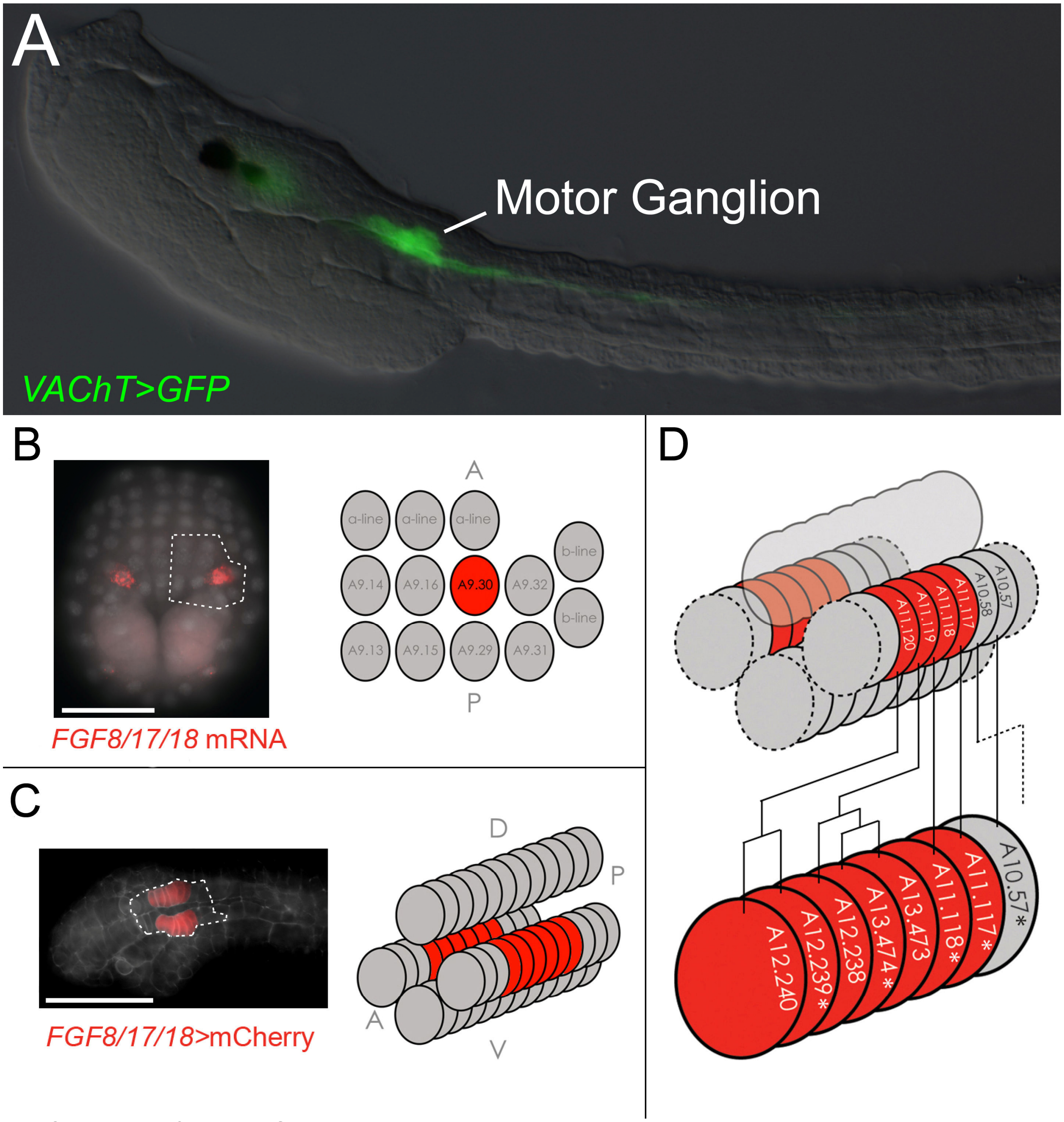

Fig.1 **Cell lineages of the Motor Ganglion.**
(**A**) Visualization of the Motor Ganglion in the swimming tadpole by electroporation of *VAChT>GFP* reporter, which labels cholinergic neurons. (**B**) Dorsal view of a late gastrula embryo with A9.30 blastomeres labeled by *in situ* hybridization for *FGF8/18/19* mRNA in red. Cell nuclei are counterstained by Hoechst stain. Outlined are the cells represented in the cartoon diagram to the right, representing the right half of the bilaterally symmetric posterior neural plate. (**C**) Lateral view of a stage E65-E70 tailbud embryo (~15 hours post-fertilization at 16°C, hpf), with descendants of A9.30 labeled by mCherry driven by the *FGF8/17/18* enhancer in red. Cell membranes are counterstained with phallicidin:BODIPY-FL. Outlined are the cells represented in the cartoon diagram to the right, representing the posterior neural tube, comprised of four rows of cells and derived from the posterior neural plate depicted in (A). The dorsal row of cells is slightly lifted to reveal descendants of both A9.30 blastomeres (red) on either side of the embryo. (**D**) Top: cartoon diagram of neural tube at E60 (~12 hpf), with A9.30 and A9.29 descendants labeled according to the established nomenclature. Dorsal row is rendered translucent for visualization of right lateral row; dashed outlines represent more anterior or posterior cells of the neural tube that have been ommitted. A9.30 descendants are highlighted in red, representing labeling by *FGF8/17/18* reporter construct (see text for details). Bottom: cartoon diagram of A9.30 lineage plus A10.57 on one side of the embryo at E75-E80 (~16 hpf). Lines between top and bottom cartoons denote invariant cell lineages. Dotted line represents posterior displacement of A10.58 by directed migration of A10.57. Putative motoneurons are denoted by asterisks. A: Anterior, P: Posterior, D: Dorsal, V: Ventral. Scale bars in (**B**,**C**) = approximately 50 μm

I next searched for enhancers in or surrounding these three genes that would be sufficient to recapitulate their cell-specific patterns. A fusion of 3.5 kb of Dmbx upstream DNA with *unc-76*-tagged enhanced Green Fluorescent Protein (GFP) recapitulated strong expression in A12.239, with slight expression in its sister cell, A12.240 (Fig. 2D). Similarly, a DNA sequence spanning the entire *Vsx* transcribed region recapitulated expression in A11.117 and A13.474 (Fig. 2E, 3B), suggesting the presence of an intronic enhancer. Finally, I have previously described an upstream enhancer of *Islet* that drives reporter gene expression in A10.57 (*'Islet>GFP',* (Stolfi et al., 2010), which I have also used in this study (Fig. 2F).

A Dmbx reporter construct labels A12.239

When embryos electroporated with such reporter constructs were allowed to develop until hatching, I was able to visualize individual, terminally differentiated neurons. A12.239, as revealed by *Dmbx>mCherry*, shows a thin axon projecting down the tail. However, it does not form the conspicuous, frondose endplates at the base of the tail revealed by electroporation of pan-neural reporter constructs (Imai and Meinertzhagen, 2007). Furthermore, the A12.239 pair project contralaterally, each axon associating with the axon bundle on the opposite side of the embryo (Fig. 3A). This is more clearly demonstrated by left/right mosaic expression, which can be achieved by consecutive electroporation of different reporter plasmid mixtures (Fig. 3D).

Thus, A12.239 is the pair of contralaterally-projecting MG neurons that were recently identified and likened to Mauthner neurons of rhombomere 4 of the fish and amphibian hindbrain (Takamura et al., 2010). Mauthner neurons are important for the escape response in which the animal rapidly turns its body away from an auditory stimulus (Eaton et al., 2001). Mauthner neuron axons cross the midline and synapse onto spinal cord motoneurons on the other side. The contralateral projection of A12.239 and their lack of endplates suggests they could serve to modulate motoneurons in a similar way, perhaps modulating the asymmetric 'tail flicking' behavior of the tadpole (Mackie and Bone, 1976). The comparison to Mauthner cells could distinguish A12.239 from the rest of the MG, giving it a higher-order status in the motor network, a rudiment of the posterior hindbrain of vertebrates. On the other hand, *Dmbx*+ v0 interneurons are definitely seen in the vertebrate spinal cord, though it has not been reported whether they project contralaterally or ipsilaterally (Ohtoshi and Behringer, 2004). I believe these *Dmbx1*+ spinal cord neurons are a stronger candidate for homology to A12.239 neurons, and that comparison to Mauthner neurons might not hold up. Certainly misleading is equating *Dmbx* expression in A12.239 to *Dmbx1* expression in the midbrain of vertebrates, as it has been used to argue for specific models of how the tripartite organization of the vertebrate CNS arose (Takahashi and Holland, 2004).

Despite a contralateral projection that could in theory help establish left/right coordination of muscle contraction during swimming, A12.239 expresses cholinergic markers and is not believed to be an inhibitory interneuron (Ikuta and Saiga, 2007). GABA/Glycinergic interneurons that arise from a different lineage are situated at the base of the tail and contact the motoneuron axon bundles in a contralateral manner

(Brown et al., 2005; Horie et al., 2010; Nishino et al., 2010). These are more likely to serve as inhibitory interneurons for modulating oscillatory left/right motoneuron firing.

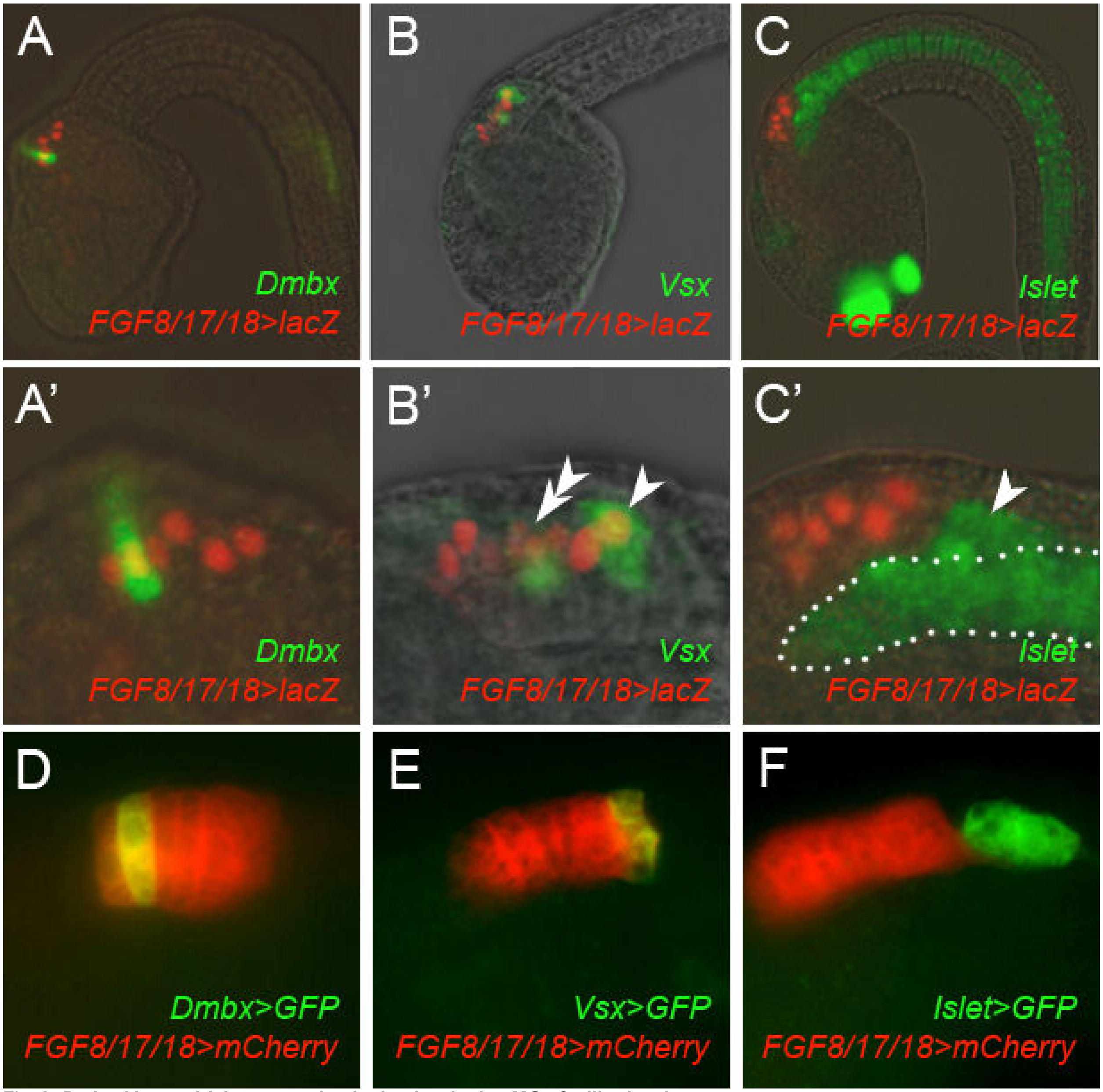

Fig. 2. ***Dmbx, Vsx,* and *Islet* expression in the developing MG of tailbud embryos.**
(**A**) *In situ* hybridization of *Dmbx* in green, showing expression in only A12.239 (**B**) *In situ* hybridization of *Vsx* in green, showing expression in A11.117 and A13.474 (arrowhead and double arrowhead in (**B'**), respectively. (**C**) *In situ* hybridization of *Islet* in green, showing expression in A10.57 (arrowhead in (**C'**)). Strong signal also seen in other tissues including notochord (dotted outline in (**C'**). All embryos counterstained by fluorescent antibody stain for Bgal (red nuclei), denoting A9.30 lineage labeled by electroporation with *FGF8/17/18>lacZ.* (**D,E,F**) Embryos co-electroporated with *FGF8/17/18>mCherry* (red) and *Dmbx, Vsx,* or *Islet>GFP* (green), respectively. Co-localization of GFP and mCherry is denoted by yellow color and corresponds to A12.239 in (**D**) and A11.117 in (**E**). *Vsx>GFP* is not seen in A13.474 in (**E**) since this cell has not been born yet. As expected, co-localization is not seen in (**F**), since A10.57 is not a part of the A9.30 lineage. Embryos in (**A-E**) are stage E65-70 (~15 hpf), embryo in (**F**) is stage E75-E80 (~16 hpf). All lateral views.

Vsx labels both A13.474 and A11.117, Pitx labels only A11.117

Neurons A13.474 and A11.117, as revealed by *Vsx>GFP* or *mCherry* (Fig. 3B), have thin axons and do not form conspicuous endplates, but do not appear to project contralaterally. Their axons never cross the midline as they project down the tail. The two pairs are distinguished by cell body size. A13.474 has a smaller cell body than that of A11.117 and the other neurons (Fig. 3B, E). Furthermore, *Vsx>GFP* revealed neurites emanating from the soma of A11.117 but not of A13.474, possibly representing dendrites (Fig. 3E). These dendrites were not seen on any of the other neurons.

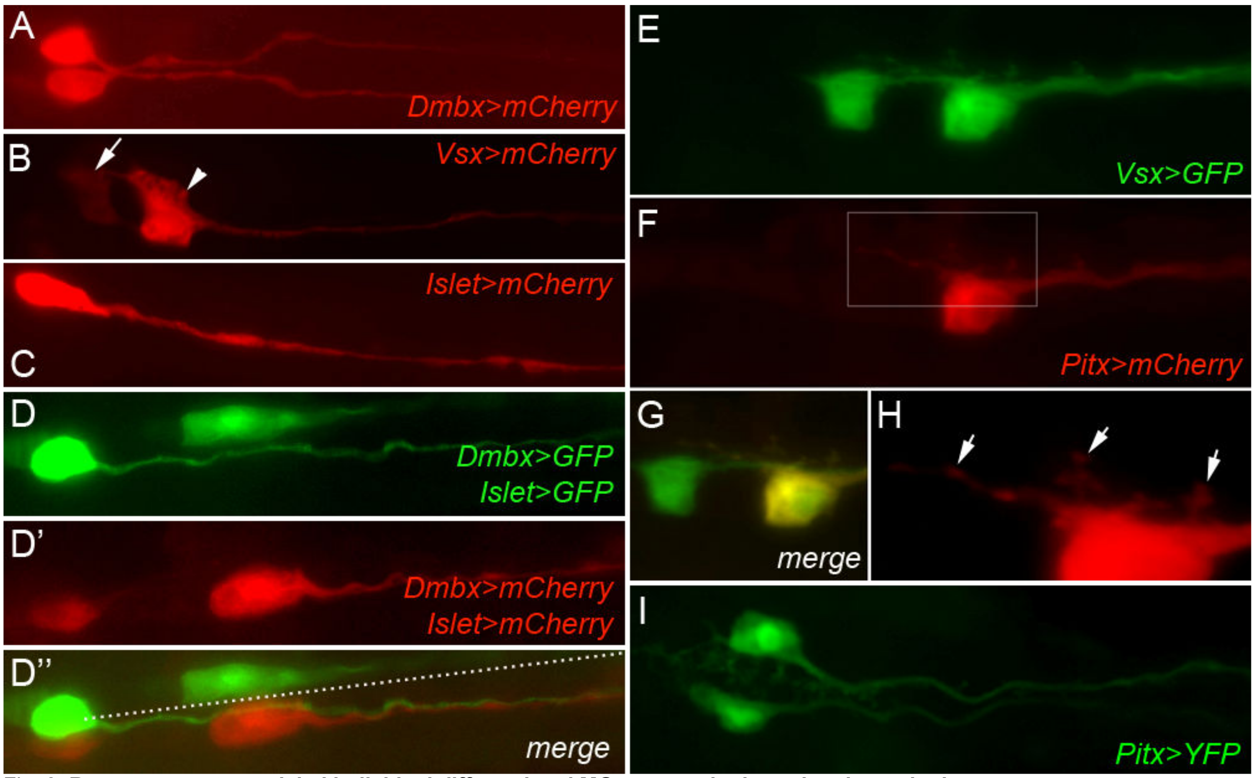

Fig. 3. **Reporter constructs label individual differentiated MG neurons in the swimming tadpole.**
(**A**) Dorsal view of A12.239 pair labeled with *Dmbx>mCherry.* (**B**) Lateral view of A13.474 (arrow) and A11.117 (arrowhead) on left side labeled with *Vsx>mCherry* (red). (**C**) Lateral view of A10.57 labeled with *Islet>mCherry.* (**D''**) Successive electroporation results in a rare tadpole with mutually exclusive left-right mosaic uptake of *Dmbx>GFP* + *Islet>GFP* and *Dmbx>mCherry* + *Islet>mCherry* plasmid combinations. (**D**) Cell bodies of A12.239 and A10.57 on the right side of the embryo labeled with GFP (**D'**) Cell bodies of A12.239 and A10.57 on the left side of the embryo labeled with mCherry. When red and green channels are merged (**D''**), the axon from GFP-labeled A12.239 on the right traverses the midline (dotted line) to associate with the mCherry-labeled axon of A10.57 on the left side, demonstrating the contralateral projections of the A12.239 pair. (**E**) Embryos electroporated with *Vsx>GFP,* which labels A13.474 and A11.117 pairs of MN. (**F**) *Pitx>mCherry* in contrast labels only A11.117. (**G**) Merged image of (**E**) and (**F**). (**H**) Magnified view of inset in F, showing putative dendrites belonging to A11.117 (arrows). Note in (**G**) that A13.474 does not appear to have dendrites. (**I**) Dorsal view of an embryo electroporated with *Pitx>YFP,* showing labeling of both left and right cells in the A11.117 pair. Note also how the dendrites are oriented towards the midline, and the axons do not project contralaterally.

The two *Vsx*-expressing pairs of neurons were separately labeled by co-electroporation with *Pitx* reporter constructs*.* A proximal genomic DNA fragment that drives the expression of the homeodomain TF *Pitx* in the visceral ganglion has been previously described (Christiaen et al., 2005). Electroporation of embryos with *Pitx>mCherry* specifically labeled A11.117 but not A13.474 (Fig. 3F,G). Co-labeling with *Vsx>GFP* and *Pitx>mCherry* also shows that A13.474 lacks the putative dendrites that are specific to

A11.117 (Fig. 3G,H). *Pitx* reporter gene expression was not seen prior to hatching (data not shown), suggesting *Pitx* is activated in A11.117 downstream of *Vsx*.

Recently, *Pitx2* was identified as a novel marker of cholinergic spinal interneurons in mouse (Enjin et al., 2010; Zagoraiou et al., 2009). A11.117 is also cholinergic and its lack of endplates further suggests a cholinergic interneuron identity. In contrast, *Vsx* orthologs are more broadly associated with interneurons arising in different nervous tissues and expressing different neurotransmitters (Kimura et al., 2006; Svendsen and McGhee, 1995). Therefore, the combination of *Vsx* and *Pitx* could be important for the specification of a cholinergic spinal interneuron identity.

An Islet reporter labels A10.57

A10.57, as revealed by *Islet>mCherry* or *GFP* and in accordance with previous studies, displays a cell body more elongated along its anterior-posterior axis than the other MG neurons (Imai and Meinertzhagen, 2007; Okada et al., 2002), but does not form prominent endplates (Fig. 3C,D). Putative motor endplates labeled by the *Islet* reporter were consistently smaller than the frondose endplates revealed by pan-neural reporter constructs (Appendix I).

Late Nkx6 expression labels A11.118

The preceding reporter constructs revealed the morphology of 4 out of 5 pairs of neurons in the MG, yet the frondose endplates still escaped cell-specific labeling. A fourth reporter construct, composed of the transcribed region of the *Nkx6* gene fused to GFP, stained frondose endplates in ~50% of transfected embryos (Fig. 4A, S2). This indicated the presence of an intronic enhancer. In half these cases, the staining was associated mainly with one cell body (Appendix II). Upon co-electroporation of *Nkx6>mCherry* and *Vsx>GFP*, this cell body was shown to be situated between A13.474 and A11.117 (Fig. 4D) and probably corresponds to A11.118.

This staining by the *Nkx6* reporter construct was unexpected, since, at the tailbud stage, *Nkx6* is expressed throughout the posterior MG (see Fig.Chapter 4). This preferential labeling of A11.118 might be due to maintenance of *Nkx6* in this cell later in development. *In situ* hybridization of *Nkx6* coupled to immunodetection of β-galactosidase in embryos electroporated with *Vsx>lacZ* is consistent with the preferential labeling of A11.118 by *Nkx6>GFP* (Fig. 4B). Co-electroporation of *Nkx6>GFP* and *Dmbx>mCherry* or *Islet>mCherry* further supported the conclusion that this late *Nkx6*+ cell is A11.118 and that it is the only motoneuron to form the frondose endplates contacting the lateral surfaces of the anterior tail muscle cells (Fig. 4C,E). In fact, co-electroporation with *Islet>mCherry* suggested that A10.57 might modulate A11.118 presynaptically, by what appears to be contacts onto the frondose endplates themselves (Fig. 4E, Appendix I).

None of the neurons exhibit an axon trajectory along the middle or ventral bands of the tail muscle, as was observed in the larvae of *Halocynthia* (Okada et al., 2002) and another ascidian species, *Dendrodoa grossularia* (Mackie and Bone, 1976). This difference in innervation could be due to the difference in size between the larger

Halocynthia and *Dendrodoa* larvae relative to *Ciona.* In *Halocynthia,* the middle band-innervating neuron is termed 'Moto-b', but it is not known whether 'Moto-b' corresponds to A11.117 or A11.118. It is conceivable that the frondose endplates of A11.118 in *Ciona* could represent the vestiges of the more ventral axon trajectories seen in *Halocynthia* and *Dendrodoa.*

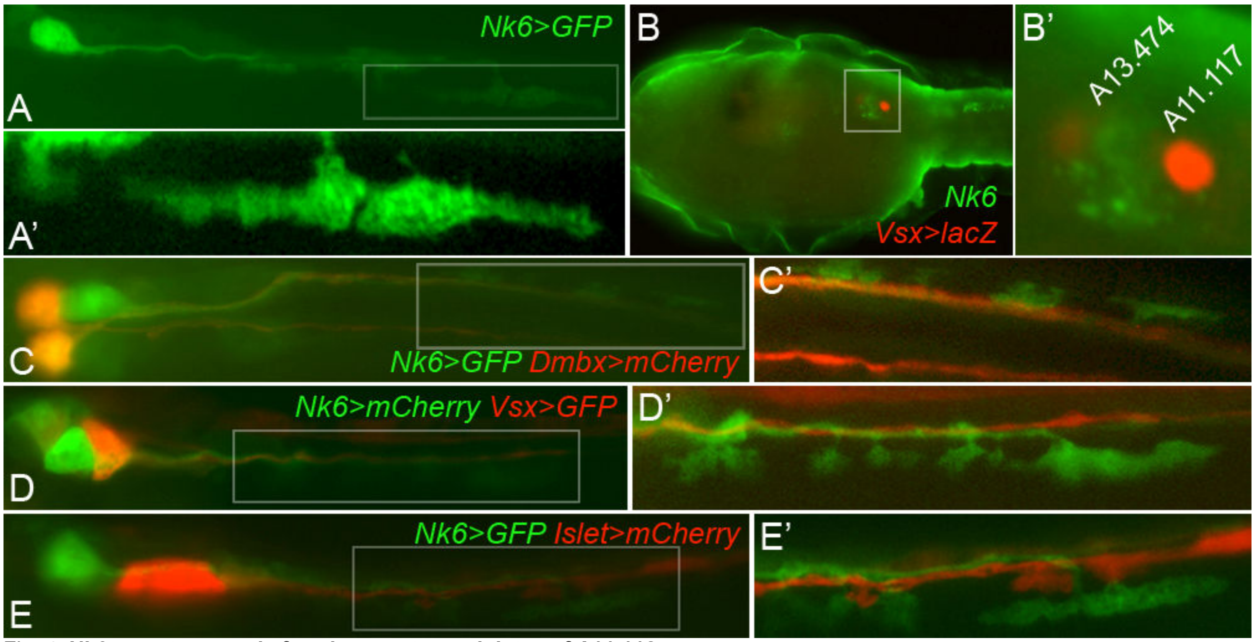

Fig. 4. **Nk6 reporter reveals frondose motor endplates of A11.118.**
(**A**) *Nk6>GFP* reporter contruct labels frondose motor endplates in 50% of electroporated embryos (see text for details). (**A'**) Magnified view of boxed area in (**A**). (**B**) Late Nk6 expression (green) seen in Stage E90 embryos in between cells A13.474 and A11.117 as revealed by antibody staining for Bgal in embryos electroporated with *Vsx>lacZ*. (**C**) Larva electroporated with *Nk6>GFP* (green) and *Dmbx>mCherry* (red). (**D**) Larva electroporated with *Nk6>mCherry* (green) and *Vsx>GFP* (red). Note inversion of false-color scheme, for consistency in the presentation of the data. (**E**) Larva electroporated with *Nk6>GFP* (green) and *Islet>mCherry* (red). (**C'-E'**) magnified or different focal planes of areas boxed in (**C-E**), to highlight frondose endplates always labeled by *Nk6* reporter construct but not by *Dmbx*, *Vsx*, or *Islet* reporters.

Ectopic Dmbx or Vsx expression abolishes A11.118-specific motor endplates

My observations on the morphological diversity of the visceral ganglion (summarized in Fig. 5) raised the possibility that the unique TF expression profile of each MG precursor might be functionally related to their particular identity. To investigate the potential role of these TFs in regulating morphology in the MG, I misexpressed Dmbx, Vsx, Islet, and Nkx6 in all differentiating MG neurons using regulatory DNA from the *COE* gene. *COE* (*Collier/Olf/Ebf*) transcription factors are involved in myriad cell fate decisions in metazoans, particularly in neurogenesis (Dubois and Vincent, 2001). A 2.6 kb genomic DNA segment located upstream of the COE gene directs expression in all of the differentiating MG neural precursors (Appendix III).

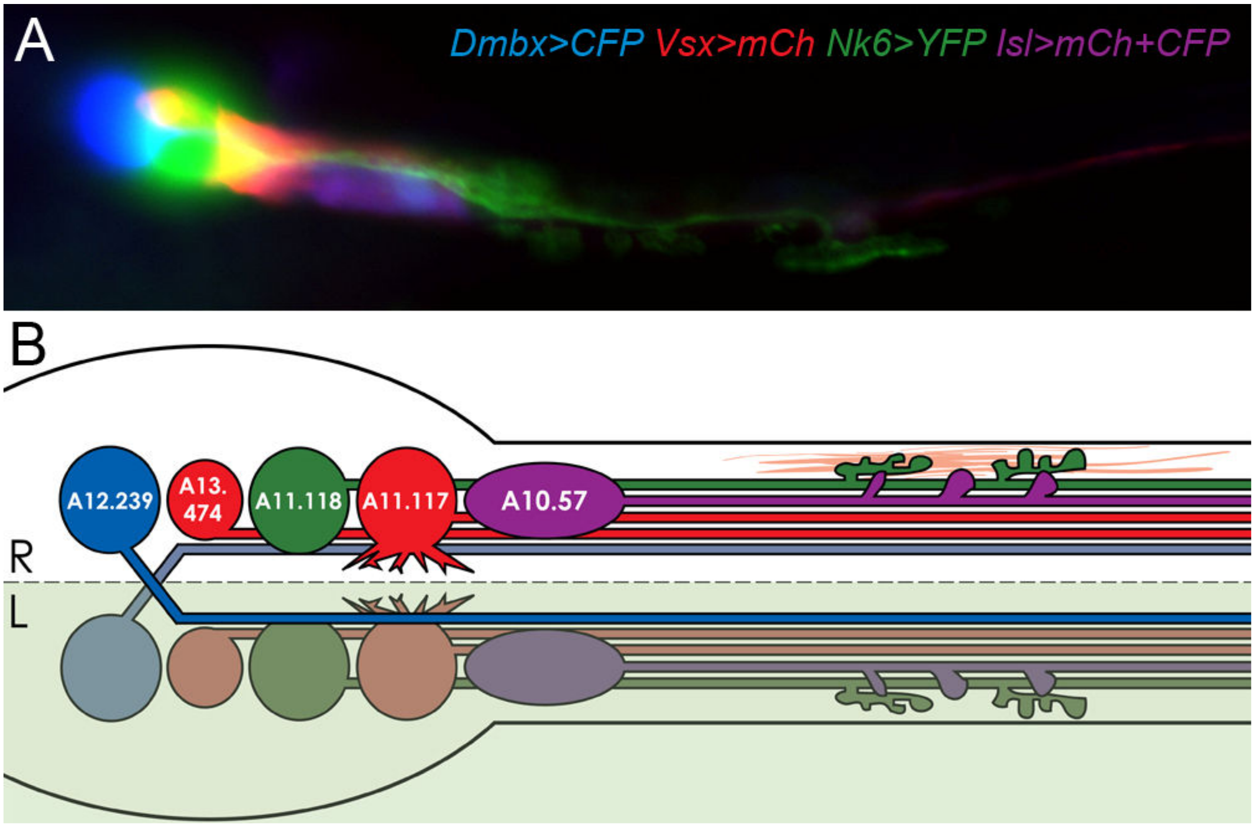

Fig. 5. **The *Ciona* Visceral Ganglion "brainbow".**
(**A**) Merged image of an imaged larva electroporated with a combination of the following plasmids: *Dmbx>CFP* (blue), *Vsx>mCherry* (red), *Nk6>YFP* (green), and *Islet>mCherry* and *Islet>CFP* (purple). Thus, five MNs are simultaneously visualized and distinguishable from one another. Green channel was imaged on a different focal plane than blue or red, to visualize *Nk6>YFP*-labeled endplates. Yellow color only indicates overlap of cell bodies, not co-localization. (**B**) Cartoon representation of the neurons depicted in (**A**) and their unique morphological traits, such as contralateral projection of A12.239 pair, smaller cell body of A13.474, frondose endplates of A11.118, dendrites on A11.117, and elongated cell body and smaller endplates of A10.57. Olive green shading indicates left side of the larva. Pink fibers represent tail muscle.

The visualization of individual neurons was sometimes compromised upon misexpression of certain TFs (Appendix IV). For example, cross-repressive interactions between Dmbx, Vsx, and Islet were revealed by *in situ* hybridization assays (Fig. 6A-C). Dmbx and Vsx strongly repress each other (Fig. 6A,B), while Dmbx and Islet have seemingly no effect on each other's expression (Fig. 6A,C). Vsx can actually induce ectopic *Islet* expression (Fig. 6C), while Islet can repress *Vsx* in A11.117, but not in A13.474 (Fig. 6B), hinting at a more complicated interaction between these two genes.

This modulation in reporter construct expression did not allow me to fully characterize the morphology of individual cells under these conditions. There were no obvious morphological defects under conditions without cross-repression (e.g. *Islet>Dmbx,* data not shown). Nonetheless, using *FGF8/17/18>GFP* to label all neurons in the A9.30 lineage I was able to visualize their axons in swimming larvae. Using this reporter, I observed multiple axons and axon growth cones originating from the MG in larvae electroporated with *COE>Dmbx* (Fig. 6A, Fig. 6D,H). These axons were all thin and did not form frondose endplates like those seen in control larvae electroporated with *COE>lacZ* (Fig. 6H). Electroporation of *COE>Vsx* also mimicked this phenotype (Fig.6E,H), suggesting that exclusion of Dmbx and/or Vsx from A11.118 might be important for its specification. In contrast, electroporation of *COE>Nkx6* or *COE>Islet* did not have a visible effect on motor endplate formation (Fig.6F-H). This observation is not surprising since *Nkx6* and *Islet* are transiently expressed in A11.118 in wild-type larvae.

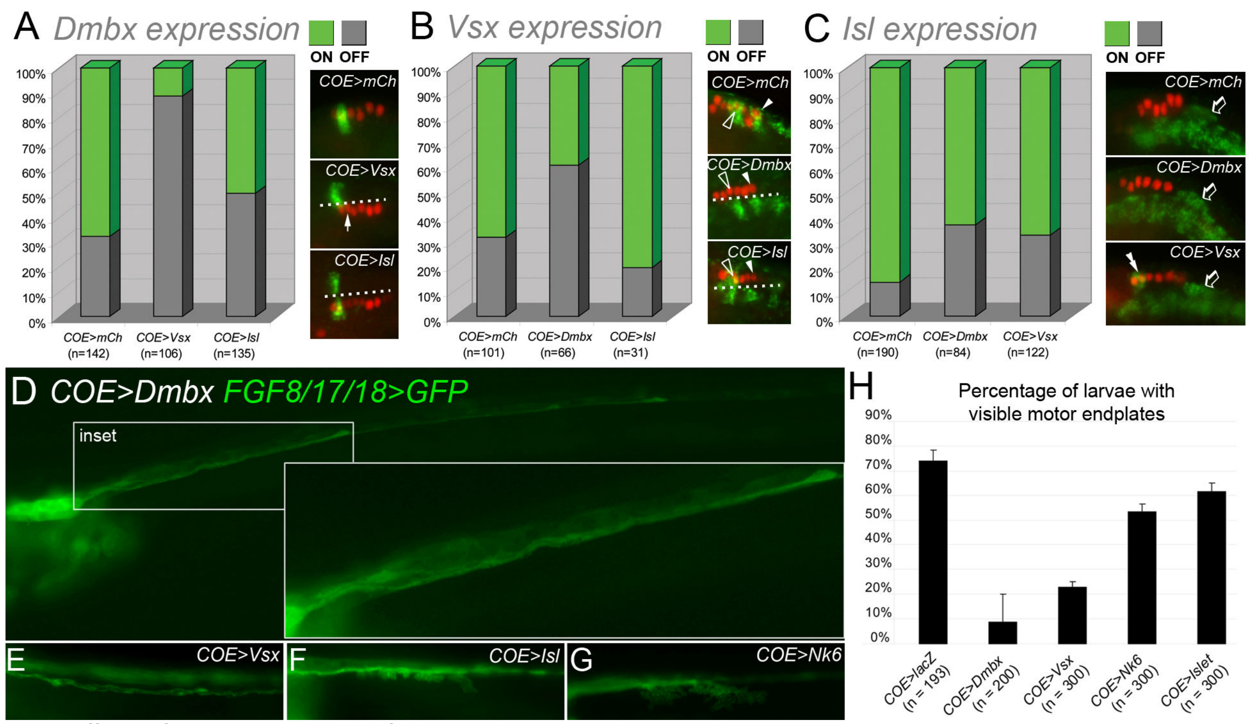

Fig. 6. **Effects of ectopic expression of Dmbx, Vsx, Isl, Nk6**
(**A**) Percent of electroporated embryos showing *Dmbx* expression upon electroporation with *COE>mCherry* (control condition), *COE>Vsx, or COE>Islet.* Only FGF8/17/18>lacZ+ embryo hemispheres (left/right) were assayed for co-localization with *Dmbx* transcript (by immunofluorescence staining for βgal coupled to fluorescent *in situ* hybridization). Green shading indicates fraction of βgal+ embryo hemispheres showing *Dmbx* expression. Grey shading indicates fraction of βgal+ hemispheres that do not show expression of *Dmbx.* Paucity of co-localization relative to control indicates that the transcription factor being overexpressed likely represses *Dmbx*. Panels to the right of the graph are representative embryos from each condition, showing A9.30 lineage in red and *Dmbx* expression in green. Dotted line represents embryo midline. In second and third panels, both hemispheres are visible but only the left side has been electroporated. In *COE>Vsx* condition, *Dmbx* expression is seen mainly in un-electroporated hemispheres, indicating that *Vsx* represses *Dmbx.* Left-right mosaic incoporation of plasmid thus provides us with an internal control. In *COE>Islet, Dmbx* expression is just as likely to be seen in electroporated hemispheres as in un-electroporated hemispheres. This indicates relative lack of repression of *Dmbx* by Islet. (**B**) Same as in (**A**), instead looking at effects of Dmbx and Islet overexpression on *Vsx*. Open arrowhead indicates A13.474 cell, solid arrowhead indicates A11.117. Dmbx appears to repress *Vsx* in both cells, while Islet appears to repress *Vsx* in A11.117 but not in A13.474. Thus, although in our quantitative assy *COE>Islet* is indistinguishable from the control, there is a qualitative difference between the two (A11.117-specific loss of *Vsx).* (**C**) Same as in (**A**) and (**B**), instead looking at effects of Dmbx and Vsx overexpression on *Islet (Isl). Islet* is expressed in A10.57 (open arrows), therefore we scored for "adjacent" *FGF8/17/18>lacZ* and neuronal *Islet* expression, instead of co-localization. *Islet* expression is also seen in the notochord, just ventral to the nerve cord. This notochord expression was not assayed. Double arrowhead indicates ectopic *Islet* expression in A12.239 caused by overexpression of *Vsx.* All *in situ* hybridizations carried out on a mixture of embryos at stages 23-25, from at least three independent electroporations per condition. (**D**) Larva electroporated with *COE>Dmbx* and *FGF8/17/18>GFP*. Axons from A9.30 descendants in the MG project down the tail but do not form motor endplates (inset). (**E**) Larva electroporated with *COE>Vsx* and *FGF8/17/18>GFP*, showing lack of endplates as in (**D**). (**F**) Larva electroporated with *COE>Islet* and *FGF8/17/18,* showing endplates typical of control larvae. (**G**) Same as in (**F**), but in a larva electroporated with *COE>Nk6* instead. (**H**) Quantification of endplate formation under conditions represented in panels (**D-G**), plus *COE>lacZ* control. Larvae were assayed for frondose endplates visible by GFP fluorescence, from *FGF8/17/18>GFP* expression in A9.30 lineage. Bars represent percentage of embryos showing endplates, averaged over three replicates. Embryos were from a batch of mixed stages, from E65-E80.

Discussion

Here I have used enhancers associated with TFs expressed in specific MG neuronal precursors to visualize the neurons controlling the swimming behavior of the *Ciona* tadpole. I have shown that neuronal subtypes in the *Ciona* MG arise in a stereotyped manner from cells expressing distinct combinations of TFs, which correlate with specific morphological features such as contralaterally-projecting axons and frondose motor endplates (summarized in Fig.5). These qualitative traits were largely invariant, though gross errors in axon outgrowth and targeting were sporadically seen in embryos displaying other non-specific developmental defects attributed to the electroporation protocol. My observations on cell-specific morphological attributes such as cell shape and axon trajectory are consistent with previous studies that distinguished each neuron based on its position within the MG (Imai and Meinertzhagen, 2007; Takamura et al., 2010).

These neuron-specific reporter constructs should be useful for the visualization and manipulation of individual neurons *in vivo.* In fact, with a combination of three enhancers and three different fluorescent reporter genes, I was able to distinguish five pairs of neurons in a single tadpole through co-electroporation and multi-plexed fluorescent imaging (Fig. 5). This *Ciona* 'brainbow' (Livet et al., 2007) demonstrates the potential usefulness of these constructs as a tool for future studies on the ascidian CNS.

Chapter 4:

Patterning of Motor Ganglion precursors by Ephrin/FGF/MAPK and Delta/Notch signaling pathways

Rationale

The results from the preceding chapter are consistent with the idea that a transcription factor code is required for the specification of morphologically distinct neuron subtypes. However, the cross-repressive interactions noticed upon misexpression of select transcription factors not only interfered with our ability to distinguish individual cell bodies and axons, they also meant that certain driver>transgene combinations (e.g. *Vsx>Dmbx*) could not work due to strong auto-repression. In an effort to circumvent this problem I manipulated instead candidate upstream cell signaling events. The goal was to change the identity of some cells without losing expression of the reporter constructs used for visualizing morphology and axon trajectories.

In the vertebrate spinal cord, different neuronal subtypes are specified as a result of dorsal-ventral (D-V) patterning by opposing BMP and Shh morphogen gradients (Briscoe and Novitch, 2008; Briscoe et al., 1999; Ericson et al., 1996; Lee et al., 2000). Surprisingly, a recent study showed that BMP and Shh do not appear to be involved in motoneuron specification in the *Ciona* MG (Hudson et al., 2011). This was not the expectation, given the conserved expression of BMP2/4 and Shh ligand expression in the dorsal and ventral neural tube cells respectively.

This was also surprising given that orthologs of vertebrate spinal cord patterning genes downstream of BMP and Shh gradients are also expressed in the *Ciona* MG (Fig 7A). From anterior to posterior, the transcription factors *Engrailed (En), Pax3/7, Pax6, Nkx6,* and *Lhx3* have partially overlapping expression domains that mirror the D-V patterning of the vertebrate spinal cord (Fig.7B) (Imai et al., 2009). In developing neural tube of chick and mouse, *Pax3* and *Pax7* are expressed dorsally. *Pax6* expression overlaps that of *Pax3/Pax7* but extending further ventrally to overlap also with expression of *Nkx6.1* and *Nkx6.2*. These *Nkx6* genes in turn delineate the ventral regions of the neural tube, where *Lhx3* is expressed ventral to *Engrailed*. In the A9.30 lineage of *Ciona,* expression of the corresponding orthologs are arrayed in the same order, from anterior to posterior. Due to the greatly reduced number of cells in ascidian embryos, the neural tube is composed of only four rows of cells: one dorsal, two lateral, and one ventral. Since the neurogenic domain of the ascidian MG is limited to the two lateral rows, it is logical that an ancestral D-V pattern (conserved in vertebrates and the more basal cephalochordates) would have been 'compressed' into an A-P layout, as we see in the *Ciona* MG

Given this re-oriented but conserved expression of transcription factors and the non-involvement of BMP and Shh in setting this pattern up, I asked what could be patterning the MG precursors, if not the usual suspects. Two of the candidate pathways most easily amenable to perturbation were the FGF/MAPK and Delta/Notch pathways, which have also been implicated in many instances of cell fate specification in the *Ciona* neurogenic ectoderm (Bertrand et al., 2003; Hudson et al., 2007). I thus sought to test their involvement in patterning of the *Ciona* MG.

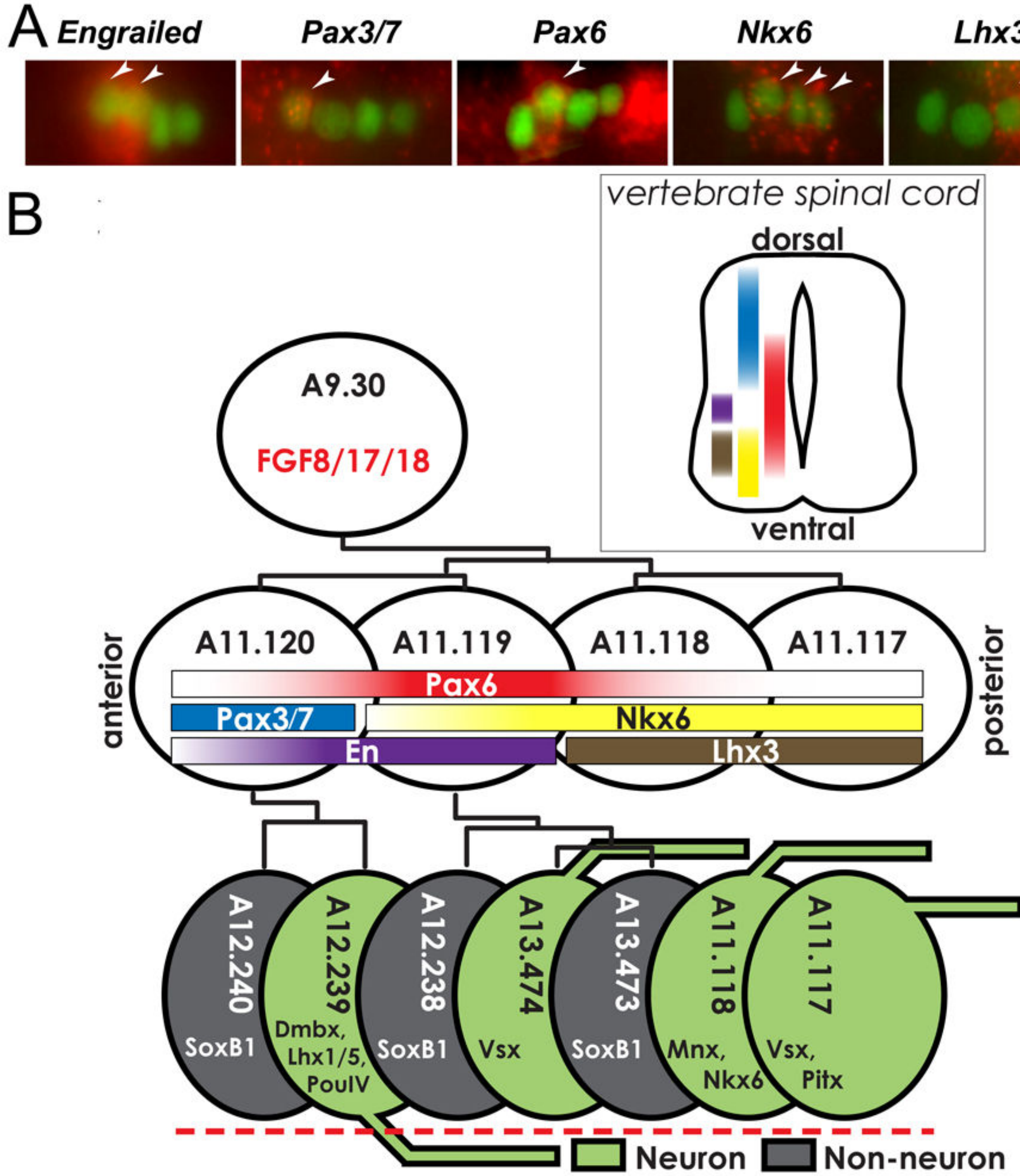

Fig. 7 **Conservation of transcription factor expression pattern despite D-V to A-P shift in neuronal subtype layout**
(**A**) Fluorescent In situ hybridization of transcription factors expressed when the A9.30 lineage is comprised of four cells. Nuclei of the A9.30 lineage are visualized by immunofluorescent detection of Bgal protein driven by the *FGF8/17/18* driver (*FGF8/17/18>lacZ*) (**B**) Diagram of the A9.30 lineage that gives rise to 4 of the 5 MG neurons. *FGF8/17/18* is expressed in the A9.30 and is used as a marker for the lineage through visualization of *FGF8/17/18* reporter constructs. Transcription factor gene expression at the four-cell stage of the lineage is denoted by colored bars. "Fading out" of colored bars represents weak and/or transient expression. The final differentiated neurons resulting from the lineage are shown at the bottom, with their respective non-neuronal sister cells. The transcription factors known to mark these neurons post-mitotically are indicated. *SoxB1* is a neural progenitor factor that is maintained in non-neuronal cells of the lineage. The embryo midline is indicated by a dotted red line. The axon trajectory of the neurons is indicated. A12.239 is the only confirmed contralaterally-projecting neuron in the MG, although the axon of A13.474 has yet to be convincingly visualized in isolation (indicated by dashed outline). Inset contains a diagram comparing A9.30 lineage gene expression to expression of orthologs of *Pax3/7* (*Pax3* and *Pax7*, blue), *Pax6* (red), *Nkx6* (*Nkx6.1* and *Nkx6.2*, yellow), *En* (purple), and *Lhx3* (brown) along the D-V axis of the vertebrate spinal cord, viewed in sagittal . (Based on Briscoe et al., 2000)

Results

Conversion of MG precursors into ectopic A11.117-like neurons by perturbation of FGF signaling

I asked whether FGF signaling is involved in specifying the identity of the various neuron subtypes in the MG. The *FGF8/17/18* enhancer was used to drive expression of a truncated, FGF ligand-sequestering form of FGF Receptor (dnFGFR) (Davidson et al., 2006b) in A9.30. Lineage-specific perturbation of signaling downstream of FGFR resulted in ectopic A11.117-like cells. In 90% (n=90) of electroporated embryos, all A9.30 descendants express *Vsx>GFP (*Fig. 8B). In contrast, ectopic *Vsx>GFP* expression (in cells other than A11.117 and A13.474) is seen in only 11% (n=75) of control embryos co-electroporated with *FGF8/17/18>lacZ*. These ectopic A11.117-like cells all project axons down the tail but do not form endplates (Fig. 8C). These neurons also express *Pitx>YFP,* albeit more weakly, indicating perhaps some later requirement for FGF signaling in *Pitx* activation or an inhibitory effect of excess Vsx (data not shown).

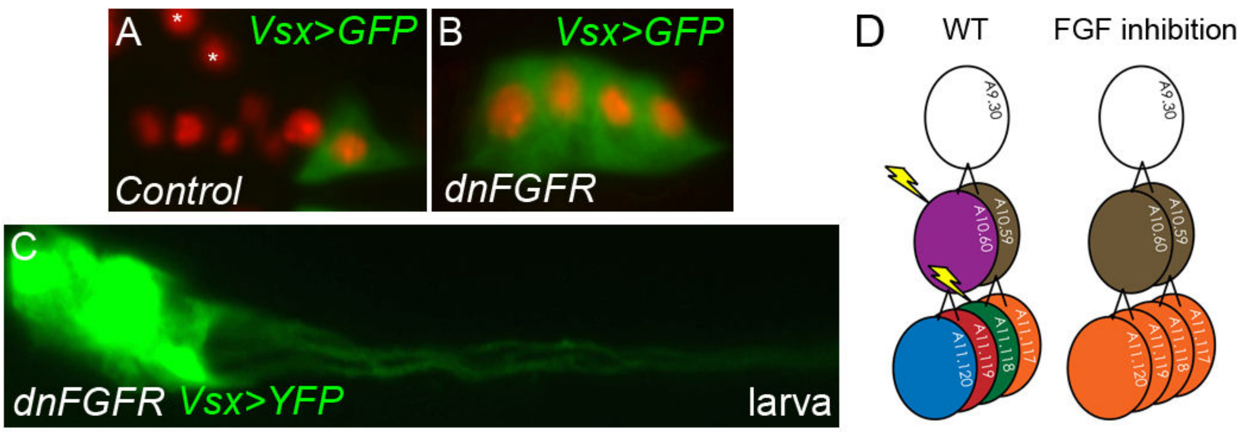

Fig. 8. **Inhibition of FGF and Notch signaling pathways alters the specification of MG neural precursors.** (**A**) At stage E75 (15.5 hpf), *Vsx>GFP* (green) is normally visible only in A11.117. (**B**) A9.30 descendants at stage E75 uniformly expressing *Vsx>GFP* upon perturbation of FGF signaling by *FGF8/17/18>dnFGFR*. (**C**) Ectopic *Vsx+* neurons in a swimming tadpole electroporated with *FGF8/17/18>dnFGFR.* (**D**) Cartoon diagram of the mitotic history of the A9.30 lineage from stages E50 to E80 (from top to bottom), indicating putative FGF signaling events (yellow thunderbolts) distinguishing A10.60 from A10.59 and A11.118 from A11.117 in wild-type embryos (left). Inhibiting FGF signaling (right) would transform the entire lineage to an A11.117-like fate (orange), as seen in (**B**).

These results are consistent with a conversion of the entire lineage to an A11.117-like identity (Summarized in Fig. 8D). Ectopic dendrites were not seen. This could be due to non-cell autonomous effects of having multiple A11.117 cells in contact with each other, or could be related to lower levels of *Pitx* expression. However, the lack of endplates, the ipsilateral axon trajectory, and cell shape and size indicate an acquisition of the A11.117 fate. Thus, there is a correlation between transcriptional state (*Vsx+, Pitx+*) and neuronal morphology in the MG.

MEK inhibitor treatment reveals timing of MAPK-dependent fate choices

I next sought to better characterize the requirement for MAPK downstream of FGF signaling in the early patterning of the A9.30 lineage. Embryos were treated at different timepoints with the irreversible MEK (MAPKK) inhibitor U0126 (Fig.9A). Expression of

En, Mnx, and *Vsx* was monitored using two-color fluorescent *in situ* hybridization, to assess the effects on cell fate choice in the daughter cells (A10.60 and A10.59) and grand-daughter cells (A11.120, A11.119, A11.118, A11.117) of A9.30. *En* is initially expressed in A11.120 and A11.119 before being maintained only in A11.119 and its descendants. *Mnx* and *Vsx* are expressed in A11.118 and A11.117, respectively. U0126 treatment at 6 hpf results in all grand-daughter cells expressing *Vsx,* and a loss of *En* expression. We interpret this as a conversion of A10.60 to an A10.59 fate, and subsequently conversion of all four grand-daughter cells to an A11.117 fate.

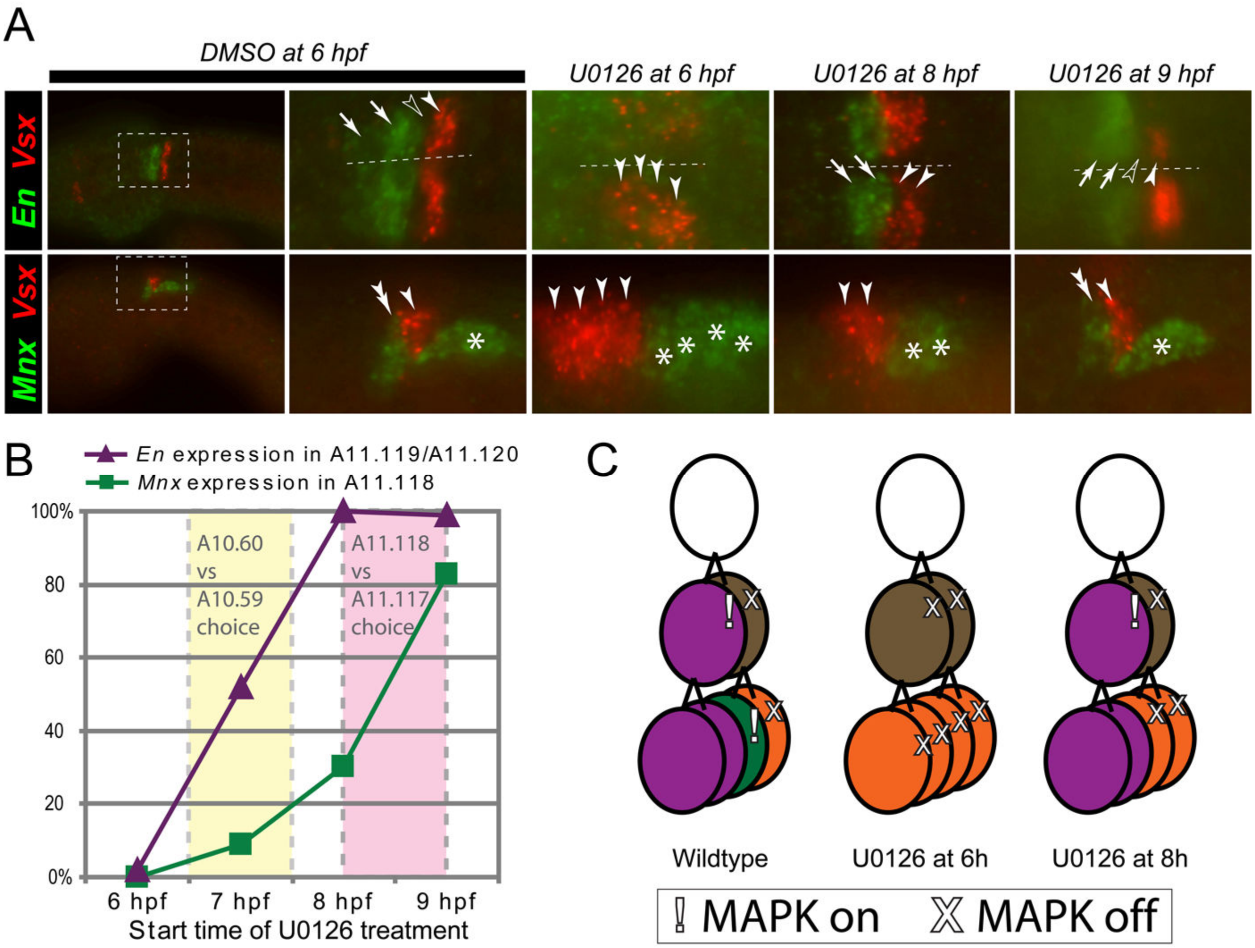

Fig. 9. **Treatment with MEK inhibitor U0126 reveals MAPK-dependent cell fate choices**
(**A**) Embryos were treated with either DMSO (control vehicle) or the irreversible MEK inhibitor U0126 starting at 1 hour intervals from 6 hpf to 9 hpf, at 20 degrees C. Embryos were fixed at 10 hpf and double fluorescent in situ hybridization was performed to simultaneously assay expression of *Engrailed* and *Vsx* (top panels) or *Mnx* and *Vsx*. Boxed areas in first panels represent area of magnified views in the second panels. TOP PANELS: *En* (green) is normally expressed in A11.120 and A11.119 (arrows), while *Vsx* is expressed in A11.117 (white arrowhead). The gap between *En* and *Vsx* expression represents A11.118 (open arrowhead). Treatment with U0126 at 6 hpf results in loss of *En*, and expression of *Vsx* in all four descendants of A9.30. Expression of *En* is not lost upon U0126 treatment starting at 8 hpf, though *Vsx* is still ectopically expressed in A11.118. Expression of both *En* and *Vsx* is normal with U0126 treatment starting at 9 hpf. BOTTOM PANELS: *Mnx* is normally expressed in A11.118 (double arrowhead), and in A10.57 (asterisk), which lays outside the A9.30 lineage. Treatment with U0126 at 6 hpf results in loss of *Mnx* from A11.118, but curiously leads to expansion of *Mnx* in the A9.29 lineage (asterisks). *Mnx* expression in A11.118 is only seen in embryos treated with U0126 starting at 9 hpf. (**B**) Fraction of embryos showing *En* (purple triangles) and *Mnx* (green squares) expression plotted over start time of U0126 treatment. Shaded yellow area represents likely time window for A10.60 vs. A10.59 fate choice, as determined by *En* expression in A11.119/A11.120 (daughter cells of A10.60). Shaded pink area represents time window for A11.118 vs. A11.117 fate choice, as determined by *Mnx* expression in A11.118. (**C**) Schematic of MAPK signaling events in wildtype embryos or embryos treated with U0126 at 6 hpf or 8 hpf. Colors correspond to cell identity as determined by *En* (purple), *Mnx* (green), or *Vsx* (orange) expression. Brown cell = A10.59 (mother cell of green + orange). Anterior is to the left in all panels.

In contrast, treatment with U0126 at 7 and 8 hpf does not abolish *En* expression. Instead, *Vsx* is ectopically expressed only in A11.118, at the expense of *Mnx.* This indicates a conversion of A11.118 into an A11.117 fate. Treatment with vehicle (DMSO) or with U0126 at 9 hpf does not alter gene expression. Taken together, these results suggest that two MAPK-dependent fate choices are made in the first two rounds of cell division in the A9.30 lineage: first, MAPK is required for A10.60 versus A10.59 fate choice, then MAPK is again required for A11.118 versus A11.117 fate choice. Since U0126 is an irreversible MEK inhibitor, treatment at 6 hpf affects both fate choices, resulting in four A11.117-like cells (Fig.9B,C).

Interestingly, *Mnx* is expanded in the A9.29 lineage upon U0126 treatment (Fig.9A). *Mnx* is usually only expressed in motoneuron A10.57, the posterior daughter cell of A9.29. Thus, ectopic *Mnx* expression in both daughter cells of A9.29 suggests that this fate choice also involves MAPK.

Ephrin is the positional cue for MAPK-dependent fate choice in the MG

The findings from the U0126 treatment are consistent with the previous dnFGFR overexpression study; both convert the entire A9.30 lineage into *Vsx*+ A11.117 interneurons, as a result of inhibiting both A10.60 and A11.118 fates. However, since *FGF8/17/18* is expressed in the A9.30 cell, presumably FGF ligand is equally available to all A9.30 descendants and thus cannot provide a localized cue for the MAPK-dependent fate choices. Consistent with this observation, targeted expression of a self-dimerizing form of the FGF receptor (*FGF8/17/18>caFGFR*) does not alter any of the aforementioned MG fate decisions (Fig. 10C, Appendix V). This suggested another cue must be involved in localized downregulation of MAPK downstream of such constitutive FGF receptor activation.

It has been shown that, in *Ciona,* Ephrins provide the localized cue required for MAPK-dependent fate choices (Picco et al., 2007; Shi and Levine, 2008). Ephrins are membrane-anchored ligands that signal to Eph receptor tyrosine kinases. In *Ciona,* Ephrin-Eph signaling suppresses MAPK in receiving cells, inhibiting FGF- and MAPK-dependent cell specification. This has been proposed to act at the level of Ras, which lies downstream of the FGF receptor but upstream of MEK in the intracellular signaling cascade (Miao et al., 2001; Picco et al., 2007). EphrinA-b is expressed in A9.29, which is situated just posterior to A9.30 (Appendix V). The A9.29 lineage thus is always in contact with the posterior-most cell of the A9.30 lineage. As such, EphrinAb is a strong candidate as the positional cue for specification of A10.59 and A11.117.

Involvement of Ephrin-Eph signaling was suggested by expression of the Eph3 receptor lacking the intracellular domain (*FGF8/17/18>Eph3ΔC*). Using *En>YFP* and *Vsx>mCherry* reporter constructs, the entire lineage was shown to be converted to *En*+ cells (Fig. 10B,C). This is consistent with MAPK being activated in these cells, due to the sequestration of Ephrin ligand by Eph3ΔC. Conversely, a self-dimerizing form of Eph3 (caEph3) is sufficient to abolish *En* reporter expression, though ectopic activation of *Vsx* reporter was not fully penetrant (Appendix V). Overexpression of other truncated Eph receptors did not produce a noticeable outcome (Appendix V).

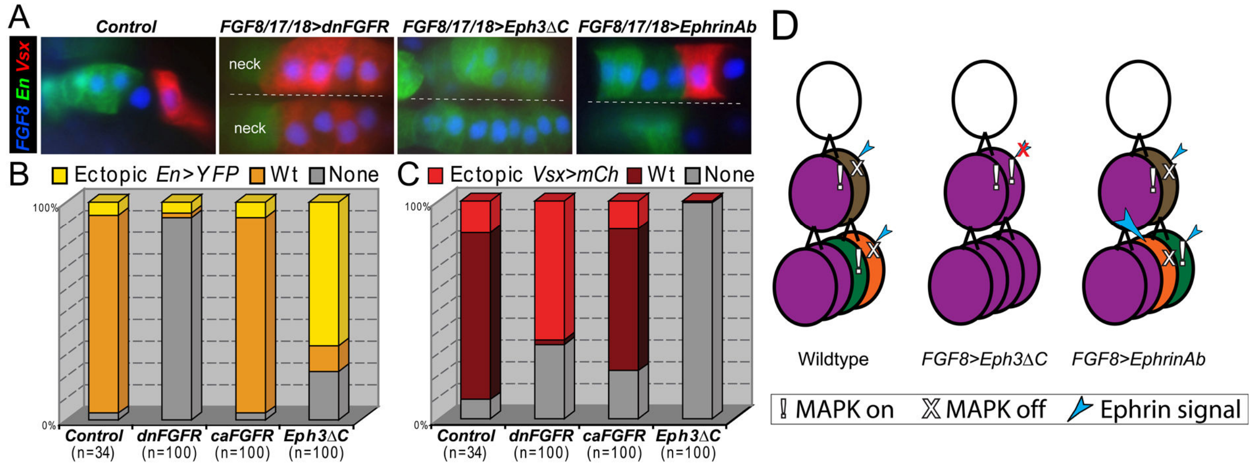

Fig. 10. **Ephrin-Eph signaling is the positional cue for MAPK-dependent fate choices**
(**A**) Embryos co-electroporated with *FGF8/17/18>H2B::CFP* (blue nuclei), *En>YFP* (green), and *Vsx>mCherry* (red) reporters and one of the following perturbation constructs: *FGF8/17/18>lacZ* (control), *FGF8/17/18>dnFGFR* (FGF receptor lacking intracellular domain), *FGF8/17/18>Eph3ΔC* (Eph3 receptor lacking intracellular domain), or *FGF8/17/18>EphrinAb*. All fixed at 15.5 hpf at 16 degrees C. In control embryos, *En>YFP* marks the anterior A9.30 lineage (descendants of A11.120 and A11.119), *Vsx>mCherry* marks A11.117, while A11.118 forms a 'gap' between *En>YFP* and *Vsx>mCherry* expression. *FGF8/17/18>dnFGFR* results in loss of *En>YFP* and ectopic *Vsx>mCherry* expression, as predicted. Note *En>YFP* still expressed in the neck, which is outside the A9.30 lineage and thus is not affected by *FGF8/17/18*-driven perturbation constructs. In contrast, *FGF8/17/18>Eph3ΔC* results in the converse phenotype: *En>YFP* expression is expanded to the whole lineage at the expense of *Vsx>mCherry* expression. *FGF8/17/18>EphrinAb* results in a distinct phenotype in which *Vsx>mCherry* expression is now seen in A11.118, but not A11.117, indicating an identity 'swap' between these two cells. Dotted line indicates midline. (**B**) Fractions of embryos showing ectopic (yellow), wildtype ("wt", orange), or no (grey) *En>YFP* expression in the A9.30 lineage in each of the conditions represented in B with the exception of *FGF8/17/18>EprhinAb* and with the addition of embryos overexpressing a self-dimerizing (constitutively active) form of the FGF receptor (*FGF8/17/18>caFGFR*). *Ectopic En>YFP* expression was taken as any expression in the posterior MG (A11.118/A11.117), whereas "wildtype" expression was taken as expression in the anterior (descendants of A11.120/A11.119 only). (**C**) Same as in (B), but scoring for ectopic (red), wildtype ("wt", maroon), or no (grey) *Vsx>mCherry* expression. Ectopic expression was defined as expression in any cell other than A11.117, and "wildtype" as expression only in A11.117. (**D**) Schematic of model incorporating Ephrin-dependent downregulation of MAPK in wildtype or perturbation conditions. Large blue arrow in right-most panel indicates overexpression of Ephrin ligand in A9.30 lineage, which can signal to A11.118 and result in preferential *Vsx>mCherry* activation in this cell in relation to its sister cell. Coloring scheme reflects that used in Figure 9C.

Electroporation with *FGF8/17/18> EphrinA-b* results in a phenotype distinct from either *FGF8/17/18>dnFGFR* (all *Vsx*+ cells) or *FGF8/17/18>Eph3ΔC* (all *En*+ cells). Instead, A11.118 and A11.117 fates appeared to be 'swapped' (Fig. 10A). In 52% of electroporated embryos (n=100), *Vsx* reporter was on in A11.118 but not in A11.117. Since Ephrin signaling is not thought to signal *in cis* to suppress MAPK, overexpression of EphrinAb in A9.30 should not affect the first fate choice between A10.60 and A10.59 if this fate choice is decided as the mother cell is dividing [as has been proposed (Picco et al., 2007)]. However, as A10.59 is dividing, it would encounter higher levels of EphrinAb from A10.60 (anterior) relative to the A9.29 lineage (posterior), thus resulting in a 'swap' of A11.118/A11.117 daughter cell fates along the A-P axis (summarized in Fig. 10D).

Overexpression of the other four *Ciona* EphrinA ligands with the *FGF8/17/18* driver did not cause the same fate swapping as seen for EphrinA-b. However, electroporation with *FGF8/17/18>EphrinA-c* and *FGF8/17/18>EphrinA-d* results in twice as many cells labeled with the *FGF8/17/18* reporter at the tailbud stage (data not shown). Due to the position of these ectopic *FGF8/17/18*+ cells in the tail, we interpreted this as a duplication of the A9.30 lineage at the expense of the A9.29 lineage. This suggests

EphrinA-c and/or EphrinA-d are involved in the earlier MAPK-dependent fate choice between A9.30 and A9.29 (Hudson et al., 2007).

Conversion of visceral ganglion precursors into ectopic A12.239-like neurons by perturbation of Notch signaling

Having shown that Ephrin-mediated suppression of MAPK downstream of FGF is required for proper specification of the posterior descendants of A9.30 I then asked: what is going on anteriorly, where A10.60 divides and gives rise to A11.120 and A11.119? A11.120 expresses *Pax3/7* and later gives rise to the *Dmbx*+ decussating A12.239 neuron, while A11.119 expresses *Pax6* and *Nkx6* and will give rise to the *Vsx*+ A13.474 neuron. The first clue that A11.120/A11.119 fate choice depends not on another Ephrin-MAPK-FGF interaction but rather on the Delta/Notch pathway came from the observation that, upon inhibition of Notch signaling in the A9.30 lineage using the *FGF8/17/18* enhancer to express a mutant form of Su(H) incapable of binding DNA (*Su(H)-DBM)* (Hudson and Yasuo, 2006), both A12.237 and A12.239 (the posterior daughter cells of A11.119 and A11.120, respectively) express Dmbx. As a result, a striking "OFF-ON-OFF-ON" GFP pattern is seen in 66% (n=100) of embryos electroporated with *FGF8/17/18>Su(H)-DBM* and *Dmbx>GFP* (Fig. 11B). In 100% (n=100) of wild-type embryos, A12.239 is the only cell that expresses *Dmbx* (Fig. 11A). An alternating pattern of endogenous *Dmbx* expression is also seen by *in situ* hybridization in embryos electroporated with *FGF8/17/18>Su(H)-DBM* (Fig. 11C), and the OFF-ON-OFF-ON pattern is also seen in embryos treated with the γ-secretase inhibitor DAPT, which inhibits the activation of Notch receptor (Appendix VI). These findings all point to a requirement for Notch signaling for expression of *Dmbx* in only A12.239 and not A12.237. In contrast, perturbation of Notch signaling in the A9.30 lineage did not affect the specification of A11.117 and A11.118, based on the lack of ectopic *Dmbx>GFP* expression in these cells, and normal *Vsx>GFP* expression in A11.117 (Appendix VI)

Strikingly, in 25% (n=300) of *FGF8/17/18>Su(H)-DBM*-electroporated embryos, ectopic *Dmbx*+ neurons grew axons that crossed the midline (Fig 11D). Thus, ectopic *Dmbx*+ neurons project contralaterally, a feature unique to the *Dmbx*+ A12.239 pair within the MG. This observation suggests that the contralateral projection of A12.239 correlates with a unique transcriptional state as assayed by *Dmbx* expression; duplicating a transcriptional state results in a duplicate neuron with the same axon trajectory.

The "OFF-ON-OFF-ON" phenotype also suggested that the specification of an ectopic A12.239-like neuron was not due to a simple breakdown in lateral inhibition of neurogenesis (Beatus and Lendahl, 1998). Rather, it suggested a conversion of A11.119 into an A11.120-like progenitor cell upon inhibition of Notch signaling. Given that perturbation of FGF signaling in these cells does not appear to convert A11.119 into A11.120 or vice-versa (see chapter 5), I hypothesized that the control of A11.119/A11.120 cell fate choice is effected by Delta/Notch signaling (summarized in Fig. 11F).

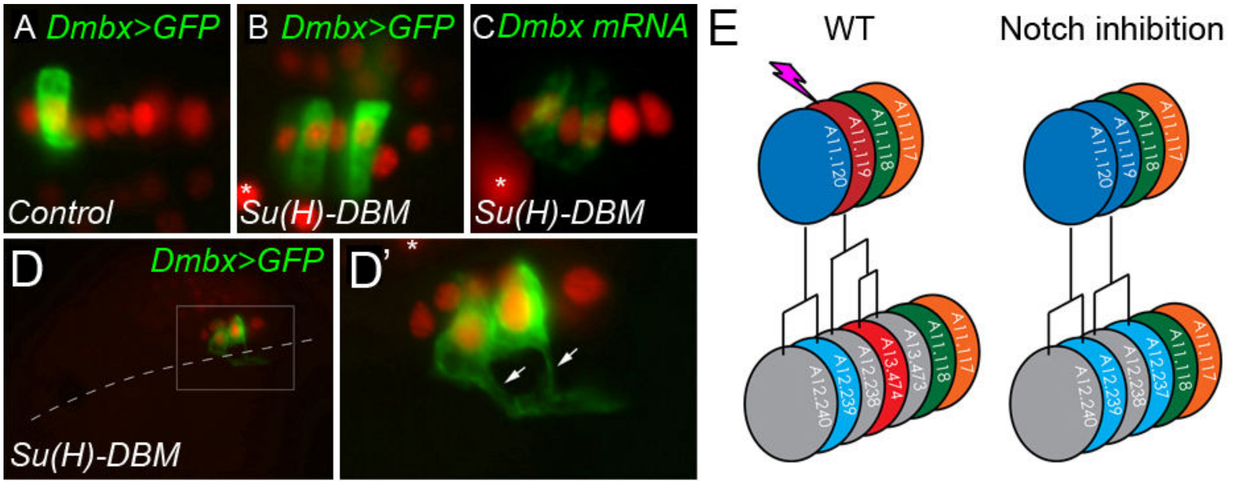

Fig. 11. **Conversion of visceral ganglion precursors into ectopic A12.239-like neurons by perturbation of Notch signaling** (**A**) Control (co-electroporated with *Dmbx>GFP* and *FGF8/17/18>lacZ)* embryo showing *Dmbx>GFP* expression (green) in A12.239 at stage E75. (**B**) Upon inhibition of Notch signaling by co-electroporation with *FGF8/17/18>Su(H)DBM* , *Dmbx>GFP* is seen to be expressed in two A9.30 descendants, instead of just one (same stage as in (**A**), see text for details) (**C**) Ectopic *Dmbx* expression confirmed by *in situ* hybridization (green) at stage E65 (14.5 hpf). (**D**) Dorsal view of a stage E90 (17.5 hpf) embryo electroporated with *FGF8/17/18>Su(H)DBM* and *Dmbx>GFP* (green). Embryonic midline marked by dashed line. (**D'**) Magnified view of inset in (**D**), showing both *Dmbx+* cells growing axons, both of which are crossing the midline (arrows). A9.30 lineage labeled with *FGF8/17/18>Histone2B::mCherry* or *lacZ* (red). (**E**) Cartoon diagram of A9.30 mitotic history from E55 to E80. Pink thunderbolt indicates putative Notch signaling event required for specification of A11.119. Upon inhibition of Notch, A11.119 adopts a A11.120 fate, giving rise to an ectopic A12.239-like descendant (light blue) as seen in (**F-G**). Asterisks denote mesenchyme cells expressing *FGF8/17/18.*

Delta/Notch signaling is required for specification of an A11.119 precursor fate

I reasoned that the duplication of *Dmbx* expression is not due to a breakdown in lateral inhibition as clearly both A11.120 and A11.119 were giving rise to one non-neuronal cell and one neuron. Furthermore, the neuron born from A11.119 was now *Dmbx+/PouIV+/Lhx1/5+* just like the neuron born from A11.120 (Fig. 12A). This was thus interpreted as A11.119 adopting an A11.120 fate.

To demonstrate more clearly this loss of A11.119 specification upon Notch perturbation, I electroporated embryos with *FGF8/17/18>Su(H)-DBM* and performed *in situ* hybridization for *Pax3/7,* a key marker of A11.120 and its descendants (Fig. 12B). Although *Pax3/7* was reported to be expressed in both A11.119 and A11.120 (Imai et al., 2009), I found that in control embryos, *Pax3/7* is initially expressed in A11.120 and later the daughter cells of A11.120, with a slight bias to A12.239 (posterior daughter cell of A11.120). In contrast to the previous report, *Pax3/7* expression was not normally seen in A11.119 or its descendants. However, in 68% of embryos electroporated with *FGF8/17/18>Su(H)-DBM* (n=100)*, Pax3/7* expression is expanded into the daughter cells of A11.119 (Fig. 12B,C).

Further evidence for conversion of A11.119 into an A11.120-like fate was obtained by assaying expression of A11.119-specific markers *Pax6* and *HesB.* Expression of these transcription factor genes in A11.119 was abolished by electroporation with *FGF8/17/18>Su(H)-DBM* (Appendix VII)*.* Furthermore, A11.119-specific maintenance of the transcription factor *SoxB1* was lost in embryos electroporated with *FGF8/17/18>Su(H)-DBM.* In wildtype embryos, expression of *SoxB1* is very dynamic throughout the neural tube during development (Ikuta and Saiga, 2007). It is initially expressed in both A11.120 and A11.119, but is specifically down-regulated in A11.120. Upon electroporation with *FGF8/17/18>Su(H)-DBM,* both A11.120 and A11.119 show either no or equally weak expression of *SoxB1* (Fig. 12B).

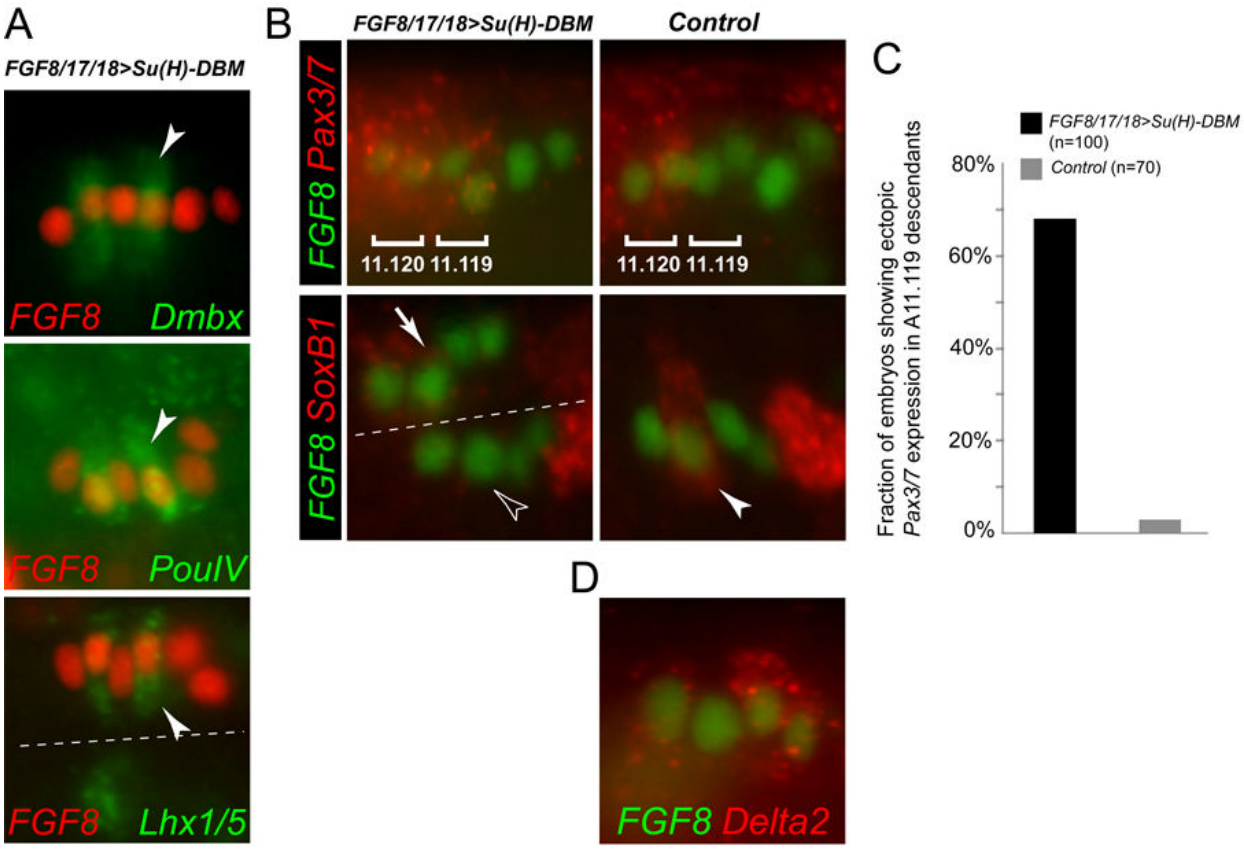

Fig. 12. **Notch signaling is required for specification of A11.119**
(**A**) In situ hybridization of A12.239 markers *Dmbx, PouIV,* and *Lhx1/5* (green) upon inhibition of Notch signaling by electroporation of FGF8/17/18>Su(H)-DBM, a form of the Notch-ICD transcriptional co-factor that cannot bind DNA. This condition results in ectopic expression of A12.239 markers in the posterior daughter cell of A11.119 (arrowhead). Expression of *Dmbx* was scored under this condition, and found to be ectopically expressed in the posterior daughter cell of A11.119 in 66% of embryos electroporated with *FGF8/17/18>Su(H)-DBM* (n=100). In contrast, control animals never show this ectopic expression. Dotted line indicates midline. Note normal *Lhx1/5* expression in A12.239 only in un-electroporated half of embryo. A9.30 lineage is visualized by electroporation with *FGF8/17/18>lacZ* (red, abbreviated as 'FGF8'). Embryos fixed at 14.5 hpf at 16 degrees C. (**B**) In situ hybridization of A11.120-descendant marker *Pax3/7* (top panels, red) and A11.119 marker *SoxB1* (bottom panels, red). Embryos in top panels fixed at 12.5 hpf at 16 degrees C, embryos in bottom panels fixed 11-12 hpf at 16 degrees C. Embryos were electroporated with either *FGF8/17/18>Su(H)-DBM* or *FGF8/17/18>GFP* (control). Note that GFP fluorescence is destroyed during the *in situ* procedure, and thus is only used as a neutral plasmid relative to the perturbation plasmid, to control for defects arising from higher transfection load. *Pax3/7* expression is expaned into A11.119 descendants upon electroporation with *FGF8/17/18>Su(H)-DBM*. Compare to control. This correlates with abolished (open arrowhead) or weak (arrow) expression of *SoxB1* in A11.119 under the same conditions. Compare to strong maintenance of *SoxB1* in A11.119 in control embryo (solid arrowhead). Dotted line indicates midline. (**C**) Scoring of embryos showing expanded *Pax3/7* expression pattern under *FGF8/17/18>Su(H)-DBM* and control conditions shown in (B). (**D**) In situ hybridization for *Delta2* (red) in A9.30 lineage (visualized by *FGF8/17/18>lacZ*: 'FGF8', green). Note expression in cells flanking A11.119, consistent with Delta/Notch-dependent specification of A11.119 fate.

I then looked for a localized source of Delta ligand that could activate notch in A11.119. Indeed, *Delta2* expression is seen in A11.118, which contacts A11.119 but not A11.120 (Fig. 12C) (Imai et al., 2009). Later, *Delta2* is activated in A11.120. I have already shown that *HesB* is activated in A11.119, and that this expression is lost upon electroporation with *FGF8/17/18>Su(H)-DBM*. These observations are consistent with

Delta2 signaling to activate Notch receptors specifically in A11.119, since *Hairy/Es(Spl)* genes are direct targets of Notch signaling (Kageyama and Ohtsuka, 1999).

Pax3/7 activates Dmbx in A12.239

Since an ectopic *Pax3/7+* A11.120-like progenitor gives rise to an extra *Dmbx+/PouIV+/Lhx1/5+* A12.239-like neuron, I hypothesized that *Pax3/7* in A11.120 is required for proper specification of its daughter cell A12.239. It was shown previously that knockdown of *Pax3/7* by morpholino oligonucleotide injection results in loss of *PouIV* and *Lhx1/5* (Imai et al., 2009). Although *Dmbx* expression was not assayed upon *Pax3/7*-morpholino injection, I extrapolate from these data that *Lhx1/5, PouIV,* and *Dmbx* are co-regulated by *Pax3/7.*

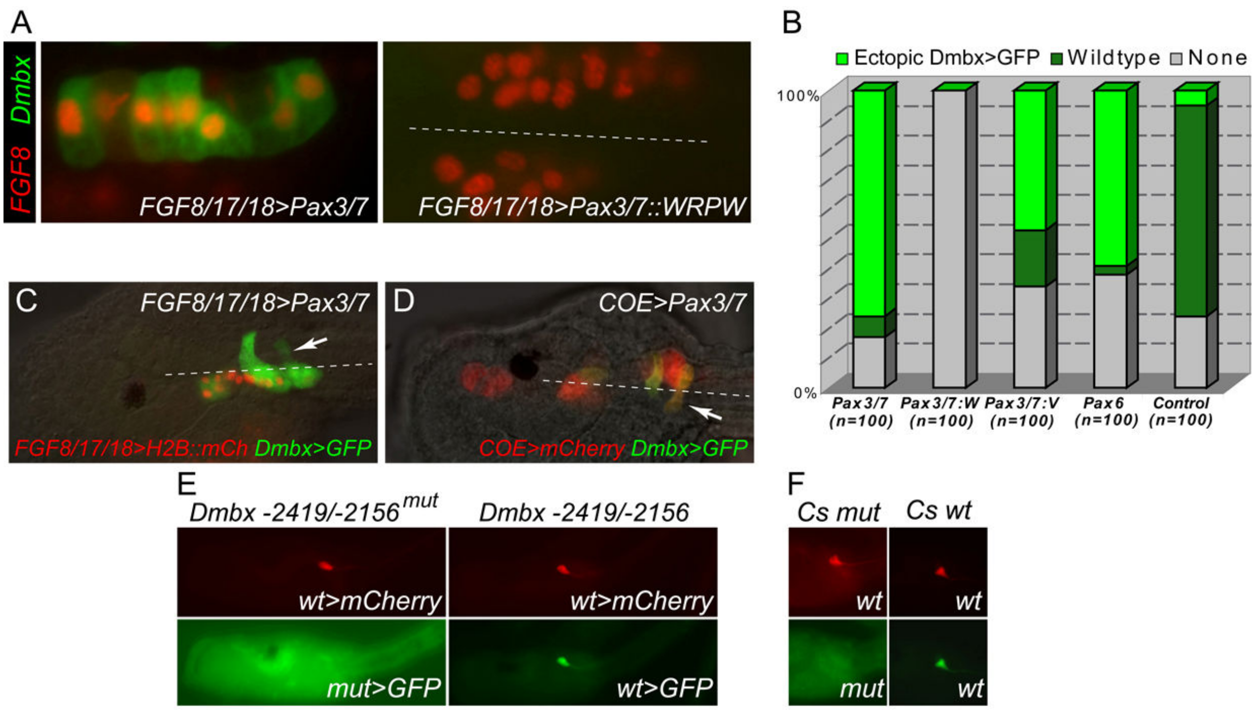

Fig. 13. **Pax3/7 as a direct transcriptional activator of *Dmbx***
(**A**) Embryos co-electroporated with *FGF8/17/18>H2B::mCherry* (red), *Dmbx>GFP* (green), and *FGF8/17/18>Pax3/7* (left panel) or *FGF8/17/18>Pax3/7::WRPW* (right panel). Pax3/7 overexpression activates ectopic *Dmbx>GFP* expression throughout the lineage, whereas Pax3/7::WRPW (a repressor form of Pax3/7) completely abolishes *Dmbx>GFP* expression. Dotted line indicates midline. Embryos fixed at 15.5 hpf at 16 degrees C. (**B**) *Dmbx>GFP* reporter expression analysis in embryos in which Pax3/7, Pax3/7::WRPW (Pax3/7:W), Pax3/7::VP16 (Pax3/7:V, a recombinant activator analog of Pax3/7), Pax6 or Bgal (lacZ) were overexpressed using the *FGF8/17/18* driver. Embryos fixed at 15.5 hpf at 16 degrees C. Wildtype *Dmbx>GFP* expression was defined as strongest expression in A12.239, while ectopic expression was defined as equal or stronger expression in other cells in addition to A12.239. (**C**) Embryo co-electroporated with *FGF8/17/18>H2B::mCherry* (red), *Dmbx>GFP* (green), and *FGF8/17/18>Pax3/7,* fixed at 17.5 hpf at 16 degrees. Midline indicated by dotted line. Note ectopic *Dmbx+* neuron extending a nascent axon across the midline (arrow). (**D**) Embryo co-electroporated with *COE>mCherry* (red), *Dmbx>GFP* (green), and *COE>Pax3/7,* fixed at 17.5 hpf at 16 degrees. Midline indicated by dotted line. Note ectopic *Dmbx+* neuron extending a nascent axon across the midline (arrow). (**E**) Swimming larvae co-electroporated with wild-type and/or mutated minimal *Dmbx* reporter constructs. The mutation in question is the disruption of a putative Pax3/7 binding site within a fragment -2419/-2156 bp upstream of the *Dmbx* start codon. Mutagenesis of the putative Pax3/7 site (*Dmbx -2419/-2156 mut* or simply *mut>GFP,* green*)* abolishes GFP reporter activity (99/100 larvae, bottom left panel). Green channel overexposed to show lack of GFP fluorescence intensity above background. Activity of co-electroporated wild-type reporter (*Dmbx -2419/-2156* or simply *wt>mCherry,* red) is not affected (top left panel). Compare to co-electroporation of both *GFP* and *mCherry* wildtype reporters (*wt>GFP* and *wt>mCherry,* right panels). Expression of the wildtype minimal *Dmbx* reporter in A12.239 is seen in 8% of larvae (n=600). (**F**) Disruption of the conserved, putative Pax3/7 binding site in the *C.savigny* minimal *Dmbx* reporter also selectively abolishes expression, when tested in *C. intestinalis* (bottom left panel). Only 2/21 larvae expressing *Dmbx-Cs wt*>mCherry (wt, red) were also expressing *Dmbx-Cs mut>GFP* (mut, green), compared to 22/23 co-expressing *Dmbx-Cs wt>mCherry* and *Dmbx-Cs wt>GFP* (right panels).

To further test the regulation *Dmbx* by Pax3/7, I mis-expressed Pax3/7 using the *FGF8/17/18* driver. Electroporation of *FGF8/17/18>Pax3/7* results in ectopic *Dmbx* reporter expression in all A9.30 descendants (Fig. 13A). This result is mimicked by the paired and homeobox domains of Pax3/7 fused to the VP16 transactivation domain (Pax3/7::VP16, Fig. 13B). In contrast, expression of a fusion of the paired and homeobox domains of Pax3/7 to the co-repressor motif WRPW (Pax3/7::WRPW) completely abolishes *Dmbx* reporter expression (Fig. 13A,B). These findings suggest *Pax3/7* promotes *Dmbx* activation through its activity as a transcriptional activator. Electroporation with *FGF8/17/18>Pax6* also results in weak but ectopic *Dmbx* reporter expression (Fig. 13B, data not shown), suggesting that Pax6 can partially substitute for Pax3/7 in activation of *Dmbx* and that other determinants of A11.119 fate (e.g. *SoxB1, HesB, Nkx6*) are likely important for repressing *Dmbx* in A11.119 descendants.

Ectopic *Dmbx* reporter expression was also achieved by mis-expressing Pax3/7 in differentiating MG neurons using the *COE* driver. Electroporation of either *FGF8/17/18>Pax3/7* or *COE>Pax3/7* results in ectopic *Dmbx*+ decussating neurons (Fig. 13C,D). Taken together, these results suggest that Pax3/7 is sufficient to specify a decussating, A12.239-like identity, in part by regulating A12.239 markers such as *Dmbx, Lhx1/5,* and *PouIV*.

To strengthen the case for direct activation of *Dmbx* transcription by Pax3/7 we analyzed the sequence of a minimal cis-regulatory module, or enhancer, from the *Dmbx* gene. A ~300 bp fragment situated -2.4 kb upstream of the *Dmbx* transcription start site was found to drive expression of GFP in A12.239 (Fig. 13E). This minimal *Dmbx* enhancer shows high sequence similarity to the corresponding sequence from the genome of the related species *Ciona savigny*. A sequence resembling a known Pax3 binding site in an *Fgfr4* enhancer of mouse (Lagha et al., 2008) was identified and mutated. Mutation of this putative Pax3/7 site disrupts minimal reporter gene expression (Fig. 13E). Mutation of the same site within the context of the larger *Dmbx* upstream regulatory region also results in loss of reporter expression (from expression in 52% of embryos for the wildtype reporter down to 12% for the mutated reporter, data not shown). Mutation of the corresponding site in the *Ciona savigny Dmbx* enhancer similarly abolished reporter expression, when tested in *C. intestinalis* (Fig. 13F). These data suggest an evolutionarily conserved putative Pax3/7 binding site is required for *Dmbx* activation.

Discussion

I have begun to dissect the signaling pathways and regulatory networks underlying the patterning of the *Ciona* MG. Despite a reduction in size and complexity relative to the spinal cord of vertebrates, some parallels between the *Ciona* MG and its vertebrate counterpart are evident. I have shown that by perturbing Notch and Ephrin/FGF signaling at different timepoints we can alter neuronal subtype specification in the MG of the *Ciona* larva. This is in contrast to patterning of the vertebrate spinal cord by long-range gradients of BMP and Shh. Despite these differences in signaling pathways employed for patterning, there is a rough D-V to A-P correspondence suggested by conserved expression of transcription factors, albeit with some clear differences.

I have shown that Ephrin/FGF/MAPK and Notch signaling result in *Pax3/7* expression in A11.120. In vertebrates, *Pax3* and *Pax7* are required for ventral commissure formation in the spinal cord (Mansouri and Gruss, 1998), and *Lhx1/5* is a known marker of commissural (decussating) dorsal spinal cord interneurons (Gowan et al., 2001; Reeber et al., 2008). As I have also shown, Pax3/7 regulates the expression of *Dmbx* and *Lhx1/5* expression in the decussating putative interneuron A12.239 and is sufficient to impose a contralateral projection when mis-expressed in other MG neurons. Thus, ascidians and vertebrates may share a conserved *Pax3/7*-dependent regulatory network to specify a decussating interneuron identity. Further comparisons between vertebrate and ascidian neuronal subtype repertoires and the transcription factors controlling their specification could shed light on the evolution of the vertebrate CNS.

Chapter 5:

Signaling requirements and transcriptional regulation of neuronal differentiation: a case study in A12.239

Rationale

Having uncovered the signaling pathways required for patterning of the A9.30 lineage up to its second generation, I asked what was regulating fate choice in the third generation. I focused on that between A12.239 and its sister cell A12.240. The A12.239 cell was of special interest due to its unique contralateral projection, and the useful *Dmbx* reporter construct that only labels A12.239. While A12.239 is a neuron, A12.240 expresses *SoxB1* and goes on to give rise to 4 small non-neuronal cells, either ependymal cells or quiescent precursors.

In many cases, the fate choice between a neuron and its non-neuron neighbors involves lateral inhibition through the Notch pathway (Beatus and Lendahl, 1998). However, as was shown in chapter 4, inhibition of Notch signaling did not appear to have a strong effect on A12.240/A12.239 cell fate, as evidenced by the OFF-ON-OFF-ON phenotype of *Dmbx* expression. In both the 'normal' and the 'ectopic' pair of sister cells, an invariant non-neuron/neuron fate choice was still being successfully carried out.

FGF is another pathway that can influence neural differentiation. FGF signaling appears to inhibit neurogenesis and promote a neural precursor-like state (Mathis et al., 2001). I therefore asked if differential FGF signaling could account for the fate choice between A12.239 neuron, and A12.240 non-neuron.

Results

Downregulation of FGF/MAPK is required for specification of A12.239 neuron
I could not simply perturb FGF signaling by electroporation with *FGF8/17/18>dnFGFR* like before, as that would block the specification of the entire anterior MG and thus my cells of interest. Thus, I carried out late perturbation of FGF/MAPK signaling by treatment with U0126 MEK inhibitor at 12 hpf at 16 degrees C (Fig. 14A). Looking at *Dmbx* reporter expression under this condition of late U0126 treatment revealed a 'twinning' of A12.239: both A12.239 and its more anterior sister cell, A12.240 now express *Dmbx*. Ectopic *Dmbx* reporter expression is not seen in descendants of A11.119, unlike the OFF-ON-OFF-ON pattern of *Dmbx* expression seen with Notch inhibition.

The twinning phenotype was mimicked by late overexpression of dnFGFR in the anterior MG using the *Engrailed* driver. Using the same driver to express Su(H)-DBM results in the OFF-ON-OFF-ON expression of *Dmbx* seen with *FGF8/17/18>Su(H)-DBM* (Fig. 14A). When combined, perturbation of Notch and late FGF signaling by co-electroporation of *FGF8/17/18>Su(H)-DBM* and *En>dnFGFR,* all four *En*+ cells go on to express *Dmbx* (Fig. 14A). These results suggest that FGF-MAPK is required for A12.240 fate. Indeed, late U0126 treatment results in loss of *SoxB1* specifically in A12.240 (Fig. 14B).

Overexpression of FGF ligand, caFGFR, Ephrin ligands, or truncated Eph receptors had no effect on *Dmbx* reporter expression (data not shown), suggesting FGF ligand availability and/or Ephrin signaling are not positional cues for this FGF/MAPK-dependent cell fate decision. Thus, FGF-MAPK appears to be permissive for A12.240 fate, whereas a localized instructive cue governing cell fate choice between A12.240 and A12.239 remains to be identified.

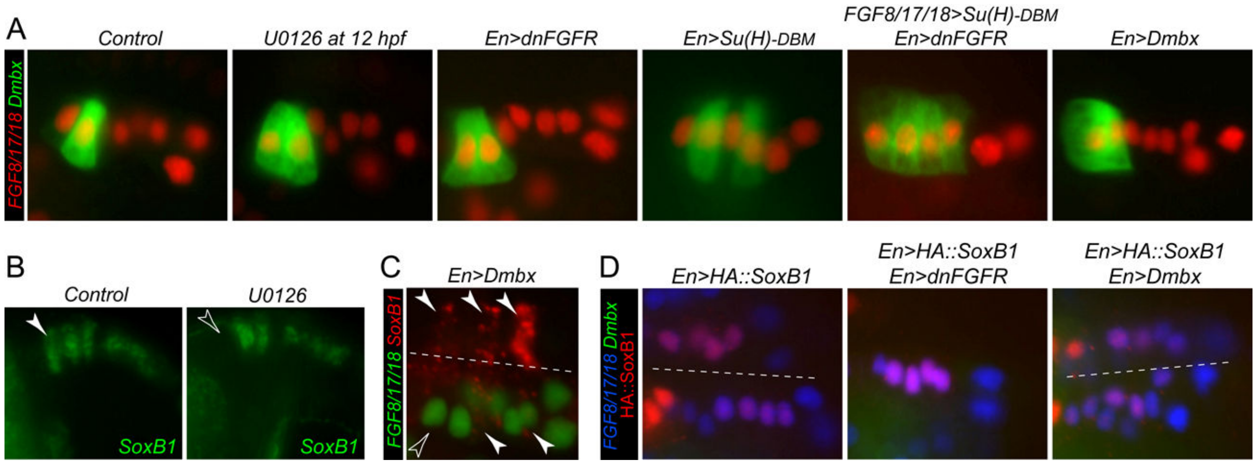

Fig. 14. **Involvement of FGF/MAPK, Dmbx, and SoxB1 in A12.240 vs. A12.239 cell fate decision**
(**A**) Embryos electroporated with *FGF8/17/18>H2B::mCherry* (red) and *Dmbx>GFP* (green) subjected to various perturbations and fixed between 15.5 hpf and 17 hpf at 16 degrees C. Control embryos (treated with DMSO at 12 hpf at 16 degrees C at the far left, showing *Dmbx>GFP* expression only in A12.239. Treatment with the MEK inhibitor U0126 at 12 hpf at 16 degrees C results in 'twinning' of *Dmbx* expression, converting non-neuronal A12.240 into an A12.239-like neuron. This effect is recapitulated by overexpression of dnFGFR relatively late using the *Engrailed* driver (*En>dnFGFR).* Electroporation of *En>Su(H)-DBM* does not mimic this 'twinning' but rather recapitulates the effect of *FGF8/17/18>Su(H)-DBM,* showing a strong, specific effect of FGF/MAPK perturbation on A12.240 vs. A12.239 cell fate choice. Combining both Notch and late FGF perturbation by co-electroporation of *FGF8/17/18>Su(H)-DBM* and *En>dnFGFR* results in four *Dmbx+* cells (two sets of 'twins'), as predicted. Unexpectedly, electroporation of *En>Dmbx* also results in 'twinning' of A12.239, suggesting Dmbx could downregulate FGF/MAPK signaling. (**B**) *In situ* hybridization of *SoxB1* (green) in embryos either treated with DMSO (control) or U0126 at 11 hpf at 16 degrees C. In 71% of control embryos (n=41) SoxB1 expression is seen in three non-neuronal cells of the MG, including A12.240 (solid arrowhead). U0126 treatment specifically abolished SoxB1 in A12.240 (open arrowhead) in 80% of treated embryos (n=45). (**C**) *SoxB1 in situ* hybridization (red) in an embryo electroporated with *FGF8/17/18>lacZ* (red) and *En>Dmbx. SoxB1* is lost specifically in A12.240 (open arrowhead). Note *SoxB1* expression is still visible in other cells (solid arrowheads), including in A12.240 in the unelectroporated half of the embryo. This suggests Dmbx and SoxB1 are mutually repressive, in the context of A12.240/A12.239 fate choice. (**D**) Embryos co-electroporated with *FGF8/17/18>H2B::CFP* (blue), *Dmbx>YFP* (green), *En>HA::SoxB1* (detected by HA-tag immunodetection, red), and one of the additional perturbation constructs: *FGF8/17/18>lacZ* (control), *FGF8/17/18>dnFGFR,* or *En>Dmbx*. HA::SoxB1 overexpression completely abolishes *Dmbx>YFP* expression, even overriding the 'twinning' effects of dnFGFR or Dmbx overexpression (in over 100 embryos looked at each). This suggests SoxB1 can repress *Dmbx* downstream of FGF/MAPK. Embryos fixed at 15.5 hpf at 16 degrees C. Dotted line indicated midline

Dmbx overexpression recapitulates FGF/MAPK downregulation

When Dmbx itself was overexpressed using the *En* driver, the 'twinning' effect of FGF/MAPK inhibition was also unexpectedly recapitulated (Fig. 14A, Appendix VIII). If Dmbx were directly auto-activating itself, we would expect to see *Dmbx* reporter expression in all descendants of *En*-expresssing cells. Instead, I hypothesize that Dmbx is downregulating FGF/MAPK signaling, due to the indistinguishable phenotypes of *En>dnFGFR* and *En>Dmbx*. However, this hypothesis was not tested, due to my inability to constitutively activate FGF/MAPK signaling.

Electroporation of *En>Dmbx* was found to abolish *SoxB1* specifically in A12.240, like U0126 treatment does (Fig. 14C). In vertebrates, Dmbx1 is thought to act as a repressor, and I found that a repressor form of Dmbx (Dmbx::WRPW) recapitulates the activity of the full-length protein (data not shown) in *Ciona*. Thus, I hypothesize that

Dmbx can promote its own expression through repression of *SoxB1* and/or a component of the FGF/MAPK pathway upstream of *SoxB1.*

It should be noted that axon targeting of these 'twin' neurons appeared abnormal, sometimes projecting anteriorly towards the sensory vesicle instead of posteriorly into the tail (Appendix VIII). Given that ectopic contralaterally-projecting Dmbx+ neurons were usually observed next to a non-neuronal Dmbx- cell (data not shown), I believe that homotypic adhesion between two A12.239-like neurons may perturb their normal axon trajectory. However, the contralateral projection itself, the act of crossing the midline, did not seem to be inhibited (data not shown). More careful studies will be needed to reveal the cell-autonomous and non-cell-autonomous factors governing axon guidance in this neuron.

SoxB1 represses Dmbx downstream of FGF

When A12.240 is born, this cell goes on to express *SoxB1* while A12.239 expresses *Dmbx*. In vertebrates, *SoxB1* genes promote a neural progenitor identity but repress neural differentiation, independently of the Delta/Notch/Hes lateral inhibition program (Bylund et al., 2003; Graham et al., 2003; Holmberg et al., 2008). Thus I hypothesized that SoxB1 is involved in keeping A12.240 in a neural progenitor state and inhibiting neurogenesis. I asked whether SoxB1 could repress *Dmbx* expression. To test this, SoxB1 was overexpressed using the *En* driver. This results in complete abolishment of *Dmbx* reporter expression, consistent with inhibition of differentiation of A12.239 (Fig. 14D). Electroporation of *En>SoxB1* also overrides the 'twinning' phenotype of *En>dnFGFR* or *En>Dmbx,* suggesting SoxB1 operates downstream of FGF signaling to inhibit A12.239 differentiation (Fig 14D). Taken together, *SoxB1* and *Dmbx* appear to mutually repress each other, in the specific context of the A12.240 versus A12.239 cell fate decision.

Discussion

FGF signaling has been shown to repress neural differentiation at several levels. In light of this, it is not surprising that FGF impacts A12.240/A12.239 fate choice by inhibiting differentiation of A12.240 into an ectopic *Dmbx+* neuron. However, what is interesting is the invariant specification of the posterior cell A12.239 as a neuronal cell opposite its non-neuronal, anterior sister cell. Although A12.240 fate requires FGF/MAPK signaling, we were unable to determine the localized cue for this asymmetry in fate, and could not implicate a usual suspect in localized MAPK suppression, Ephrin.

Although I observed a strong effect of FGF/MAPK downregulation on A12.240 vs. A12.239 fate choice, I cannot rule out a role for Delta/Notch in this process also. Firstly, the Delta/Notch lateral inhibition effectors *HesB* and *Neurogenin (Ngn)* show mutually exclusive expression in these cells that mirrors that of *SoxB1* and *Dmbx*, respectively (Appendix VIII). Secondly, in some embryos electroporated with *En>Su(H)-DBM, Dmbx* expression is seen equally in A12.240 (and the ectopic A12.240-like cell) as in A12.239 or the ectopic A12.239-like cell (Appendix VIII). This suggests that the strongest levels of Notch perturbation can mimic FGF/MAPK downregulation and have some input on A12.240 vs. A12.239 fate choice.

In light of the mutual repression of *SoxB1* and *Dmbx,* I suspect that Delta/Notch could be the asymmetric cue that feeds into the FGF/MAPK-dependent A12.240 vs A12.239 fate choice. *SoxB1* has been shown to interfere with neurogenesis by inhibiting proneural gene activity (Graham et al., 2003). In *Ciona,* the repressive effect of *SoxB1* on *Dmbx* expression is rescued by co-electroporation of the proneural gene *Ngn* (Appendix VIII). Notch signaling could be biasing *Ngn* and *Dmbx* expression in A12.239, while biasing *SoxB1* in A12.240. *Dmbx* in A12.239 would result in downregulation of FGF/MAPK and/or *SoxB1* in this cell, resulting in cell-cycle exit and differentiation. Meanwhile, *SoxB1* would continue to keep A12.240 in a progenitor like state (as long as FGF/MAPK signaling were still occurring), inhibiting *Ngn* and/or repressing *Dmbx*. *Dmbx1* has been shown to promote cell-cycle exit in vertebrates (Wong et al., 2010), supporting the idea of a *Dmbx*-dependent integrator circuit for differentiation downstream of FGF and Notch inputs (Appendix VIII).

How does the asymmetry in Delta/Notch signaling arise? In the A9.30 lineage, *Delta2* is expressed in A10.59 (data not shown) as a result of some combination of earlier regulatory cascades and extrinsic signals. Later, *Delta2* is maintained in A11.118, while HesB is expressed in A11.119. From this one can model the later *Ngn/HesB* expression pattern observed as a simple consequence of lateral inhibition within the lineage (Appendix VIII). This also raises the idea that the FGF and Notch pathways are not independent in their patterning of the MG. Perhaps proper Ephrin/FGF/MAPK-mediated specification of the posterior MG, where *Delta2* is expressed, is critical for setting up Notch-mediated specification of A11.119, as well as later specification events in the anterior MG. Indeed there is evidence for this, as embryos electroporated with *FGF8/17/18>Eph3ΔC* (which abolishes the *Delta2*-expressing posterior MG, but not the anterior MG) show aberrant *Pax3/7, Pax6,* and *Dmbx* expression (data not shown).

Chapter 6:

Conclusions

I have begun to document the morphological diversity of the ascidian MG, and the exact signaling events and transcriptional regulators involved in setting this up (summarized in Fig. 15A). Namely, Ephrin/FGF/MAPK and Delta/Notch signaling pathways can account for all the cell fate decisions that give rise to 4 out of the 5 MG neurons. By manipulating these pathways I can predictably obtain embryos with radically different configurations of motoneuron and interneuron subtypes (Fig. 15B). This provides a foundation for studying how these neurons assemble into a CPG to control the swimming behavior of the larva.

Unfortunately, the dechorionation/electroporation protocol used in our experiments perturbs larval tunic formation as well as other small defects in tail shape that leads to extremely aberrant swimming. To address this issue, transposon-mediated stable transgenesis (Sasakura et al., 2003) should be used for any serious behavioral studies. Nonetheless, the reductive nature of the MG, with only five pairs of neurons, could provide a simple yet powerful model for studying the neural basis of chordate locomotion.

Downregulation of FGF signaling is required for onset of spinal cord patterning genes (del Corral et al., 2002), and Notch has been shown to regulate neuronal subtype diversification (Peng et al., 2007). However, the role of Delta and Ephrin ligands as localized inductive cues for neural tube patterning seen here could very well be derived. Conserved or not, why have Delta/Notch and Ephrin/FGF taken on such a prominent role in patterning *Ciona* MG*?* These two pathways are also heavily involved in other early progenitor fate choices in *Ciona* (Hudson et al., 2007). I propose that Ephrin/FGF/MAPK and Delta/Notch constitute ideal pathways for cell fate choice in the context of invariant cell lineages. As transmembrane ligands, Ephrin and Delta might be able to quickly relay transient yet precise cell-cell interactions into equally precise gene expression patterns in a way that diffuse gradients might not.

While the invariant cell fate choices are regulated by such cell-cell contacts, diffuse signals could still be required for broad activation of MG-specific factors. In vertebrates, retinoic acid (RA) is required for activation of patterning genes in spinal cord progenitors as they escape FGF signaling (del Corral et al., 2003). RA also has a later role in activating motoneuron specification genes in vertebrates (Novitch et al., 2003). In *Ciona,* the RA-synthesizing gene *RALDH2* is expressed in anterior tail muscles and is required for *Hox1* expression in the anterior MG (Imai et al., 2009; Nagatomo and Fujiwara, 2003). Perhaps RA emanating from the tail is also important for activating other MG transcription factors. It will be interesting to address the roles of RA and other signaling molecules showing conserved expression patterns. Although the Shh-expressing floor plate cells in *Ciona* are not required for motoneuron induction, the conserved expression pattern of Shh belies an important, if yet unknown function.

Although the signaling events are not necessarily shared with vertebrates, I believe the transcriptional networks operating downstream of cell fate choice may prove to be more conserved, and thus more interesting from a comparative standpoint. In vertebrates, Pax6 and Nkx6.1/Nkx6.2 restrict the competence for Olig2 expression and subsequent motoneuron induction to a more ventral region of the spinal cord (Briscoe et al., 2000; Novitch et al., 2001). An ortholog of *Olig2* has not been identified in the *C. intestinalis* genome, and in the A9.30 lineage *Pax6* and *Nkx6* overlap in a non-motoneuron precursor (A11.119), though *Nkx6* extends to the posterior cells of lineage*,* including the motoneuron A11.118. This motoneuron expresses *Lhx3* and *Mnx,* which are part of a conserved 'motoneuron code' that also includes *Islet.* In flies and vertebrates, the combinatorial activity of Islet and Lhx3 specifies primary motoneurons, while interneurons are specified in the absence of Islet, through action of Chx10/Vsx2 (Lee et al., 2008; Thaler et al., 2002; Thor et al., 1999). However, in *Ciona* sustained expression of *Islet* is seen only in motoneuron A10.57, which arises from the A9.29 lineage and also expresses *Lhx3* and *Mnx* but not *Nkx6.* Thus these two similar but distinct motoneuron subtypes arise from different lineages expressing overlapping sets of conserved motoneuron determinants.

In *Ciona,* FGF signaling is required for *Mnx* expression in motoneuron A11.118 yet appears to play the opposite role in the A9.29 lineage, where treatment with the MEK inhibitor U0126 results in ectopic *Mnx*+ A10.57-like motoneurons (Fig. 9A). Thus, two distinct motoneuron programs could be operating in *Ciona:* one, in the presence of Nkx6 and FGF and the other in the absence of Nkx6 and FGF. Future work will be needed to define the regulatory networks specifying these two motoneuron subtypes, and how they relate to their counterparts in other animals.

Future work will be required to determine the causal link between TFs and morphology in the MG. A gene network analysis might reveal the regulation of rate-limiting cellular effectors responsible for some of the distinctive properties of MG neurons. For instance, presumably something is transcriptionally downstream of Pax3/7, perhaps downstream of or in parallel to *Dmbx,* to cause neurons to project their axon over the midline, as is the case of neurons ectopically expressing Pax3/7. It is also possible that some TFs might regulate transient cellular processes, such as morphogenetic movements, rather than subtype identity. Furthermore, some possibly also represent 'selector genes', directly regulating the terminal differentiation genes responsible for subtype-specific physiological properties (Hobert et al., 2010). Future work on how these distinct neurons interconnect to control swimming will bring us closer to understanding how gene regulatory networks create behavior in a chordate.

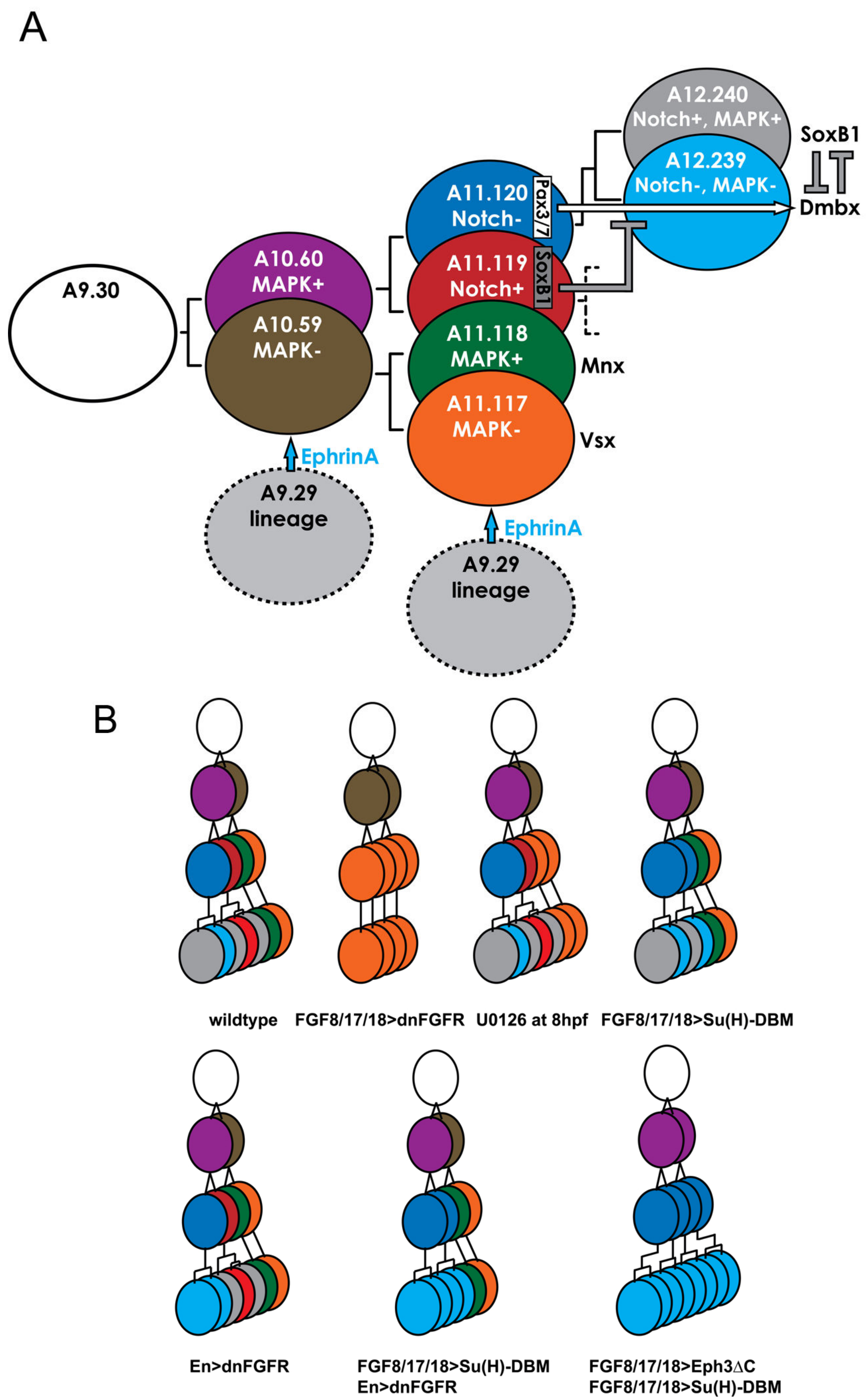
A
A9.30
A10.60
MAPK+
A10.59
MAPK-
A11.120
Notch-
Pax3/7
A11.119
Notch+
SoxB1
A11.118
MAPK+
A11.117
MAPK-
A12.240
Notch+, MAPK+
A12.239
Notch-, MAPK-
SoxB1
Dmbx
Mnx
Vsx
EphrinA
A9.29
lineage
EphrinA
A9.29
lineage
B
wildtype
FGF8/17/18>dnFGFR
U0126 at 8hpf
FGF8/17/18>Su(H)-DBM
En>dnFGFR
FGF8/17/18>Su(H)-DBM
En>dnFGFR
FGF8/17/18>Eph3ΔC
FGF8/17/18>Su(H)-DBM

(Previous page) Fig. 15. **Summary diagrams.**

(**A**) Summary of cell signaling events and transcriptional regulation setting up the specification and differentiation of A12.239. Anterior is at the top, posterior is at the bottom. (**B**) Summary of different MG configurations resulting from the various perturbation conditions described in the paper. The dramatic phenotype of an entirely *Dmbx*+ A9.30 lineage in embryos co-electroporated with *FGF8/17/18>Eph3ΔC* and *FGF8/17/18>Su(H)-DBM* can be explained by 1) First converting all cells of the lineage at the four-cell stage to *En*+ precursors by inhibition of Ephrin-mediated FGF/MAPK suppression, 2) then making all four *En*+ precursors express *Pax3/7* by inhibiting Notch, 3) then converting all daughter cells of the four *En*+ precursors into *Dmbx*+ neurons due to a breakdown in FGF and/or Notch pathways resulting from the constructs electroporated (direct) and/or loss of positional cues dependent on earlier patterning (indirect).

Chapter 7:

Early chordate origins of the vertebrate Second Heart Field: an epilogue

Rationale

During the course of my thesis work, the *Islet* reporter described in Chapter 3 unexpectedly showed expression in atrial siphon muscle (ASM) precursors, a serendipitous finding that allowed for an entire side project relating to the origin of the vertebrate Second Heart Field (SHF), which I will briefly recount in this chapter.

The vertebrate heart initially forms as a linear tube from a population of precursor cells within the first heart field (FHF). Cells from the adjacent second heart field (SHF) are then progressively added to the developing heart (Abu-Issa and Kirby, 2007; Buckingham et al., 2005). Both heart fields arise from common mesodermal progenitors, although the detailed lineage relationships between FHF and SHF remain uncertain (Buckingham et al., 2005; Meilhac et al., 2004). In avian and mammalian hearts, the FHF contributes mainly to the left ventricle, while the SHF gives rise to the outflow tract and large portions of the right ventricle and atria. SHF-like territories have been identified in frogs (Brade et al., 2007; Gessert and Kuhl, 2009), zebrafish (de Pater et al., 2009) and lamprey (Kokubo et al., 2010), yet evidence for a deeper evolutionary origin remains obscured by the absence of a clear SHF in invertebrates (Perez-Pomares et al., 2009).

Studies on *Ciona intestinalis* have revealed conserved regulatory mechanisms underlying chordate heart development (Davidson, 2007). The *Ciona* heart arises from the B7.5 pair of cells in gastrulating embryos (Satou et al., 2004). Localized expression of *MesP* in B7.5 cells determines their competence to form heart (Fig. 16A)(Christiaen et al., 2009a; Satou et al., 2004). Subsequently, FGF signaling induces expression of *FoxF* and heart determinants *NK4* (*tinman/Nkx2.5*), *GATAa* and *Hand-like/NoTrlc* in the anterior B7.5 grand-daughter cells (the trunk ventral cells, or TVCs) (Fig. 16B)(Beh et al., 2007; Davidson et al., 2006a). FoxF activates downstream target genes that control the migration of the TVCs to the ventral trunk region (Fig. 16C)(Beh et al., 2007; Christiaen et al., 2008).

After metamorphosis, some descendants of the B7.5 lineage give rise to the heart (Fig. 16D). B7.5 descendants also generate the atrial siphon muscles (ASMs) that surround the excurrent openings of the peribranchial atrium (Fig. 16D), as well as longitudinal muscles (LoMs) arising from the ASMs during metamorphosis. The contribution of the B7.5 lineage to ASMs is consistent with conventional lineage tracing performed in the distantly related ascidian *Halocynthia roretzi* (Hirano and Nishida, 1997). Both heart and ASMs express the structural muscle gene *Titin*, but the expression of two Myosin Heavy Chain (MHC) genes, *MHC2* and *MHC3* (Ogasawara et al., 2002) distinguish the heart and ASMs, respectively (see results). Thus, cardiomyocytes and ASMs constitute distinct muscle types arising from common progenitor cells. How do these distinct tissues residing in different parts of the juvenile arise from a common progenitor? Here my co-authors and I attempted to show just how.

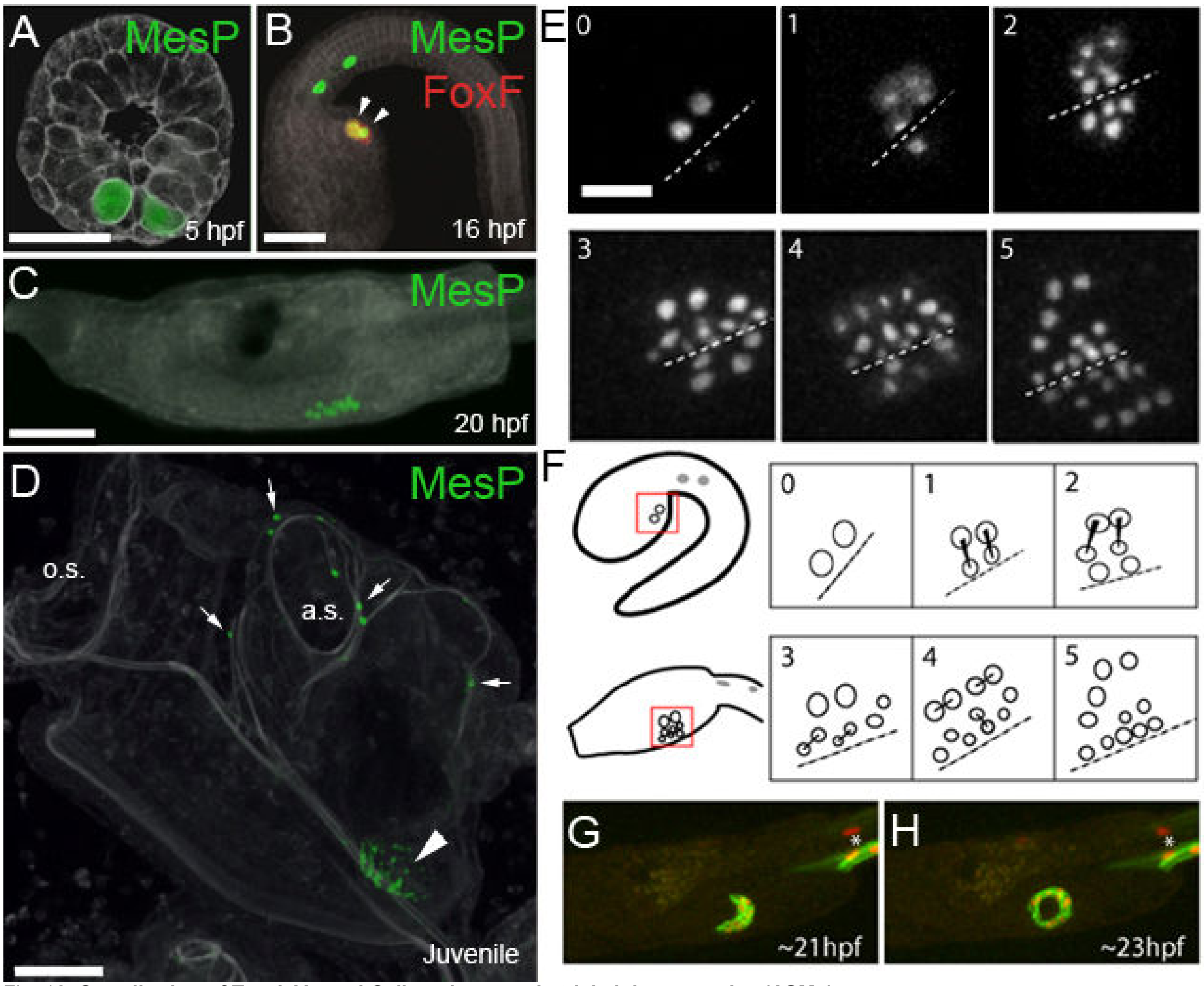

Fig. 16. **Contribution of Trunk Ventral Cells to heart and atrial siphon muscles (ASMs).**
(**A**) Immunodetection of β-gal expression (green) in B7.5 cells in a gastrulating embryo transfected with *MesP>lacZ* transgene. (**B**) Visualization of *MesP>lacZ* (green) and *FoxF[TVC enhancer]>mCherry* (red) expression in B7.5 descendants in a tailbud stage embryo. (**C**) Expression of a *MesP>Histone2B(H2B)::GFP* fusion protein (green) in a tadpole.) (**D**) Visualization of *MesP>H2B::CFP* (green), in a stage 38 juvenile (~100 hours post fertilization, hpf). Expression is visible in the heart (arrowhead), ASMs and longitudinal muscles (LoMs)(arrows). *MesP* is only activated in the B7.5 pair of cells at the gastrula stage. a.s= atrial siphon, o.s.= oral siphon (**E**) Frames from timelapse movies. Dashed line indicates ventral midline. Right-side cells partially visible in 1 and 2. Stereotyped cell divisions (see text) result in four lateral TVCs on either side of the embryo flanking ~16 medial TVCs. The four lateral TVCs on either side detach and migrate to form ASMs. Medial cells form the heart. Cells were visualized as two independent time-lapse sequences (0-2 and 3-5) of embryos transfected with *MesP>H2B::GFP/CFP*. (**F**) Cartoon representing the events in E. (**G,H**) Left side ASM precursors expressing *MesP>H2B::mCherry* (red) and *MesP>PH::GFP* (green). ASM precursors encircle the siphon primordium, between 21 hpf (G) to 23 hpf (H). Scale bars in A-D= 50 µm. Scale bar in E= 20µm.

Results

A common progenitor for heart and pharyngeal muscles in *Ciona*

Live imaging of the B7.5 lineage allowed the characterization of events leading to the separation between heart and ASM (Fig. 16E). Following their migration to the ventral trunk region, each TVC undergoes two successive asymmetric divisions along the medio-lateral axis to produce 6 cells on either side of the ventral midline (Fig. 15E,F timepoints 0-2). The larger daughter cells (lateral TVCs) are positioned lateral to the smaller medial TVCs. Subsequent symmetric cell divisions result in an array of ~24 cells: 8 lateral TVCs (four on either side) bracketing 16 medial TVCs (Fig. 16E,F)(Davidson et al., 2005).

A second migration occurs several hours after hatching. This time, each group of four lateral TVCs detach from the medial TVCs and migrate dorsally as a polarized cluster of cells on either side of the trunk (Fig 16G). They eventually form a ring of cells underneath the ectodermal placodes that produce the atrial siphon openings of the juvenile. Targeted inhibition of TVC specification blocked the formation of ASMs (data not shown). These observations clearly document that the lateral TVCs correspond to the precursors of the ASMs.

Molecular and developmental parallels to jaw muscle precursors/Second Heart Field of vertebrates

The ASMs are thus evocative of vertebrate jaw muscles arising from lateral/splanchnic mesoderm (SpM): *Ciona* TVCs and vertebrate anterior SpM both express orthologs of *Nkx2.5* and *FoxF* and derive from progenitors that expressed *MesP* during gastrulation (Gessert and Kuhl, 2009; Kang et al., 2009; Prall et al., 2007). In chick and mouse embryos, much of the anterior SpM gives rise to the SHF, but some precursors migrate into the first branchial arch and form intermandibular muscles (Nathan et al., 2008). A key marker of the anterior SpM and SHF is the LIM-homeodomain transcription factor, *Islet1* (*Isl1*) (Brade et al., 2007; de Pater et al., 2009; Gessert and Kuhl, 2009; Nathan et al., 2008). The single *Ciona Islet* (Giuliano et al., 1998b) gene is expressed in several tissues including the ASM precursors, which maintain *Islet* expression during their migration away from the medial TVCs (Appendix IX). The latter possibly show weak and transient *Islet* expression (data not shown), which is reminiscent to that reported in the FHF of vertebrates (Prall et al., 2007).

Islet expression was further characterized using defined enhancers (Appendix IX). Reporter transgenes containing ~3.2 kb of the *Islet* 5' flanking region exhibit localized expression in the lateral TVCs and ASMs (not heart) in juveniles (Fig. 17). In contrast, *MesP* reporter transgenes label the entire B7.5 lineage, including both ASMs and heart (e.g., Fig. 16C,D). The heart primordium is situated ventrally and medially to the *Islet*$^+$ ASM progenitors (Fig. 17A). This is reminiscent of the positioning of the FHF relative to *Isl1*$^+$ SHF/pharyngeal mesoderm in basal vertebrates (Brade et al., 2007; Gessert and Kuhl, 2009). Furthermore, LoM precursors segregating from the ASMs express the *Ciona* ortholog of *Tbx1* (Takatori et al., 2004), an important regulator of cardiac and pharyngeal mesoderm development in vertebrates (Zhang et al., 2006) (Fig. 17D-F). Taken together, these results suggest homology between the ASM/LoM precursors of tunicates and the progenitors of lower jaw muscles and SHF of vertebrates.

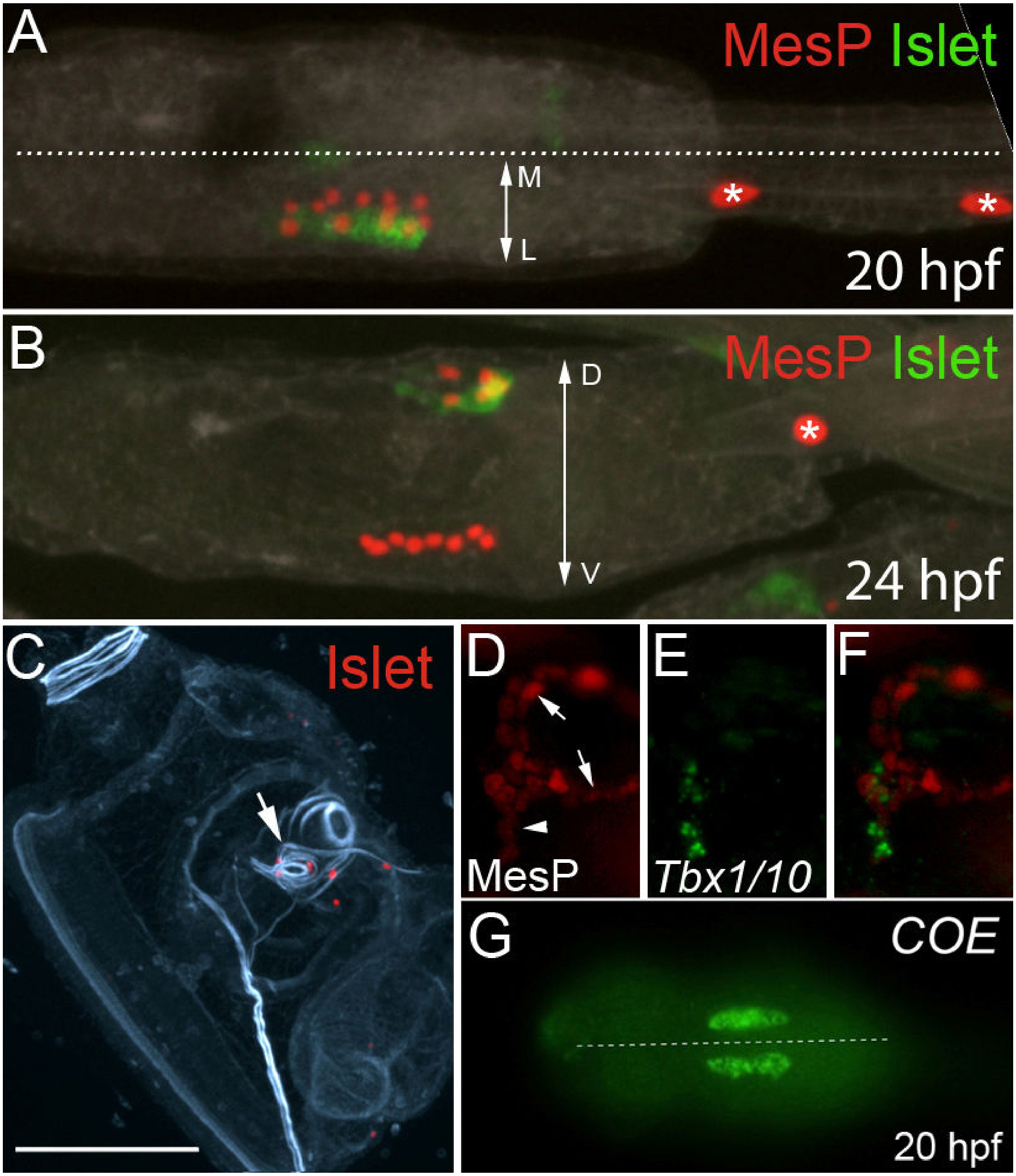

Fig. 17. **ASM-specific gene expression.**
(**A**) Dorsal view of electroporated larva exhibiting mosaic incorporation (left side) of *Islet>GFP* (green) and *MesP>H2B::mCherry* (red) transgenes at 20 hpf, before the migration of the lateral TVCs. *Islet>GFP* expression is restricted to lateral TVCs. Dotted line= midline. (**B**) Lateral view of larva expressing same transgenes as in A, at 24h, after migration of *Islet>GFP*-positive lateral TVC descendants around atrial siphon primordium. (**C**) Juvenile (~100 hpf) raised from embryo transfected with *Islet>H2B::mCherry* (red), with transgene expression visible around atrial siphons (arrow) and longitudinal muscles (arrowheads), but not heart (Ht). F-actin stained by phallacidin (blue-green). Scale bar= 100μm (**D**) Magnified view (see Fig. S7) of LoMs (arrowhead) segregating from ASMs (arrows) during metamorphosis, visualized by *MesP>lacZ* expression (red). Panel width ~100 μm (**E**) *In situ* hybridization of *Tbx1/10* (green). (**F**) Merged view of D and E, showing activation of *Tbx1/10* in LoMs. (**G**) *COE* expression in lateral TVCs at 20 hpf revealed by *in situ* hybridization. Dotted line= midline.

COE regulates the choice between heart and ASM

Preliminary functional assays suggest that Islet is not instructive for the specification of ASMs (data not shown). In the course of these studies we found that the transcription factor *Collier/Olf1/EBF* (*COE)* is expressed early in the ASM precursors (Fig. 17G). To determine whether this localized expression is instructive for ASM specification, COE was misexpressed in all TVCs using the *FoxF* minimal TVC enhancer (Beh et al., 2007). Strikingly, in 96% of transfected embryos, all TVC descendants migrated towards the atrial siphon placodes and expressed *Islet>GFP* (Fig. 18B). 56% of transfected embryos grew into juveniles that lacked a heart but still had ASMs (Fig. 18B,E,I,J, F), suggesting that COE is sufficient to specify a lateral TVC identity and subsequent ASM fate.

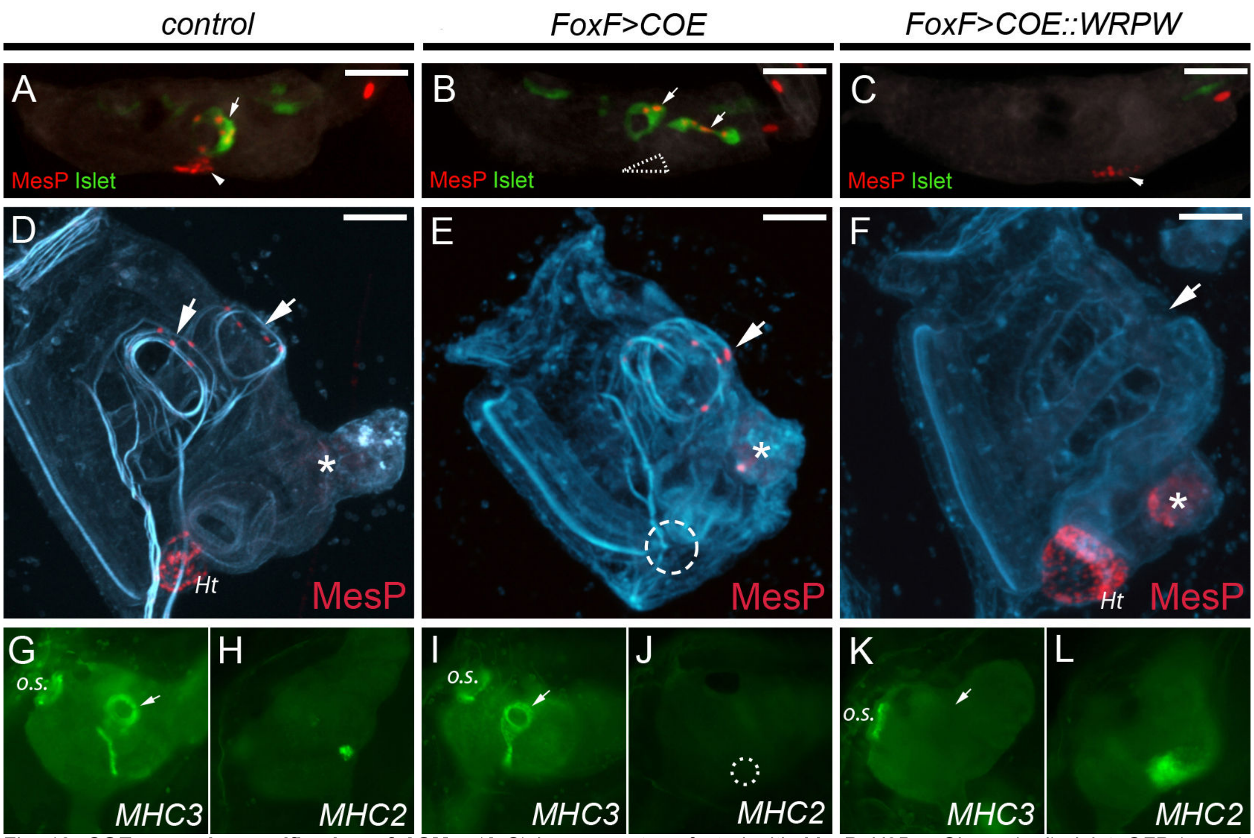

Fig. 18. **COE controls specification of ASMs**. (**A-C**) Larvae co-transfected with *MesP>H2B::mCherry* (red), *Islet>GFP* (green), and: **A**) *FoxF*>lacZ, (**B**) *FoxF>COE*, or **C**) *FoxF>COE::WRPW*. (**B**) All TVCs are transformed into ASM precursors (arrows). No heart primordium is formed (dashed triangle). (**C**) All TVC descendants form heart (arrowhead) with no *Islet>GFP* expression. (**D**) Juveniles raised from embryos transfected with *MesP>H2B::mCherry* (red), counterstained with phallacidin (blue-green). H2B::mCherry+ B7.5 descendants populate the heart (Ht) and ASMs (arrows) (residual larval muscle staining indicated by asterisks). (**E**) co-transfection with the *FoxF>COE* transgene, resulting in no heart (usual location indicated by dashed circle) but normal ASMs (arrow). (**F**) coexpression of the *FoxF>COE:WRPW* transgene. TVCs form an expanded heart and there are no ASMs (arrow). (**G,H**) *In situ* hybridization on wildtype juveniles showing *MHC3* and *MHC2* expression in ASMs (arrow) and heart, respectively. (**I,J**) *FoxF>COE* results in loss of *MHC2* expression (dashed circle), but not *MHC3* expression (arrow). (**K,L**) *FoxF>COE::WRPW* abolishes *MHC3* expression (arrow) and leads to expanded *MHC2* expression. Scale bars= 50μm. o.s.= oral siphons

Similar targeted misexpression assays with a repressor form of COE (COE::WRPW) resulted in the reciprocal phenotype: all TVC descendants remained in the ventral trunk and *Islet>GFP* expression was abolished (Fig. 18C). Upon metamorphosis, TVC descendants differentiated into enlarged hearts (Fig. 18F,L). Inhibition of COE function thus transforms the entire TVC lineage to heart, indicating that COE activity is required for ASM specification.

Conservation of a COE ortholog in the pharyngeal mesoderm of vertebrates

The COE homolog Collier/Knot is involved in muscle type specification in *Drosophila* (Crozatier and Vincent, 1999), but a role for COE in vertebrate SHF or jaw muscle development has not been reported. As a first step towards determining whether COE factors might play a conserved role in vertebrates, our collaborator John J. Young in the Harland Lab performed *in situ* hybridization of *COE* orthologs *Xebf2* and *Xebf3* in *Xenopus tropicalis* embryos (Fig. 19A-C). *Xebf2* expression was seen in *Nkx2.5*$^{+}$ / *Isl1*$^{+}$ anterior lateral mesoderm, where *Tbx1* is also expressed (Gessert and Kuhl, 2009).

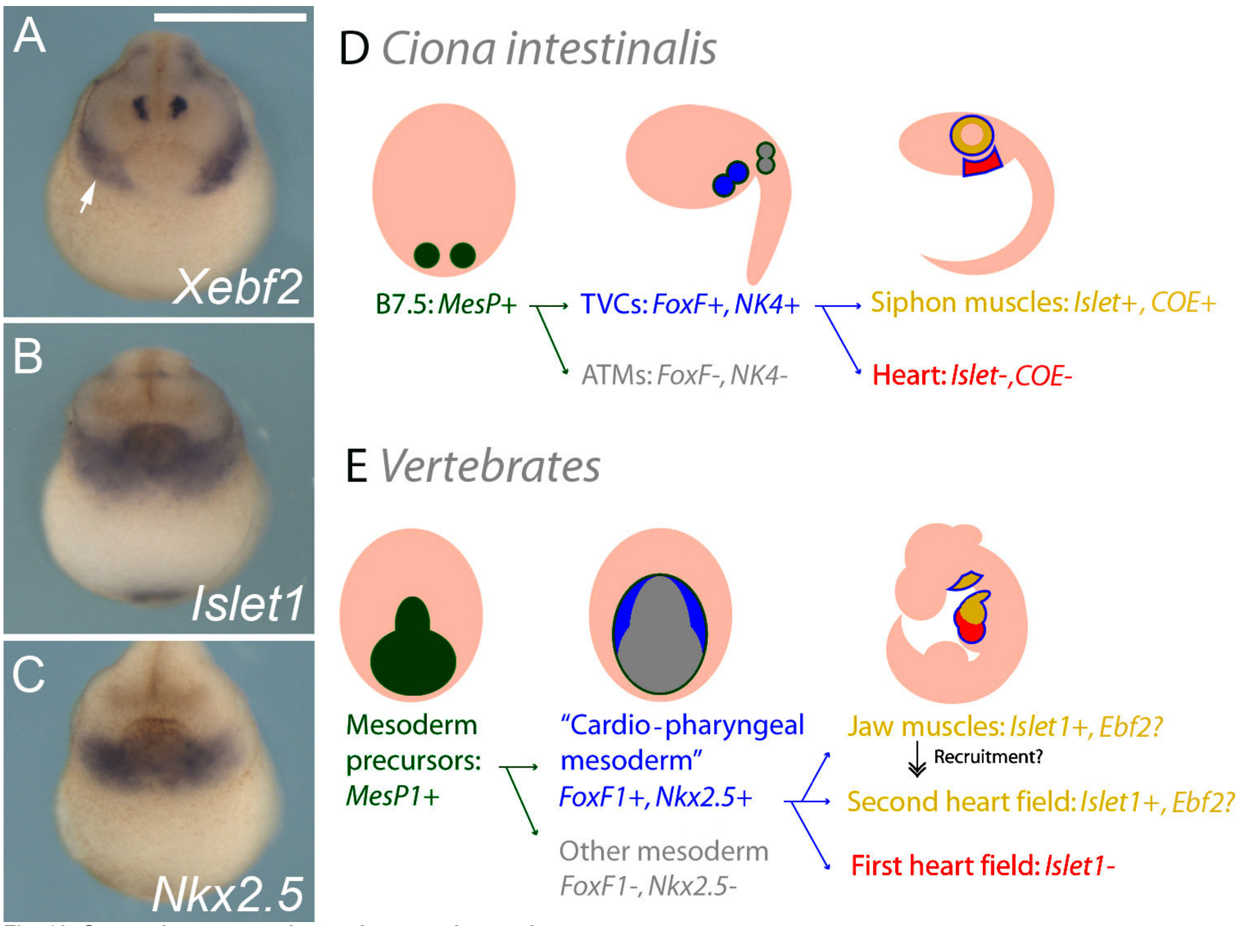

Fig. 19. **Comparison to vertebrate pharyngeal mesoderm**.
(**A-C**) Expression of the *COE* ortholog *Xebf2* and anterior lateral mesoderm/SHF markers *Nkx2.5* and *Islet1* in *Xenopus tropicalis* embryos at NFstage20. (**A**) Expression of *Xebf2* (white arrow) partially overlaps that of (**B**) *Nkx2.5* and (**C**) *Islet1* in pharyngeal mesoderm lateral to the heart primordium. Scale bar = 500 µm (**D,E**) The cardio-pharyngeal lineages of Ciona (**D**) and vertebrates (**E**). (**D**) Summary of differential expression of selected regulatory genes in the B7.5 lineage. (**E**) Expression of orthologous genes in mouse development. Evolutionary re-allocation of *Islet1*$^{+}$ cardio-pharyngeal precursors towards the heart might have given rise to the SHF.

Discussion

The preceding results suggest that the last common ancestor of tunicates and vertebrates had a population of cardio-pharyngeal mesoderm, which 1) arose from *MesP*-expressing early mesoderm, 2) expressed orthologs of *FoxF* and *Nkx2.5* and 3) had the potential to give rise to both heart tissue and pharyngeal muscles, which 4) correlated with differential maintenance of *Islet* expression. Moreover, *COE* might play a conserved role in chordate pharyngeal mesoderm development.

I propose that the re-allocation of *Islet*$^{+}$ cells among the heart and cranial myogenic fields supported the emergence of the SHF (summarized in Fig. 19D,E). In *Ciona, Islet*+ cells do not contribute to the definitive beating heart but targeted expression of COE::WRPW was sufficient to convert them into cardiomyocytes. It is conceivable that the re-allocation of *Islet*$^{+}$ pharyngeal muscle progenitors towards SHF depended on the intercalation of cardiac regulatory network components (e.g. *GATA4, Mef2c*) downstream of *Islet (Olson, 2006).*

An ancient connection between heart and craniofacial muscles has been proposed based on the role of an *Nkx2.5* ortholog in the pharynx of the nematode *C. elegans*, which lacks a heart (Okkema et al., 1997). *Haikouella lanceolata*, a fossil chordate from the Lower Cambrian, shows a putative heart adjacent to a muscularized pharyngeal atrium (Chen et al., 1999). The shared lineage of cardiomyocytes and pharyngeal muscles in tunicates hints that a pool of common precursors could have formed both heart and pharyngeal atrium muscles in a *Haikouella*-like ancestor. Northcutt and Gans (Gans and Northcutt, 1983) proposed that muscular ventilation of the pharyngeal arches was a key transition in the evolution of the vertebrates. Therefore, the cardio-pharyngeal mesoderm could have been instrumental in the co-evolution of circulatory, respiratory, and feeding functions in tunicates and vertebrates.

References

Abu-Issa, R. and Kirby, M. L. (2007). Heart field: from mesoderm to heart tube. *Annu Rev Cell Dev Biol* **23**, 45-68.

Beatus, P. and Lendahl, U. (1998). Notch and neurogenesis. *Journal of neuroscience research* **54**, 125-136.

Beh, J., Shi, W., Levine, M., Davidson, B. and Christiaen, L. (2007). FoxF is essential for FGF-induced migration of heart progenitor cells in the ascidian Ciona intestinalis. *Development* **134**, 3297.

Bertrand, V., Hudson, C., Caillol, D., Popovici, C. and Lemaire, P. (2003). Neural tissue in ascidian embryos is induced by FGF9/16/20, acting via a combination of maternal GATA and Ets transcription factors. *Cell* **115**, 615-627.

Brade, T., Gessert, S., Kuhl, M. and Pandur, P. (2007). The amphibian second heart field: Xenopus islet-1 is required for cardiovascular development. *Dev Biol* **311**, 297-310.

Briscoe, J. and Novitch, B. G. (2008). Regulatory pathways linking progenitor patterning, cell fates and neurogenesis in the ventral neural tube. *Philosophical Transactions of the Royal Society B: Biological Sciences* **363**, 57.

Briscoe, J., Pierani, A., Jessell, T. M. and Ericson, J. (2000). A homeodomain protein code specifies progenitor cell identity and neuronal fate in the ventral neural tube. *Cell* **101**, 435-445.

Briscoe, J., Sussel, L., Serup, P., Hartigan-O'Connor, D., Jessell, T., Rubenstein, J. and Ericson, J. (1999). Homeobox gene Nkx2. 2 and specification of neuronal identity by graded Sonic hedgehog signalling. *Nature* **398**, 622-626.

Brown, E. R., Nishino, A., Bone, Q., Meinertzhagen, I. A. and Okamura, Y. (2005). GABAergic synaptic transmission modulates swimming in the ascidian larva. *Eur J Neurosci* **22**, 2541-8.

Buckingham, M., Meilhac, S. and Zaffran, S. (2005). Building the mammalian heart from two sources of myocardial cells. *Nat Rev Genet* **6**, 826-35.

Bylund, M., Andersson, E., Novitch, B. G. and Muhr, J. (2003). Vertebrate neurogenesis is counteracted by Sox1–3 activity. *Nature neuroscience* **6**, 1162-1168.

Chabry, L. (1887). Embryologie normale et tératologique des Ascidies: F. Alcan.

Chen, J. Y., Huang, D. Y. and Li, C. W. (1999). An early Cambrian craniate-like chordate. *Nature* **402**, 518-522.

Christiaen, L., Bourrat, F. and Joly, J. (2005). A modular cis-regulatory system controls isoform-specific pitx expression in ascidian stomod um. *Developmental biology* **277**, 557-566.

Christiaen, L., Davidson, B., Kawashima, T., Powell, W., Nolla, H., Vranizan, K. and Levine, M. (2008). The transcription/migration interface in heart precursors of Ciona intestinalis. *Science* **320**, 1349-52.

Christiaen, L., Stolfi, A., Davidson, B. and Levine, M. (2009a). Spatio-temporal intersection of Lhx3 and Tbx6 defines the cardiac field through synergistic activation of Mesp. *Dev Biol* **328**, 552-60.

Christiaen, L., Wagner, E., Shi, W. and Levine, M. (2009b). The Sea Squirt Ciona intestinalis. *CSH protocols* **2009**.

Cole, A. G. and Meinertzhagen, I. A. (2004). The central nervous system of the ascidian larva: mitotic history of cells forming the neural tube in late embryonic Ciona intestinalis. *Dev Biol* **271**, 239-62.

Conklin, E. G. (1905). Mosaic development in ascidian eggs. *Journal of Experimental Zoology* **2**, 145-223.
Crozatier, M. and Vincent, A. (1999). Requirement for the Drosophila COE transcription factor Collier in formation of an embryonic muscle: transcriptional response to notch signalling. *Development* **126**, 1495-504.
Davidson, B. (2007). Ciona intestinalis as a model for cardiac development. *Semin Cell Dev Biol* **18**, 16-26.
Davidson, B., Shi, W., Beh, J., Christiaen, L. and Levine, M. (2006a). FGF signaling delineates the cardiac progenitor field in the simple chordate, Ciona intestinalis. *Genes Dev* **20**, 2728-38.
Davidson, B., Shi, W., Beh, J., Christiaen, L. and Levine, M. (2006b). FGF signaling delineates the cardiac progenitor field in the simple chordate, Ciona intestinalis. *Genes & development* **20**, 2728.
Davidson, B., Shi, W. and Levine, M. (2005). Uncoupling heart cell specification and migration in the simple chordate Ciona intestinalis. *Development* **132**, 4811-8.
de Pater, E., Clijsters, L., Marques, S. R., Lin, Y. F., Garavito-Aguilar, Z. V., Yelon, D. and Bakkers, J. (2009). Distinct phases of cardiomyocyte differentiation regulate growth of the zebrafish heart. *Development* **136**, 1633-41.
Dehal, P., Satou, Y., Campbell, R. K., Chapman, J., Degnan, B., De Tomaso, A., Davidson, B., Di Gregorio, A., Gelpke, M., Goodstein, D. M. et al. (2002). The draft genome of Ciona intestinalis: insights into chordate and vertebrate origins. *Science* **298**, 2157-67.
del Corral, R. D., Breitkreuz, D. N. and Storey, K. G. (2002). Onset of neuronal differentiation is regulated by paraxial mesoderm and requires attenuation of FGF signalling. *Development* **129**, 1681.
del Corral, R. D., Olivera-Martinez, I., Goriely, A., Gale, E., Maden, M. and Storey, K. (2003). Opposing FGF and retinoid pathways control ventral neural pattern, neuronal differentiation, and segmentation during body axis extension. *Neuron* **40**, 65-79.
Delsuc, F., Brinkmann, H., Chourrout, D. and Philippe, H. (2006). Tunicates and not cephalochordates are the closest living relatives of vertebrates. *Nature* **439**, 965-968.
Dilly, N. (1964). Studies on Receptors in Cerebral Vesicle of Ascidian Tadpole .2. Ocellus. *Quarterly Journal of Microscopical Science* **105**, 13-&.
Dilly, P. N. (1962). Studies on Receptors in Cerebral Vesicle of Ascidian Tadpole .1. Otolith. *Quarterly Journal of Microscopical Science* **103**, 393-&.
Dubois, L. and Vincent, A. (2001). The COE-Collier/Olf1/EBF-transcription factors: structural conservation and diversity of developmental functions. *Mechanisms of development* **108**, 3-12.
Dufour, H. D., Chettouh, Z., Deyts, C., de Rosa, R., Goridis, C., Joly, J. S. and Brunet, J. F. (2006). Precraniate origin of cranial motoneurons. *Proc Natl Acad Sci U S A* **103**, 8727-32.
Dynes, J. and Ngai, J. (1998). Pathfinding of olfactory neuron axons to stereotyped glomerular targets revealed by dynamic imaging in living zebrafish embryos. *Neuron* **20**, 1081-1091.
Eaton, R., Lee, R. and Foreman, M. (2001). The Mauthner cell and other identified neurons of the brainstem escape network of fish. *Progress in Neurobiology* **63**, 467-485.
Enjin, A., Rabe, N., Nakanishi, S., Vallstedt, A., Gezelius, H., Memic, F., Lind, M., Hjalt, T., Tourtellotte, W. and Bruder, C. (2010). Identification of novel spinal cholinergic genetic subtypes disclose Chodl and Pitx2 as markers for fast motor neurons and partition cells. *The Journal of comparative neurology* **518**, 2284-2304.

Ericson, J., Morton, S., Kawakami, A., Roelink, H. and Jessell, T. M. (1996). Two critical periods of Sonic Hedgehog signaling required for the specification of motor neuron identity. *Cell* **87**, 661-673.
Gans, C. and Northcutt, R. G. (1983). Neural Crest and the Origin of Vertebrates: A New Head. *Science* **220**, 268-273.
Gessert, S. and Kuhl, M. (2009). Comparative gene expression analysis and fate mapping studies suggest an early segregation of cardiogenic lineages in Xenopus laevis. *Dev Biol*.
Giuliano, P., Marino, R., Pinto, M. and De Santis, R. (1998a). Identification and developmental expression of Ci-isl, a homologue of vertebrate islet genes, in the ascidian Ciona intestinalis. *Mechanisms of development* **78**, 199-202.
Giuliano, P., Marino, R., Pinto, M. R. and De Santis, R. (1998b). Identification and developmental expression of Ci-isl, a homologue of vertebrate islet genes, in the ascidian Ciona intestinalis. *Mech Dev* **78**, 199-202.
Goulding, M. (2009). Circuits controlling vertebrate locomotion: moving in a new direction. *Nature Reviews Neuroscience* **10**, 507-518.
Gowan, K., Helms, A. W., Hunsaker, T. L., Collisson, T., Ebert, P. J., Odom, R. and Johnson, J. E. (2001). Crossinhibitory activities of Ngn1 and Math1 allow specification of distinct dorsal interneurons. *Neuron* **31**, 219-232.
Graham, V., Khudyakov, J., Ellis, P. and Pevny, L. (2003). SOX2 functions to maintain neural progenitor identity. *Neuron* **39**, 749-765.
Harland, R. (1991). In situ hybridization: an improved whole-mount method for Xenopus embryos. *Methods in cell biology* **36**, 685.
Hirano, T. and Nishida, H. (1997). Developmental fates of larval tissues after metamorphosis in ascidian Halocynthia roretzi. I. Origin of mesodermal tissues of the juvenile. *Dev Biol* **192**, 199-210.
Hobert, O., Carrera, I. and Stefanakis, N. (2010). The molecular and gene regulatory signature of a neuron. *Trends in neurosciences*.
Holmberg, J., Hansson, E., Malewicz, M., Sandberg, M., Perlmann, T., Lendahl, U. and Muhr, J. (2008). SoxB1 transcription factors and Notch signaling use distinct mechanisms to regulate proneural gene function and neural progenitor differentiation. *Development* **135**, 1843.
Horie, T., Kusakabe, T. and Tsuda, M. (2008a). Glutamatergic networks in the Ciona intestinalis larva. *The Journal of comparative neurology* **508**, 249-263.
Horie, T., Nakagawa, M., Sasakura, Y., Kusakabe, T. G. and Tsuda, M. (2010). Simple motor system of the ascidian larva: neuronal complex comprising putative cholinergic and GABAergic/glycinergic neurons. *Zoolog Sci* **27**, 181-90.
Horie, T., Sakurai, D., Ohtsuki, H., Terakita, A., Shichida, Y., Usukura, J., Kusakabe, T. and Tsuda, M. (2008b). Pigmented and nonpigmented ocelli in the brain vesicle of the ascidian larva. *The Journal of comparative neurology* **509**, 88-102.
Hudson, C., Ba, M., Rouvière, C. and Yasuo, H. (2011). Divergent mechanisms specify chordate motoneurons: evidence from ascidians. *Development* **138**, 1643.
Hudson, C., Lotito, S. and Yasuo, H. (2007). Sequential and combinatorial inputs from Nodal, Delta2/Notch and FGF/MEK/ERK signalling pathways establish a grid-like organisation of distinct cell identities in the ascidian neural plate. *Development* **134**, 3527.
Hudson, C. and Yasuo, H. (2006). A signalling relay involving Nodal and Delta ligands acts during secondary notochord induction in Ciona embryos. *Development* **133**, 2855.

Ikuta, T. and Saiga, H. (2007). Dynamic change in the expression of developmental genes in the ascidian central nervous system: revisit to the tripartite model and the origin of the midbrain-hindbrain boundary region. *Developmental biology* **312**, 631-643.
Imai, J. and Meinertzhagen, I. (2007). Neurons of the ascidian larval nervous system in Ciona intestinalis: I. Central nervous system. *The Journal of comparative neurology* **501**, 316-334.
Imai, K., Levine, M., Satoh, N. and Satou, Y. (2006). Regulatory blueprint for a chordate embryo. *Science* **312**, 1183.
Imai, K., Stolfi, A., Levine, M. and Satou, Y. (2009). Gene regulatory networks underlying the compartmentalization of the Ciona central nervous system. *Development* **136**, 285.
Jiang, D., Tresser, J., Horie, T., Tsuda, M. and Smith, W. (2005). Pigmentation in the sensory organs of the ascidian larva is essential for normal behavior. *The Journal of experimental biology* **208**, 433.
Kageyama, R. and Ohtsuka, T. (1999). The Notch-Hes pathway in mammalian neural development. *Cell research* **9**, 179-188.
Kajiwara, S. and Yoshida, M. (1985). Changes in behavior and ocellar structure during the larval life of solitary ascidians. *The Biological Bulletin* **169**, 565.
Kang, J., Nathan, E., Xu, S. M., Tzahor, E. and Black, B. L. (2009). Isl1 is a direct transcriptional target of Forkhead transcription factors in second heart field-derived mesoderm. *Dev Biol*.
Katsuyama, Y., Okada, T., Matsumoto, J., Ohtsuka, Y., Terashima, T. and Okamura, Y. (2005). Early specification of ascidian larval motor neurons. *Developmental biology* **278**, 310-322.
Kimura, Y., Okamura, Y. and Higashijima, S. (2006). alx, a zebrafish homolog of Chx10, marks ipsilateral descending excitatory interneurons that participate in the regulation of spinal locomotor circuits. *Journal of Neuroscience* **26**, 5684.
Kokubo, N., Matsuura, M., Onimaru, K., Tiecke, E., Kuraku, S., Kuratani, S. and Tanaka, M. (2010). Mechanisms of heart development in the Japanese lamprey, Lethenteron japonicum. *Evol Dev* **12**, 34-44.
Lagha, M., Kormish, J. D., Rocancourt, D., Manceau, M., Epstein, J. A., Zaret, K. S., Relaix, F. and Buckingham, M. E. (2008). Pax3 regulation of FGF signaling affects the progression of embryonic progenitor cells into the myogenic program. *Genes & development* **22**, 1828.
Lee, K. J., Dietrich, P. and Jessell, T. M. (2000). Genetic ablation reveals that the roof plate is essential for dorsal interneuron specification. *Nature* **403**, 734-740.
Lee, S., Lee, B., Joshi, K., Pfaff, S., Lee, J. and Lee, S. (2008). A regulatory network to segregate the identity of neuronal subtypes. *Developmental cell* **14**, 877-889.
Livet, J., Weissman, T., Kang, H., Lu, J., Bennis, R., Sanes, J. and Lichtman, J. (2007). Transgenic strategies for combinatorial expression of fluorescent proteins in the nervous system. *Nature* **450**, 56-62.
Mackie, G. and Bone, Q. (1976). Skin impulses and locomotion in an ascidian tadpole. *Journal of the Marine Biological Association of the UK* **56**, 751-768.
Mansouri, A. and Gruss, P. (1998). Pax3 and Pax7 are expressed in commissural neurons and restrict ventral neuronal identity in the spinal cord. *Mechanisms of development* **78**, 171-178.
Marder, E. and Bucher, D. (2001). Central pattern generators and the control of rhythmic movements. *Current Biology* **11**, R986-R996.

Mathis, L., Kulesa, P. M. and Fraser, S. E. (2001). FGF receptor signalling is required to maintain neural progenitors during Hensen's node progression. *Nature cell biology* **3**, 559-566.
Meilhac, S. M., Esner, M., Kelly, R. G., Nicolas, J. F. and Buckingham, M. E. (2004). The clonal origin of myocardial cells in different regions of the embryonic mouse heart. *Dev Cell* **6**, 685-98.
Meinertzhagen, I., Lemaire, P. and Okamura, Y. (2004). The neurobiology of the ascidian tadpole larva: recent developments in an ancient chordate. *Neuroscience* **27**, 453.
Meinertzhagen, I. A. and Okamura, Y. (2001). The larval ascidian nervous system: the chordate brain from its small beginnings. *Trends in neurosciences* **24**, 401-410.
Miao, H., Wei, B. R., Peehl, D. M., Li, Q., Alexandrou, T., Schelling, J. R., Rhim, J. S., Sedor, J. R., Burnett, E. and Wang, B. (2001). Activation of EphA receptor tyrosine kinase inhibits the Ras/MAPK pathway. *Nature cell biology* **3**, 527-530.
Nagatomo, K. and Fujiwara, S. (2003). Expression of Raldh2, Cyp26 and Hox-1 in normal and retinoic acid-treated Ciona intestinalis embryos. *Gene Expression Patterns* **3**, 273-277.
Nathan, E., Monovich, A., Tirosh-Finkel, L., Harrelson, Z., Rousso, T., Rinon, A., Harel, I., Evans, S. M. and Tzahor, E. (2008). The contribution of Islet1-expressing splanchnic mesoderm cells to distinct branchiomeric muscles reveals significant heterogeneity in head muscle development. *Development* **135**, 647-57.
Nicol, D. and Meinertzhagen, I. A. (1988). Development of the central nervous system of the larva of the ascidian, Ciona intestinalis L. I. The early lineages of the neural plate. *Dev Biol* **130**, 721-36.
Nicol, D. and Meinertzhagen, I. A. (1991). Cell counts and maps in the larval central nervous system of the ascidian Ciona intestinalis (L.). *J Comp Neurol* **309**, 415-29.
Nishino, A., Okamura, Y., Piscopo, S. and Brown, E. R. (2010). A glycine receptor is involved in the organization of swimming movements in an invertebrate chordate. *BMC neuroscience* **11**, 6.
Novitch, B. G., Chen, A. I. and Jessell, T. M. (2001). Coordinate regulation of motor neuron subtype identity and pan-neuronal properties by the bHLH repressor Olig2. *Neuron* **31**, 773-789.
Novitch, B. G., Wichterle, H., Jessell, T. M. and Sockanathan, S. (2003). A requirement for retinoic acid-mediated transcriptional activation in ventral neural patterning and motor neuron specification. *Neuron* **40**, 81-95.
Ogasawara, M., Sasaki, A., Metoki, H., Shin-i, T., Kohara, Y., Satoh, N. and Satou, Y. (2002). Gene expression profiles in young adult Ciona intestinalis. *Dev Genes Evol* **212**, 173-85.
Ohmori, H. and Sasaki, S. (1977). Development of neuromuscular transmission in a larval tunicate. *The Journal of Physiology* **269**, 221.
Ohtoshi, A. and Behringer, R. (2004). Neonatal lethality, dwarfism, and abnormal brain development in Dmbx1 mutant mice. *Molecular and cellular biology* **24**, 7548.
Okada, T., Katsuyama, Y., Ono, F. and Okamura, Y. (2002). The development of three identified motor neurons in the larva of an ascidian, Halocynthia roretzi. *Developmental biology* **244**, 278-292.
Okada, T., MacIsaac, S., Katsuyama, Y., Okamura, Y. and Meinertzhagen, I. (2001). Neuronal form in the central nervous system of the tadpole larva of the ascidian Ciona intestinalis. *The Biological Bulletin* **200**, 252.
Okkema, P. G., Ha, E., Haun, C., Chen, W. and Fire, A. (1997). The Caenorhabditis elegans NK-2 homeobox gene ceh-22 activates pharyngeal muscle gene expression in combination with pha-1 and is required for normal pharyngeal development. *Development* **124**, 3965-73.

Olson, E. N. (2006). Gene regulatory networks in the evolution and development of the heart. *Science* **313**, 1922.
Peng, C. Y., Yajima, H., Burns, C. E., Zon, L. I., Sisodia, S. S., Pfaff, S. L. and Sharma, K. (2007). Notch and MAML signaling drives Scl-dependent interneuron diversity in the spinal cord. *Neuron* **53**, 813-827.
Perez-Pomares, J. M., Gonzalez-Rosa, J. M. and Munoz-Chapuli, R. (2009). Building the vertebrate heart-an evolutionary approach to cardiac development. *Int J Dev Biol* **53**, 1427-43.
Picco, V., Hudson, C. and Yasuo, H. (2007). Ephrin-Eph signalling drives the asymmetric division of notochord/neural precursors in Ciona embryos. *Development* **134**, 1491.
Prall, O. W., Menon, M. K., Solloway, M. J., Watanabe, Y., Zaffran, S., Bajolle, F., Biben, C., McBride, J. J., Robertson, B. R., Chaulet, H. et al. (2007). An Nkx2-5/Bmp2/Smad1 negative feedback loop controls heart progenitor specification and proliferation. *Cell* **128**, 947-59.
Reeber, S. L., Sakai, N., Nakada, Y., Dumas, J., Dobrenis, K., Johnson, J. E. and Kaprielian, Z. (2008). Manipulating Robo expression in vivo perturbs commissural axon pathfinding in the chick spinal cord. *The Journal of Neuroscience* **28**, 8698.
Rothbächer, U., Bertrand, V., Lamy, C. and Lemaire, P. (2007). A combinatorial code of maternal GATA, Ets and -catenin-TCF transcription factors specifies and patterns the early ascidian ectoderm. *Development* **134**, 4023.
Sasakura, Y., Awazu, S., Chiba, S. and Satoh, N. (2003). Germ-line transgenesis of the Tc1/mariner superfamily transposon Minos in Ciona intestinalis. *Proceedings of the National Academy of Sciences of the United States of America* **100**, 7726.
Sato, S. and Yamamoto, H. (2001). Development of Pigment Cells in the Brain of Ascidian Tadpole Larvae:
Insights into the Origins of Vertebrate Pigment Cells. *Pigment Cell Research* **14**, 428-436.
Satoh, N. (2003). Ciona intestinalis: an emerging model for whole-genome analyses. *Trends in Genetics* **19**, 376-381.
Satou, Y., Imai, K. S. and Satoh, N. (2004). The ascidian Mesp gene specifies heart precursor cells. *Development* **131**, 2533-41.
Shi, W. and Levine, M. (2008). Ephrin signaling establishes asymmetric cell fates in an endomesoderm lineage of the Ciona embryo. *Development* **135**, 931.
Stolfi, A., Gainous, T., Young, J., Mori, A., Levine, M. and Christiaen, L. (2010). Early Chordate Origins of the Vertebrate Second Heart Field. *Science* **329**, 565.
Svendsen, P. and McGhee, J. (1995). The C. elegans neuronally expressed homeobox gene ceh-10 is closely related to genes expressed in the vertebrate eye. *Development* **121**, 1253.
Takahashi, T. and Holland, P. (2004). Amphioxus and ascidian Dmbx homeobox genes give clues to the vertebrate origins of midbrain development. *Development* **131**, 3285.
Takamura, K. (1998). Nervous network in larvae of the ascidian Ciona intestinalis. *Development genes and evolution* **208**, 1-8.
Takamura, K., Egawa, T., Ohnishi, S., Okada, T. and Fukuoka, T. (2002). Developmental expression of ascidian neurotransmitter synthesis genes. *Development genes and evolution* **212**, 50-53.
Takamura, K., Minamida, N. and Okabe, S. (2010). Neural map of the larval central nervous system in the Ascidian Ciona intestinalis. *Zoological Science* **27**, 191-203.

Takatori, N., Hotta, K., Mochizuki, Y., Satoh, G., Mitani, Y., Satoh, N., Satou, Y. and Takahashi, H. (2004). T box genes in the ascidian Ciona intestinalis: Characterization of cDNAs and spatial expression. *Developmental dynamics* **230**, 743-753.
Thaler, J., Lee, S., Jurata, L., Gill, G. and Pfaff, S. (2002). LIM factor Lhx3 contributes to the specification of motor neuron and interneuron identity through cell-type-specific protein-protein interactions. *Cell* **110**, 237-249.
Thor, S., Andersson, S., Tomlinson, A. and Thomas, J. (1999). A LIM-homeodomain combinatorial code for motor-neuron pathway selection. *Nature* **397**, 76-80.
Tsuda, M., Sakurai, D. and Goda, M. (2003). Direct evidence for the role of pigment cells in the brain of ascidian larvae by laser ablation. *The Journal of experimental biology* **206**, 1409.
Wada, H., Holland, P., Sato, S., Yamamoto, H. and Satoh, N. (1997). Neural Tube Is Partially Dorsalized by Overexpression ofHrPax-37: The Ascidian Homologue ofPax-3andPax-7. *Developmental biology* **187**, 240-252.
Wilson, D. and Wyman, R. (1965). Motor output patterns during random and rhythmic stimulation of locust thoracic ganglia. *Biophysical journal* **5**, 121-143.
Wong, L., Weadick, C., Kuo, C., Chang, B. and Tropepe, V. (2010). Duplicate dmbx 1 genes regulate progenitor cell cycle and differentiation during zebrafish midbrain and retinal development. *BMC Developmental Biology* **10**, 100.
Yoshida, R., Sakurai, D., Horie, T., Kawakami, I., Tsuda, M. and Kusakabe, T. (2004). Identification of neuron-specific promoters in Ciona intestinalis. *genesis* **39**, 130-140.
Zagoraiou, L., Akay, T., Martin, J. F., Brownstone, R. M., Jessell, T. M. and Miles, G. B. (2009). A cluster of cholinergic premotor interneurons modulates mouse locomotor activity. *Neuron* **64**, 645-662.
Zhang, Z., Huynh, T. and Baldini, A. (2006). Mesodermal expression of Tbx1 is necessary and sufficient for pharyngeal arch and cardiac outflow tract development. *Development* **133**, 3587.

Appendix

Appendix I: Islet+ A10.57 does not form frondose endplates

Labeling MG neurons with pan-neural reporters had revealed prominent, leaf-like (i.e. frondose) motor endplates (Imai and Meinertzhagen, 2007). It was assumed that all MG motoneurons contributed to the formation of these frondose endplates. However, double-labeling with a pan-neural reporter (*Onecut>GFP)* and *Islet>mCherry* showed that neuron A10.57 did not form the frondose endplate but rather forms smaller endplates, some of which might be contacting the frondose endplates (Fig. AI). Thus, even though A10.57 expresses classic motoneuron markers such as *Islet* and *Mnx,* more work is needed on its function in synaptic excitation of the muscles.

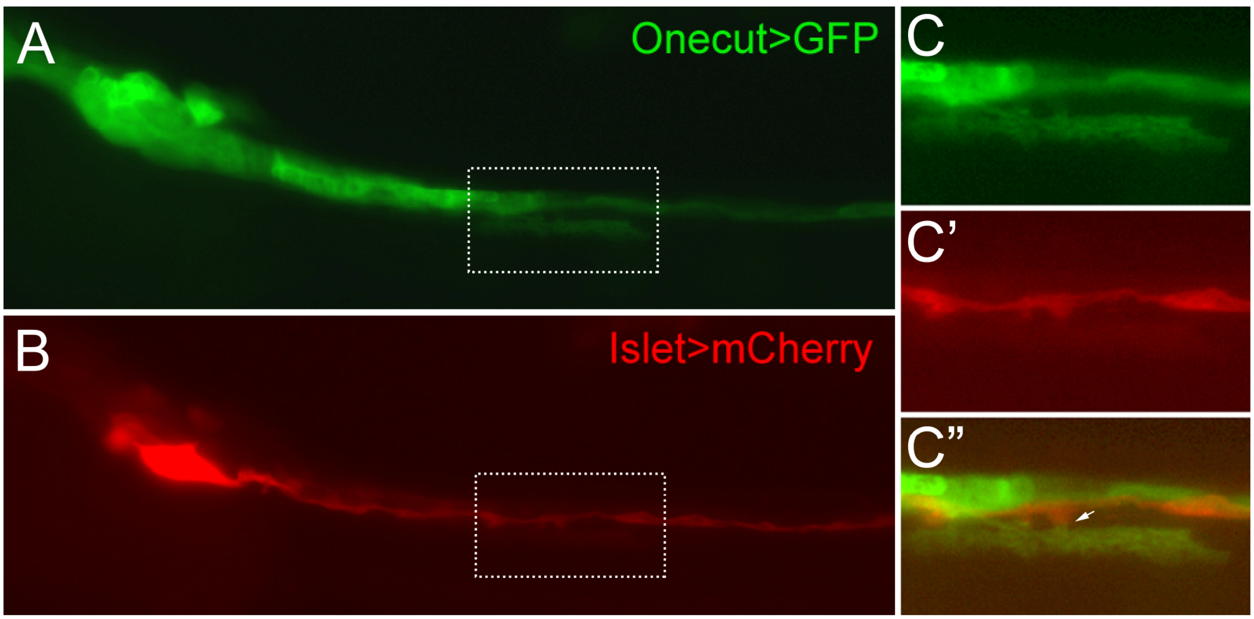

Fig. AI. **Frondose endplates stained with pan-neural reporter *Onecut>GFP*.**
(**A**) A -4.2 kb fragment immediately upstream of the transcription start site of the neuronal differentiation factor *Onecut* (also known as *HNF6*) drives reporter gene expression in differentiating neurons and nerve cord cells. This labels frondose endplates that contact the sides of the dorsal and anterior tail muscle cells. (**B**) Co-electroporation with Islet>mCherry reveals that these endplates do not belong to A10.57, which is strongly stained by this construct. (**C**) Magnification of dotted area in (**A**). **C'**) Magnification of dotted area in (**B**). (**C"**) Merged image of (**C**) and (**C'**), showing that A10.57 might even be contacting and synapsing onto the frondose endplates (arrow).

Appendix II: Nkx6 reporter preferentially labels frondose endplates

An *Nkx6>GFP* reporter preferentially labels frondose endplates in 50% of electroporated embryos (Fig. AII). In half these cases, staining is associated with a single cell body, presumably that of A11.118. This supports the conclusion that the frondose motor endplates of the *Ciona* tadpole belong to a single primary motoneuron, A11.118. The labeling of additional cells other than A11.118 by the *Nkx6>GFP* can be explained by the transient expression of *Nkx6* in the A9.30 blastomere and posterior descendants (see text for details).

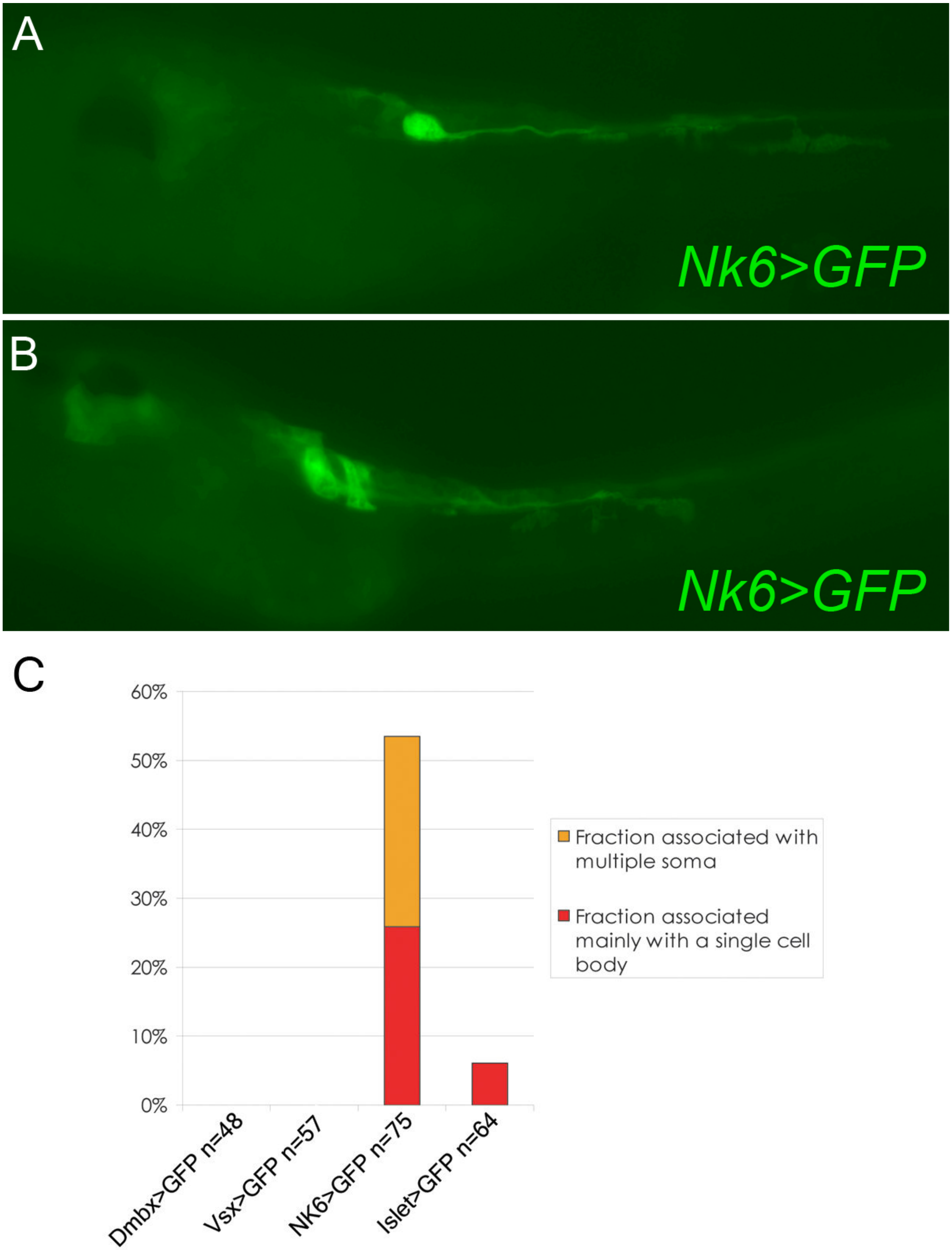
A
Nk6>GFP
B
Nk6>GFP
C
60%
50%
40%
30%
20%
10%
0%
Fraction associated with multiple soma
Fraction associated mainly with a single cell body
Dmbx>GFP n=48
Vsx>GFP n=57
NK6>GFP n=75
Islet>GFP n=64

(Previous page) Fig. AII. **Quantification of frondose endplate staining by Nkx6>GFP and other reporters**

(**A**) Some embryos electroporated with Nkx6>GFP (also called *Nk6>GFP,* based on slightly different nomenclature*)* showed frondose endplate labeling by GFP and a single cell body, or soma, strongly labeled by GFP (green). (**B**) Some embryos electroporated with Nkx6>GFP showed frondose endplate labeling by GFP, but this labeling was associated with multiple labled cell bodies. (**C**) Nkx6>GFP was compared to Dmbx, Vsx, and Islet>GFP in staining of frondose endplates. Larvae were scored for presence of visible endplates, and staining of cell bodies in the visceral ganglion. Only Islet>GFP showed residual staining of endplates. Red fraction represents cases as in (**A**) and orange fraction represents cases as in (**B**). Swimming larvae were assayed 18-24 hpf.

Appendix III: The *COE* enhancer

2.6 kb of DNA upstream from the translation start site of the *COE* gene was cloned into a reporter plasmid and electroporated into embryos. It was found that this *COE* reporter was sufficient to drive expression in CNS precursors a few cell divisions away from terminal differentiation, as evidenced by strongest GFP expression in post-mitotic neurons A10.57, A11.117, and A11.118, and weaker GFP expression in A12.239 and A12.240, presumably due to transient expression in A11.120 (Fig. AIII). In the larvae, the reporter turns on in non-neuronal CNS cells (ependymal cells), suggesting an incomplete cis-regulatory logic required for maintenance, possibly contained within intronic regions of the gene (T. Blair Gainous, personal communication).

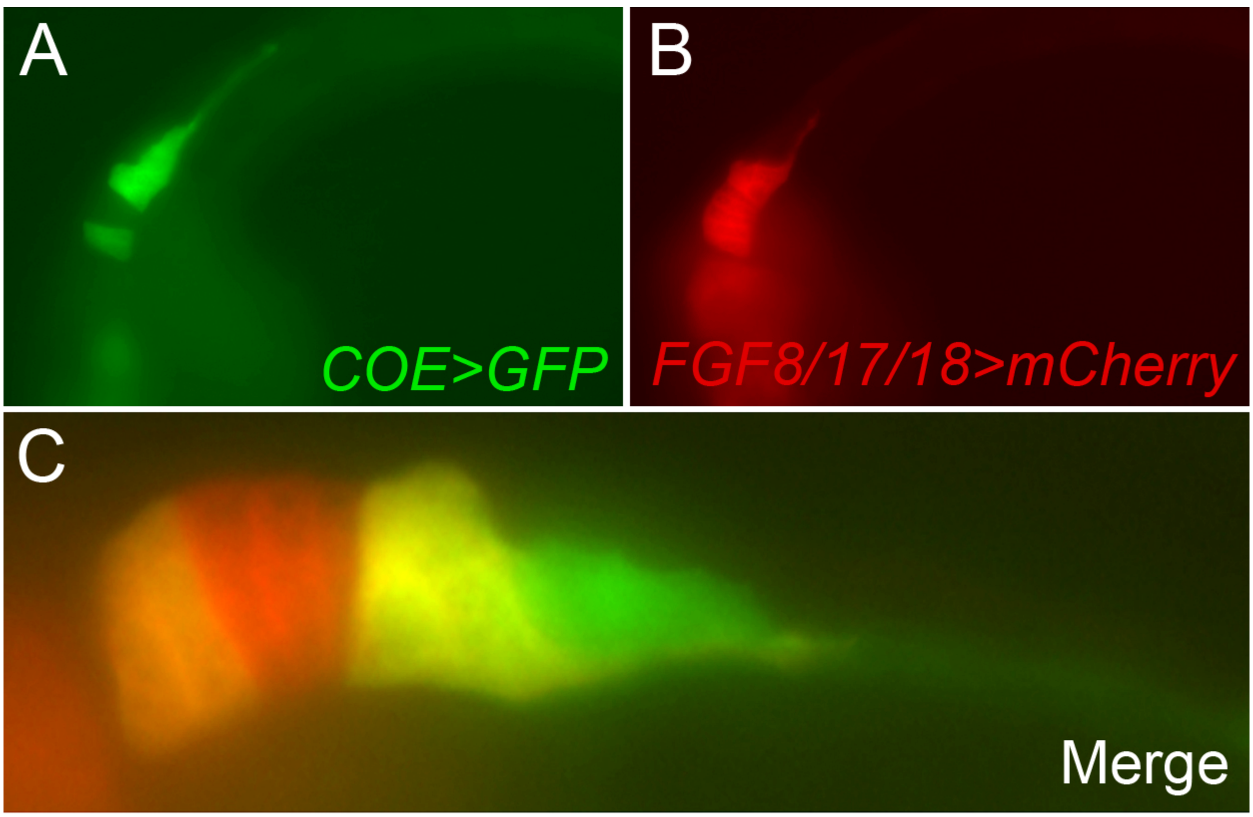

Fig. AIII. ***COE* enhancer drives reporter gene expression in differentiating neuroblasts.**
(**A**) A ~2.6 kb DNA fragment immediately upstream of the *COE* translational start codon is sufficient to drive GFP expression (green) in neural precursors that have differentiated or are starting to differentiate. (**B**) A9.30 lineage is marked by *FGF8/17/18>mCherry* (red). (**C**) Merged view of (**A**) and (**B**). *COE>GFP* marks both A12.240 and A12.239 (anterior-most cells), due to transient expression in mother cell A11.120. Endogenous *COE* expression becomes restricted to A12.239 and excluded from A12.240 starting at this time (data not shown). Embryo is stage E75-80 (~16 hpf), lateral view.

Appendix IV: Cross-repressive interactions prevent visualization of single neurons upon transcription factor overexpression.

To illustrate the "Catch-22" encountered upon overexpression of my candidate transcription factors, *Dmbx* and *Vsx* reporters were co-electroporated with *COE>Vsx* or *COE>Dmbx*, respectively (Fig. AIV). Overexpression of Vsx or Dmbx results in uniform background-level expression of my reporter constructs, thus not allowing me to ask the effect of such overexpression on morphology of say A12.239 or A11.117 neurons. Such cross-repressive interactions were confirmed by *in situ* hybridization (see text).

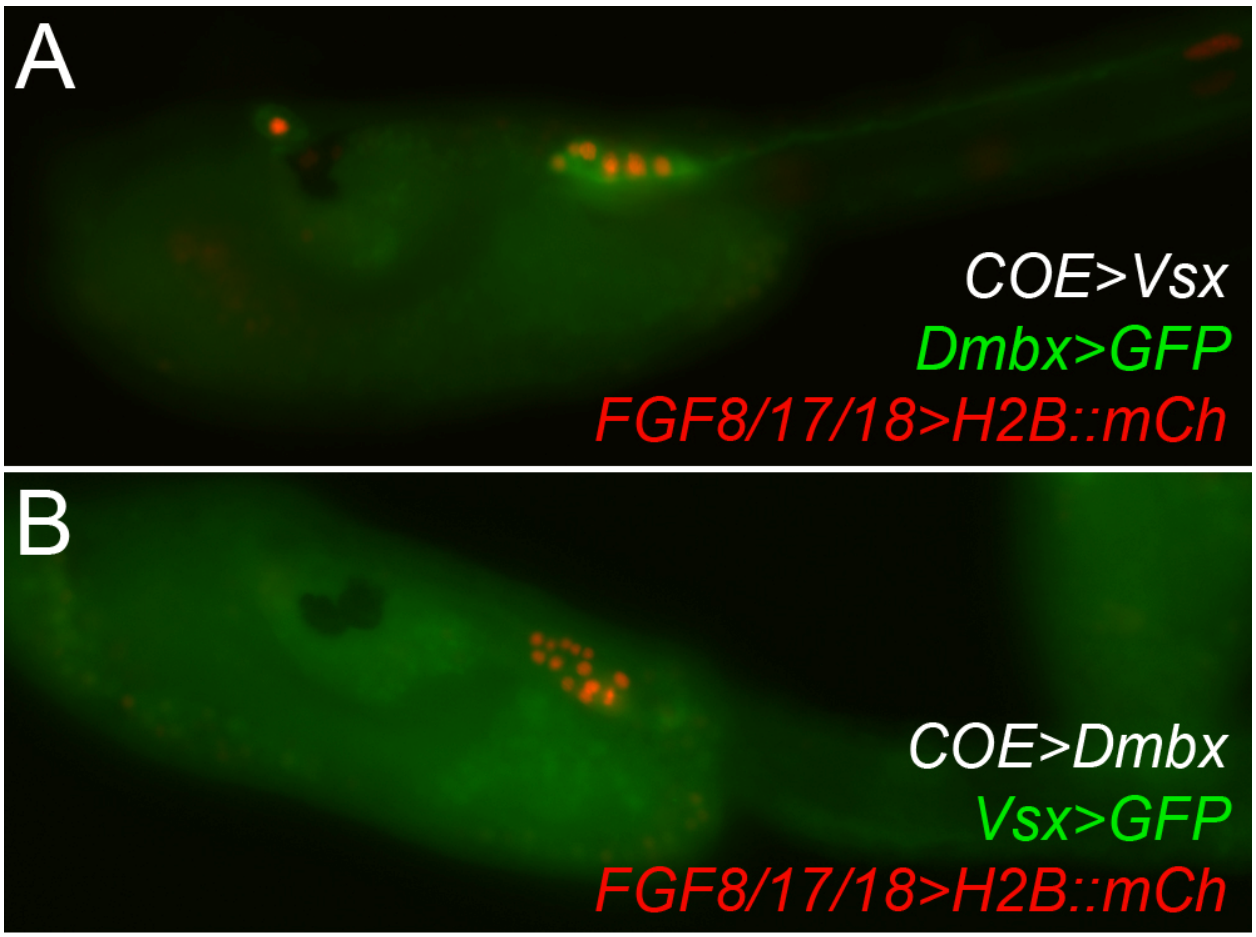

Fig. AIV. **Cross-repression between transcription factors and reporter constructs.** (**A**) Swimming larva electroporated with *COE>Vsx* and *Dmbx>GFP*. Vsx overexpression results in all VG descendants expressing baseline levels of *Dmbx>GFP* (green), still visible but barely stronger than background. (**B**) Swimming larva electroporated with *COE>Dmbx* and *Vsx>GFP*. Dmbx overexpression results in the reciprocal downregulation of *Vsx>GFP* (green). Both larvae co-electroporated with *FGF8/17/18>Histone2B::mCherry* (red) to visualize A9.30 lineage.

Appendix V: Effects of other Ephrin/FGF/MAPK perturbations on MG patterning

A constitutively-active form of the FGFR does not alter *Engrailed* or *Vsx* reporter expression (Fig. AV), consistent with the idea that it is not FGF ligand availability or FGFR activation *per se* that is limited. The hypothesis that activation of Eph receptor by localized Ephrin ligand is supported by overexpression of truncated Eph3 (Eph3ΔC, see text), as well as a constitutively-active form of the Eph3 receptor (caEph3, Fig. AV). Overexpression of truncated forms of other Eph receptors did not produce the same patterning defects as truncated Eph3 (Fig. AV and Fig. 10). EphrinAb is expressed in A9.29, and was the only Ephrin ligand to alter A11.118/A11.117 specification when overexpressed (Fig. 10 and data not shown), suggesting that EphrinAb signaling to Eph3 provides the localized cue for MAPK-downregulation required for A10.59 and later A11.117 fate choices.

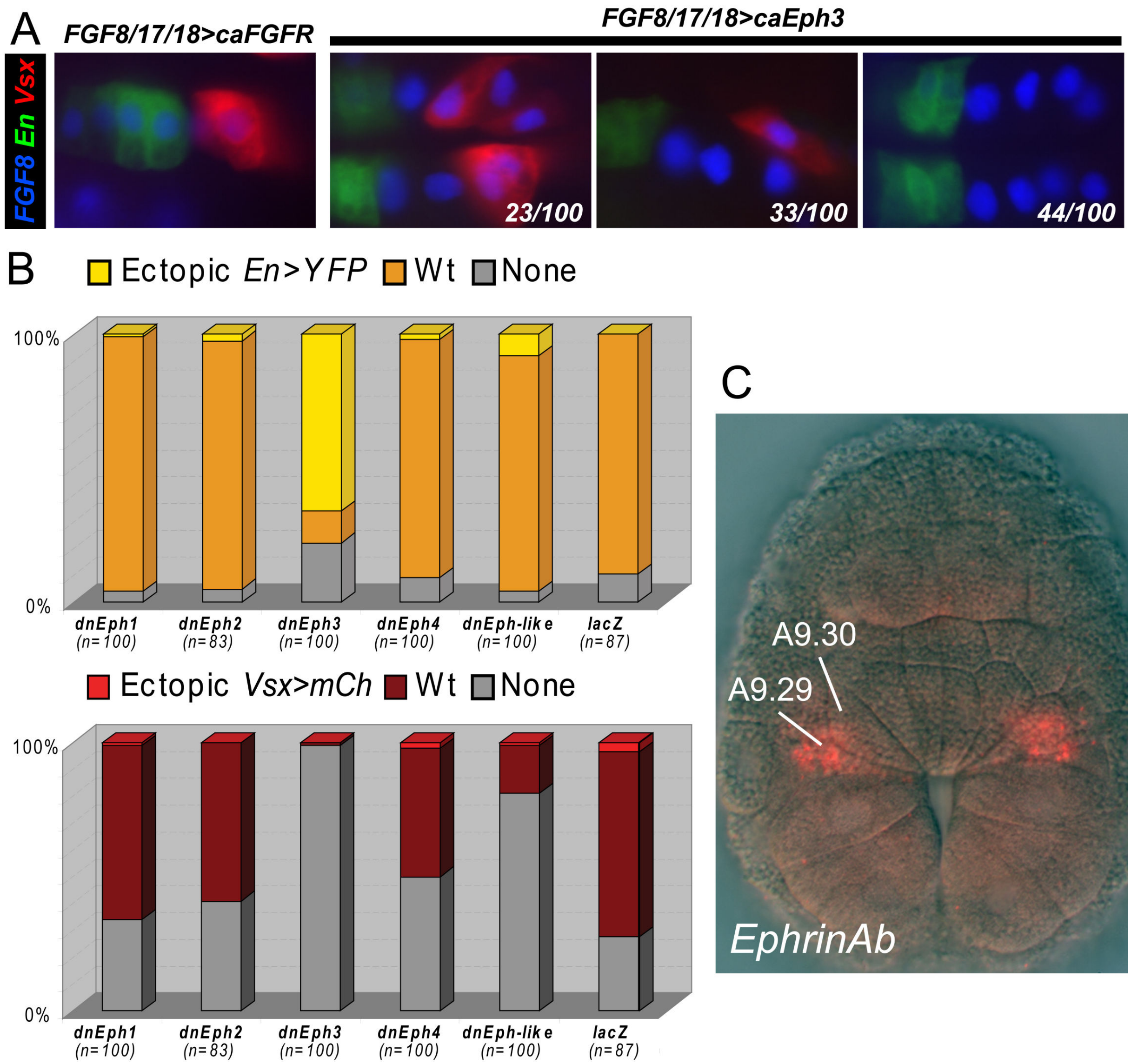

Fig. AV. **Effects of other Ephrin/FGF/MAPK perturbations on MG patterning.** (**A**) Left most panel: embryo electroporated with *FGF8/17/18>caFGFR,* and *FGF8/17/18Histone2B::CFP* (blue), *En>YFP* (green), and *Vsx>mCherry* (red). The effect of caFGFR overexpression was not distinguishable from wild-type (see text, Fig. 10). Right panels: embryos electroporated with the same reporters as in (A), in addition to *FGF8/17/18* driving *caEph3*, a self-dimerizing form of the Eph3 receptor. This resulted in complete loss of *En* reporter expression, but *Vsx* reporter expression varied from wildtype pattern, to total loss, to ectopic expression (numbers indicated embryos falling within each phenotype of *Vsx* reporter expression represented by the image). (**B**) Quantification of embryos showing of *En* and *Vsx* reporter expression status upon electroporation with other truncated Eph receptors (dnEph1-4, and dnEph-like). Truncated Eph3 = Eph3ΔC data from Fig. 10. All embryos in (A,B) fixed and assayed at 15.5 hpf at 16°C. (**C**) *In situ* hybridization showing expression of *EphrinAb* (red) in A9.29, which is posterior to A9.30. Embryo is at late gastrula stage.

Appendix VI: Details regarding Notch-dependent patterning of the MG

Here I show that the γ-secretase inhibitor DAPT can also mimic the effect of *FGF8/17/18>Su(H)-DBM.* DAPT administration proved quite challenging, as the drug appeared to be hindered in its diffusion past the embryonic tunic, which starts being synthesized at the tailbud stage, as well its poor solubility in sea water. 13/64 individuals in a pool of embryos treated with DAPT at different stages were seen to produce a OFF-ON-OFF-ON pattern of *Dmbx* expression, as visualized by *in situ* hybridization (Fig. AVI). This low percentage suggests only one of our timepoints being early enough for DAPT to penetrate and affect A11.120/A11.119 fate choice (presumable ~11 hpf at 16°C).

Furthermore, the concern was raised that Notch signaling might be involved also in A11.118/11.117 cell fate choice. I show here that this is not the case, as *Vsx* reporter expression was normal in all embryos electroporated with *FGF8/17/18>Su(H)-DBM*.

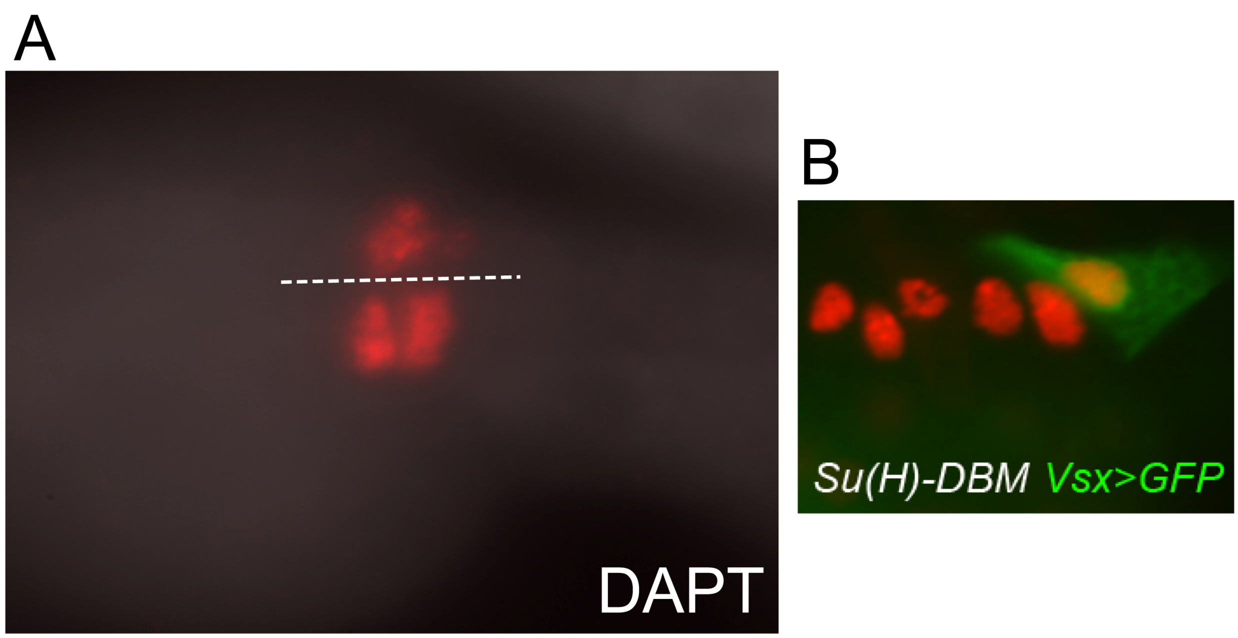

Fig. AVI. **Details regarding Notch-dependent patterning of the MG.**
(**A**) *In situ* hybridization for *Dmbx mRNA* (red) in a mid-tailbud embryo from a pool of embryos treated at different times with DAPT from 11 hpf to 13 hpf at 16°C. Midline denoted by dotted line. (**B**) Embryo co-electroporated with *FGF8/17/18>Su(H)-DBM, FGF8/17/18>Histone2B::mCherry* (red) and *Vsx>GFP* (green), showing normal *Vsx* reporter expression in A11.117. This would suggest Notch signaling is not important for proper A11.117 cell fate specification.

Appendix VII: Additional markers as evidence for A11.119 to A11.120 conversion upon Notch perturbation

Here I use additional markers of A11.119 to show that *FGF8/17/18>Su(H)-DBM* results in conversion of A11.119 to an A11.120-like fate. *HesB* and *Pax6* are both expressed in A11.119 alone at the stage where the A9.30 lineage contains 4 cells. This expression in A11.119 is abolished upon perturbation of Notch signaling by electroporation of *FGF8/17/18>Su(H)-DBM.* Coupled to loss of *SoxB1* expression, and ectopic expression of the A11.120 marker *Pax3/7* in A11.119 descendants (Fig. 12B), this further supports the interpretation that A11.119 is adopting a A11.120-like fate upon Notch inhibition.

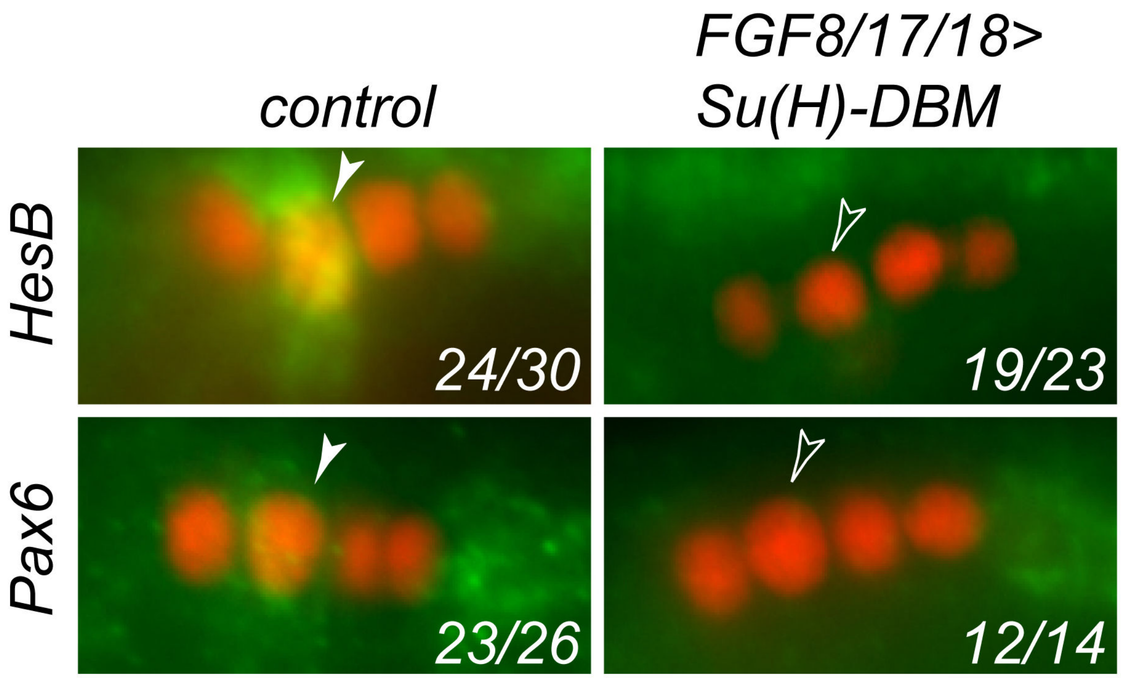

Fig. AVII. **HesB and Pax6 are lost from A11.119 upon Notch perturbation.**
In situ hybridization for *HesB* (top panels) and *Pax6* (bottom panels) *mRNA* in an embryo fixed around 11.5 hpf at 16°C. *In situ* signal is in green. A9.30 lineage counterstained by immunofluorescent detection of *FGF8/17/18>lacZ* expression (red). Note expression of *HesB* and *Pax6* in A11.119 in control embryos (white arrowheads, left panels). This expression in A11.119 is lost upon co-electroporation with *FGF8/17/18>Su(H)-DBM* (open arrowheads, right panels). Numbers indicate embryos showing represented expression pattern, out of total embryos assayed. Control embryos were co-electroporated with *FGF8/17/18>mCherry* as a neutral plasmid (i.e. in place of *FGF8/17/18>Su(H)-DBM).*

Appendix VIII: Supporting evidence for role of Delta/Notch and Dmbx in A12.240/A12.239 cell fate decision

The 'twinning' of the *Dmbx*+ A12.239 neuron has given me some insight into how this neuron is specified and differentiates. Twinning of A12.239 was initially discovered as a result of late FGF/MAPK inhibition, but Dmbx overexpression mimics it perfectly (Fig. AVIII 1), suggesting a role for Dmbx in FGF/MAPK suppression.

One interesting observation is that twinned A12.239 neurons will often project anteriorly (Fig. AVIII 1), suggesting non-cell autonomous effects on long-range axon pathfinding. Their ability to cross the midline, however, did not seem to be abolished (data not shown).

If FGF/MAPK signaling is permissive but not instructive for A12.240 and Dmbx might be involved in downregulation FGF/MAPK and/or SoxB1 in A12.239 to allow for differentiation (see text for details), then what biases Dmbx expression in A12.239? The best candidate I can come up with is Delta/Notch. *HesB* and *Ngn* show alternating expression patterns by *in situ* hybridization, with *Ngn* on in A12.239 but *HesB* on in A12.240 (Fig. AVIII 2). This is consistent with Delta/Notch-mediated lateral inhibition of neurogenesis. Perturbation of Notch via overexpression of *Su(H)-DBM* can sometimes result in twinning of A12.239 in addition to twinning of its mother cell (ON-ON-ON-ON Dmbx expression, Fig. AVIII 2, instead of the more common OFF-ON-OFF-ON pattern Fig. 11B). This twinning effect is not strong, and does not increase with increased dose of *Su(H)-DBM* expression, suggesting either non-specific effect of a limited role in promoting one fate over the other (Fig. AVIII 3).

The fact that *Ngn* is a proneural gene and is expressed in A12.239 suggested it could be promoting an A12.239 neuron fate. Consistent with this, Ngn overexpression rescues *Dmbx* reporter expression from *SoxB1*-mediated repression (Fig. AVIII 2). These facts, taken together, suggest Delta/Notch could be biasing the *Dmbx* expression and neurogenesis to A12.239. Delta/Notch could providing the 'spatial' cue, but be largely subordinate to FGF/MAPK/SoxB1 activity in A12.240/A12.239 fate. Dmbx could sit at the nexus between these two pathways to promote neural differentiation (Fig. AVIII 2). Perhaps upon loss of Delta/Notch signaling, either A12.239 or A12.240 can be twinned. Assaying SoxB1 expression upon Delta/Notch inhibition will be required to resolve this issue.

How does the *Ngn/HesB* expression pattern form at this stage? One model is that propagation of Delta/Notch-mediated lateral inhibition starting from Delta2-expression in A11.118 can organize the later pattern seen (Fig. AVIII 4). Outstanding questions are: How do A11.118 and A11.117 escape each other's Delta2 signal (i.e., how can these two neurons touch each other and co-exist?)? Does the Jagged/Serrate ligand expressed in A11.117 have anything to do with this (cis-inhibition of Notch by Jagged/Serrate could keep A11.117 from turning on HesB)? Is the proper specification of A11.118 (versus A11.117) required for setting up the proper Delta2 pattern seen, or can A11.117 substitute for A11.118? These are all questions to follow up on.

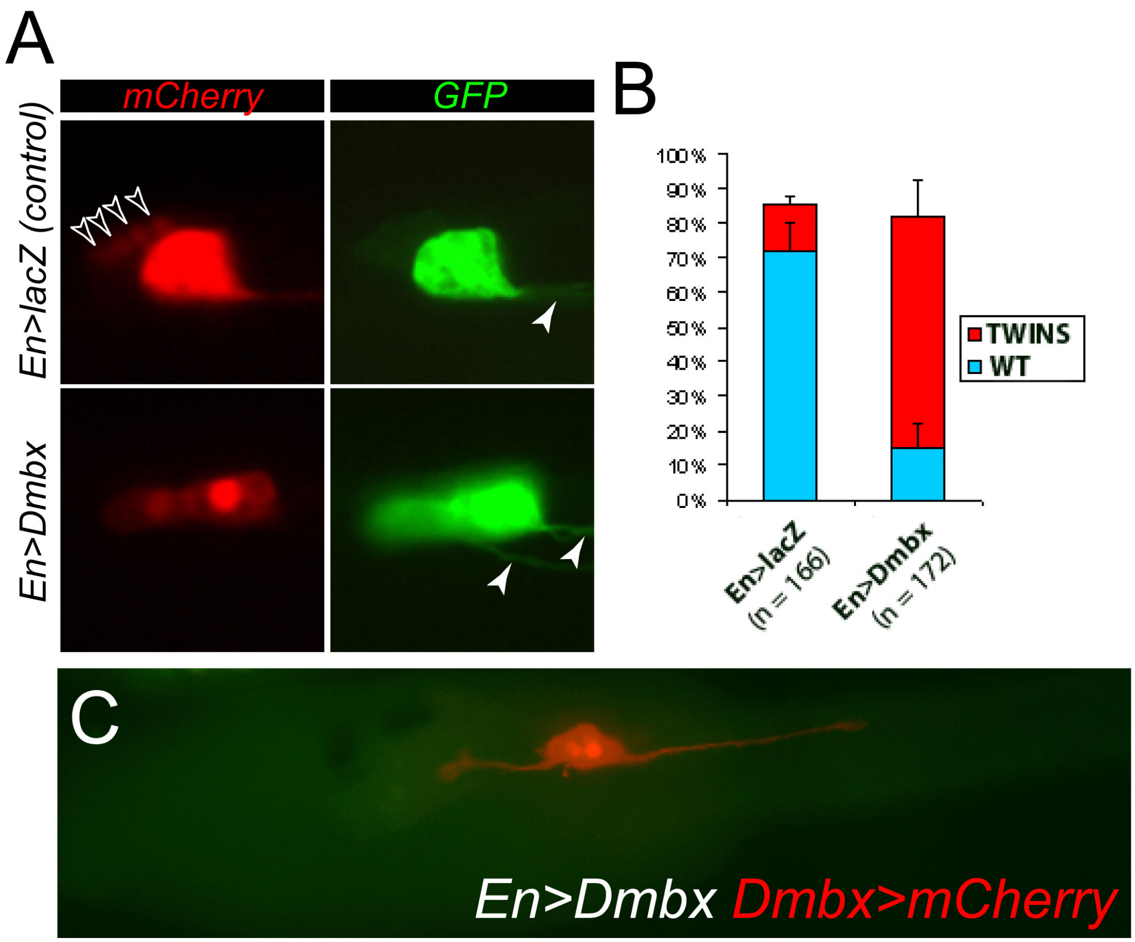

Fig. AVIII 1. **Twinning by Dmbx overexpression** (**A**) Larvae electroporated with *En>Dmbx* (bottom panels) compared to control embryos electroporated with *En>lacZ* (top panels). The *Dmbx* driver was used to drive expression of an untagged mCherry (left panels, mCherry, red) as well as an unc-76-tagged version of GFP (right panels, GFP, green). The untagged fluorophore marks the nuclei in addition to cell bodies, while the tagged GFP labels axons. Looking at untagged mCherry, one can see 4 nuclei of the 4 non-neuronal descendants of A12.240 in this tadpole, thanks to leaky/transient expression of the *Dmbx* reporter (open arrowheads). Looking at tagged GFP, one can see the axon of A12.239 (arrowhead). Upon *Dmbx* overexpression with the *En* driver, both A12.240 and A12.239 differentiate into neurons, as shown by the two axons and loss of small sister nuclei. (**B**) Quantification of twinning phenotype in (A). (**C**) Tadpole larva showing aberrant anterior axonal projection in twinned *Dmbx*+ neuron. This was seen in 31/100 tadpoles.

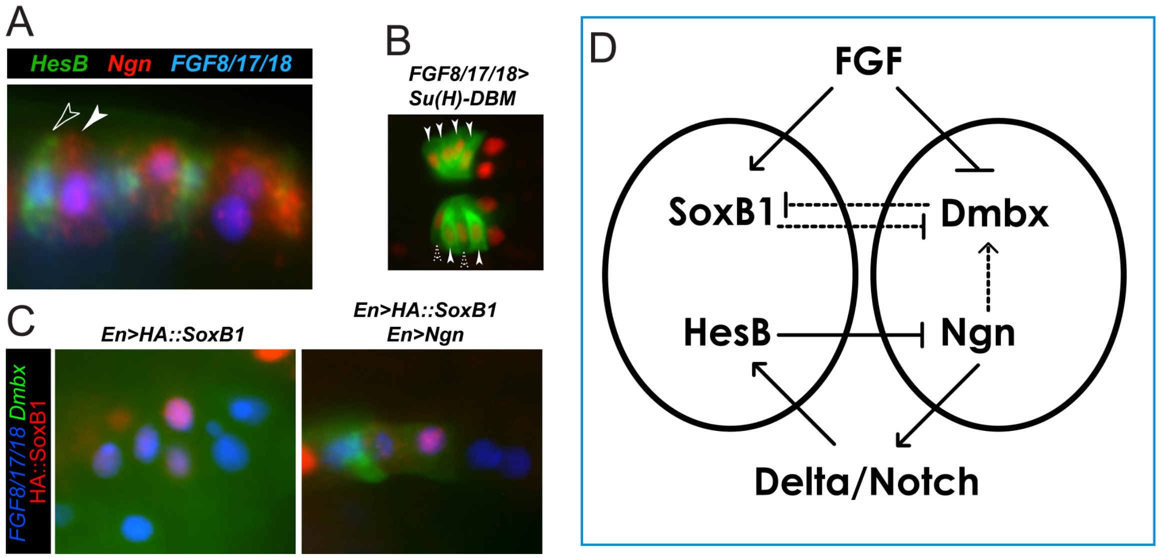

Fig. AVIII 2. **Role of Delta/Notch in A12.240/A12.239 fate**

(**A**) *In situ* hybridization for *HesB* (green) and *Ngn* (red) on embryos electroporated with *FGF8/17/18>lacZ* (detected by immunofluorescence, blue), fixed at 15 hpf at 16°C. Open arrowhead indicates A12.240, while white arrowhead indicates A12.239. Their expression of *HesB* and *Ngn,* respectively, is consistent with models of lateral inhibition of neurogenesis. (**B**) Embryo electroporated with *FGF8/17/18>Su(H)-DBM, FGF8/17/18>Histone2B::mCherry* (red) and *Dmbx>GFP* (green), imaged at 15.5 hpf at 16°C. Both left/right halves of the embryos are shown. Note the A9.30 lineage at the top appears to have lost distinction between neuron and non/neuron, suggested by *Dmbx* reporter expression in all 4 cells of the anterior MG (white arrowheads). The lineage at the bottom still retains some difference in *Dmbx* reporter expression between A12.240- and A12.239-like cells (dotted arrowhead and white arrowhead, respectively). (**C**) Embryos electroporated with *FGF8/17/18>Histone2B::CFP* (blue), *Dmbx>YFP* (green), and either *En>HA::SoxB1* alone or *En>HA::SoxB1* plus *En>Ngn.* (The embryos electroporated with *En>HA::SoxB1* alone were actually co-electroporated with *En>lacZ,* to control for transfection load). *HA::SoxB1* expression was monitored by immunofluorescence against the HA tag. *SoxB1* overexpression abolished *Dmbx* reporter expression in 82/100 embryos. Co-electroporation with *Ngn* restored *Dmbx* reporter expression in 45/100 embryos, suggesting overexpression of *Ngn* can promote *Dmbx* expression, rescuing it from *SoxB1*-mediated repression. Embryos fixed at 16 hpf at 16°C. (**D**) Model of Dmbx and SoxB1 interactions with each other and FGF and Delta/Notch pathways, based on my data. Dotted lines between TFs indicate that direct interactions (e.g. binding to an enhancer) have yet to be demonstrated.

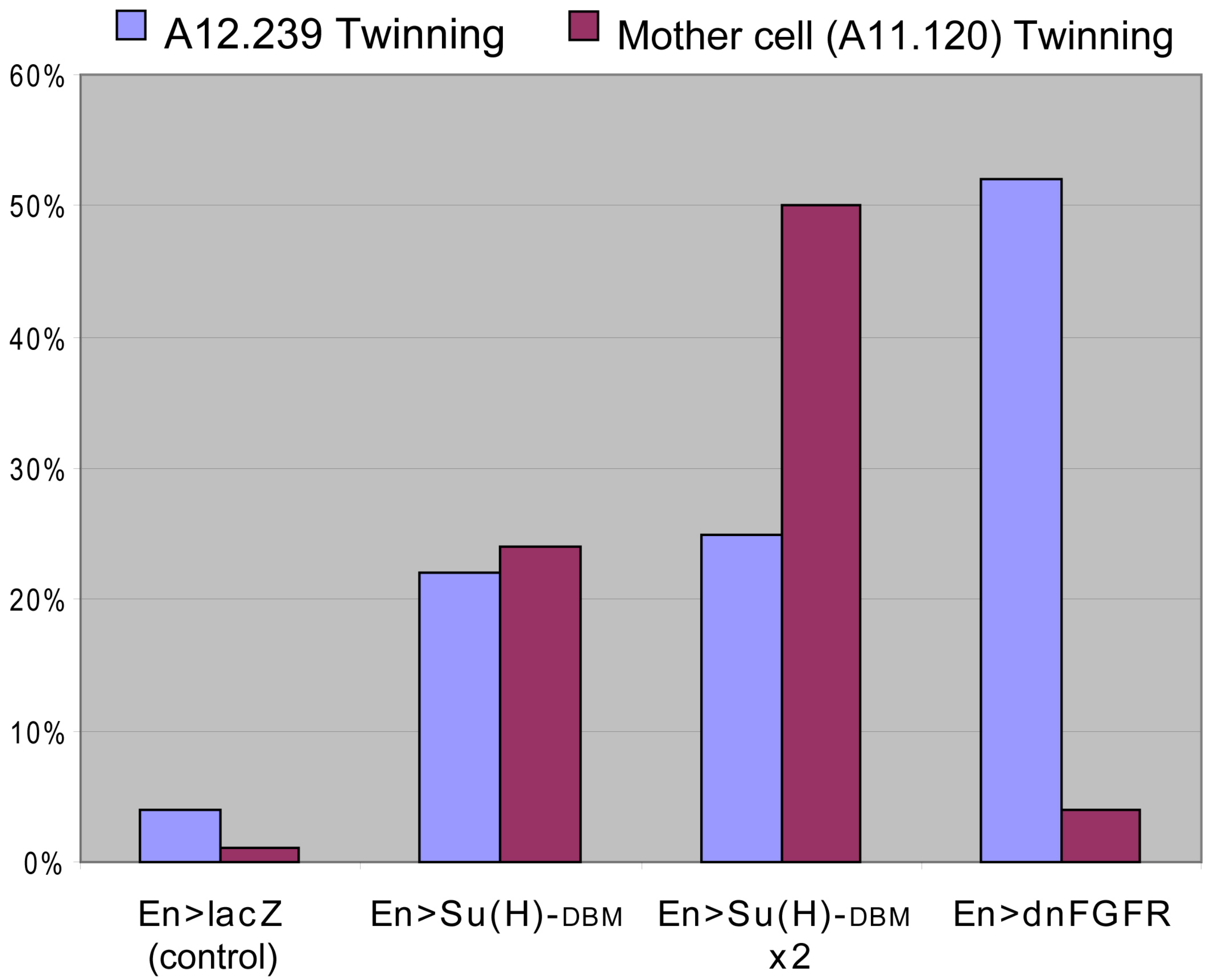

Fig. AVIII 3. **Effect of Su(H)-DBM and dnFGFR on twinning of A12.239 and/or its mother cell (A11.120).**

Embryos were electroporated with either *En>lacZ (control), En>Su(H)-DBM, or En>dnFGFR,* and fixed at 17 hpf at 16°C. Twinning status was determined by scoring for *Dmbx>GFP* reporter that had been co-electroporated. A9.30 lineage cells were counted by visualizing *FGF8/17/18>Histone2B::mCherry* reporter, also co-electroporated. Two different doses of *En>Su(H)-DBM* were administered, by doubling the amount of plasmid electroporated (120 µg vs. 60 µg per 500 µl total electroporation volume. The transfection load was kept constant by co-electroporation with 60 µg of *En>lacZ*, for the 1x dose*).* Twinning of A11.120 was assayed by expected patterns of *Dmbx* expression, with or without twinning of one or both daughter cells. At 1x the dose of *En>Su(H)-DBM*, roughly 20% embryos showed duplication of A11.120 and/or A12.239. At 2x the dose, more embryos showed duplication of A11.120, as was expected, however, twinning of A12.239 was not more frequent, as a percentage of all embryos showing *Dmbx* expression. A strong A12.239 twinning effect was seen in *En>dnFGFR*-electroporated embryos, confirming my previous experiments (see text).
n=100 for each condition.

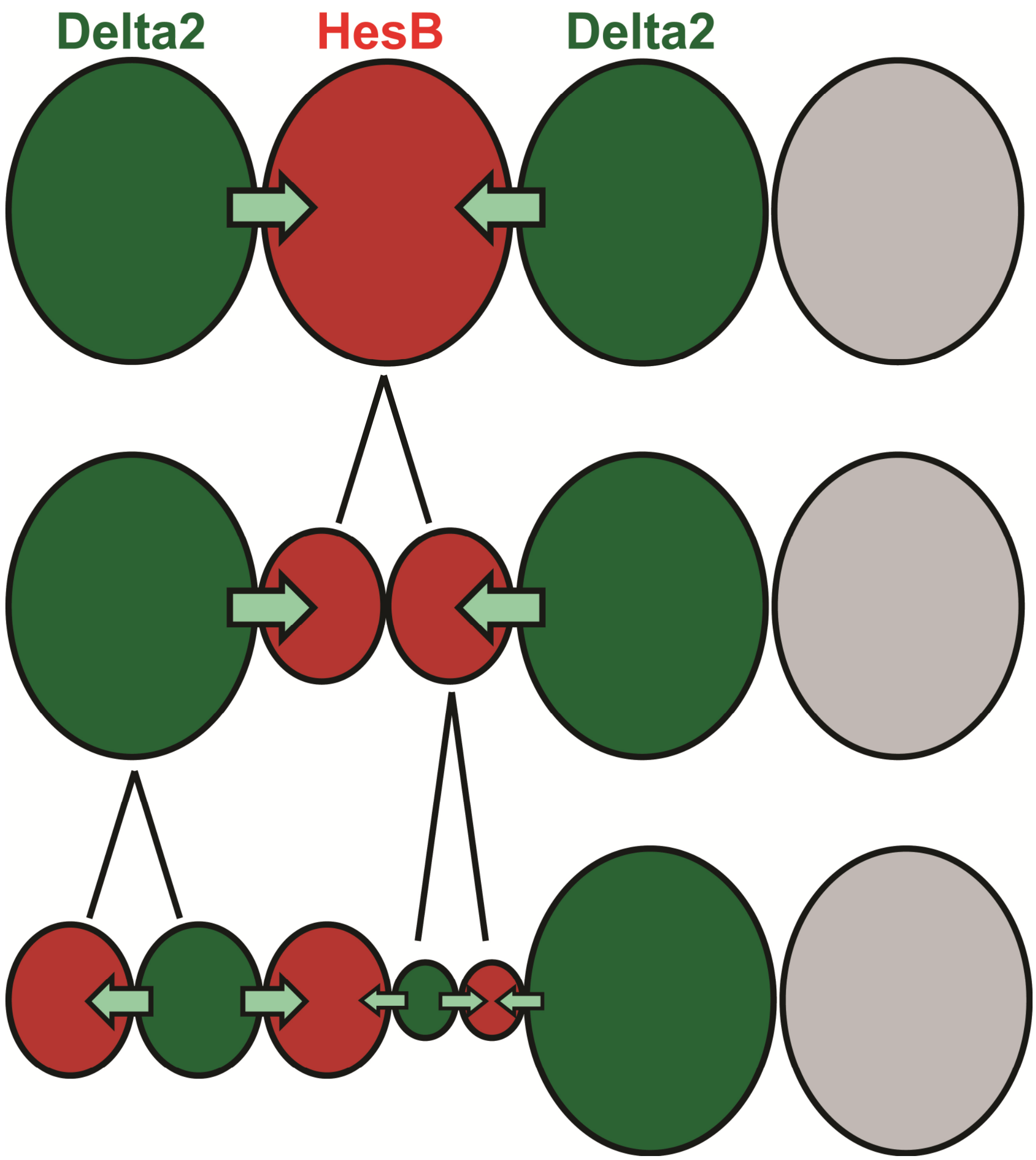

Fig. AVIII 4. **Model for self-organizing gene expression in the A9.30 lineage by Delta2/Notch-mediated lateral inhibition.**
Schematic diagram of A9.30 lineage cells expressing *Delta2* or *HesB*. Top row, *Delta2* and *HesB* patterns have been confirmed by *in situ* hybridization at 11.5 hpf at 16°C. *Delta2* (green) is expressed in A11.120 and A11.118. *HesB* (red) is expressed in A11.119. Grey cell represents A11.117, which expresses both *Delta2* and a homolog of vertebrate *Jagged/Serrate,* another ligand for Notch. Middle row, cells might try to resolve *Delta2/HesB* expression status as they divide, but ultimately the pattern is only to be resolved later. In the bottom row, when each cell is contacting a different neighbor, lateral inhibition is satisfied. This *HesB* pattern has been verified (Fig. AVIII 2), while the hypothetical expression pattern of *Delta2* is identical to actual *Ngn* expression (Fig. AVIII 2).

Appendix IX: Islet expression in lateral TVCs/ASM precursors

Islet expression as visualized by *in situ* hybridization and reporter constructs tied this pharyngeal muscle-generating lateral TVC population to the SHF/anterior splanchnic mesoderm of vertebrates. In addition to *Islet* other markers shared between these cells and the SHF/SpM of vertebrates include *Nkx2.5, Tbx1, FoxF, MesP,* and *COE* (see text).

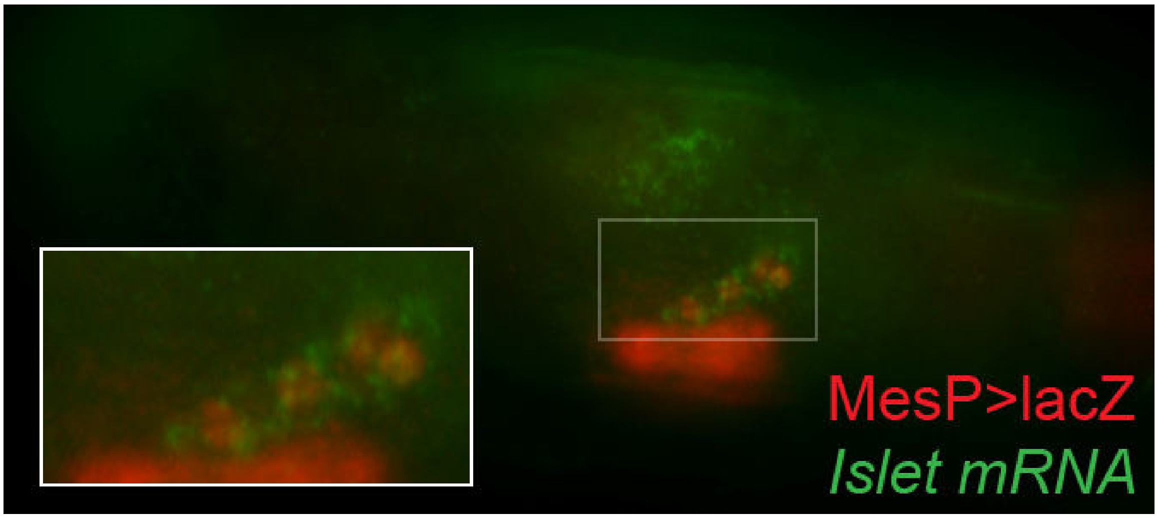

Fig. AIX 1. ***Islet* expression at larval stage**. (A) Larva expressing the *MesP>lacZ* transgene, which reveals the B7.5 lineage cells after immunostaining of the ßgalactosidase (red). *Islet* mRNAs (green) were detected by fluorescent *in situ* hybridization (FISH) at ~22 hpf. *Islet* is only expressed in lateral TVCs that are migrating to the atrial siphon placodes to later form ASMs. The heart (more ventral red staining) does not express *Islet.* Inset is a zoomed in picture of the boxed in area.

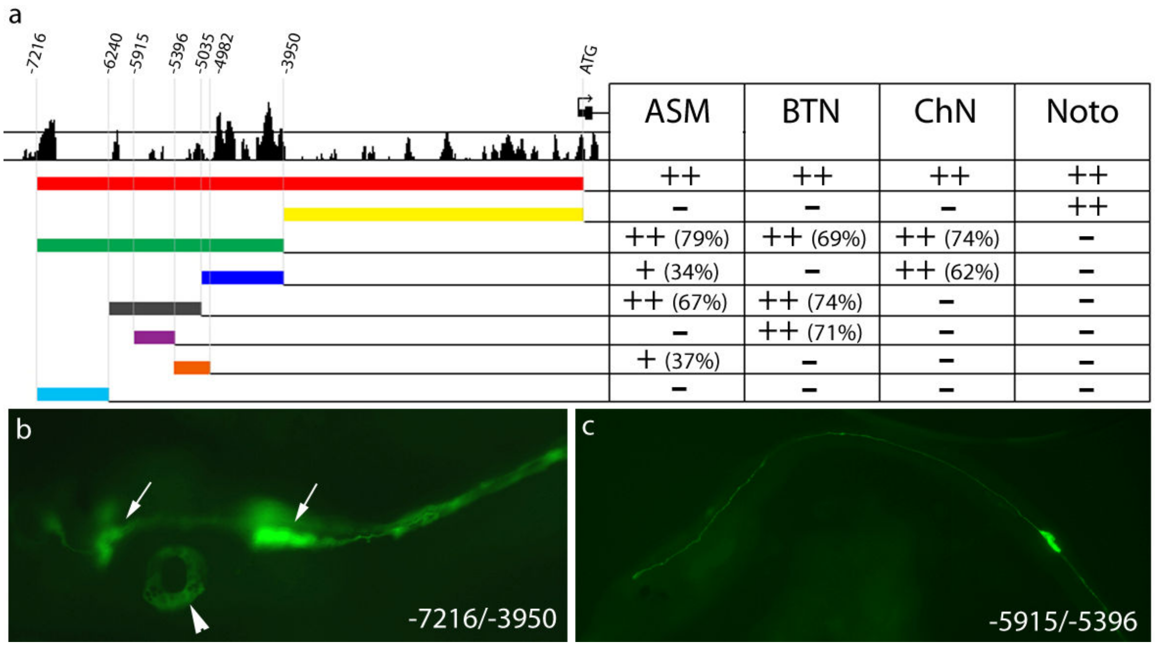

Fig. AIX 2**. Analysis of *Islet cis*-regulatory sequences**

Schematic of genomic DNA sequences upstream of predicted transcription start site of *Islet* gene. Numbers of base pairs prior to predicted start codon of *Islet* open reading frame are given in negative values. Conservation track indicating alignment with *C. savignyi* genome is taken from the CNRS mirror of the UCSC genome browser (http://genome.ciona.cnrs-gif.fr/cgi-bin/hgGateway?org=C.+intestinalis&db=ci1).

Expression in atrial siphon muscle precursors (ASM), notochord (Noto), bipolar tail neurons (BTN) and cholinergic neurons (ChN) of the central nervous system are given for each reporter construct carrying the corresponding fragment (see materials and methods). Expression is given as percentage of transfected larvae with visible GFP fluorescence in TVCs at 24 hpf (n = 35 to 195). Minus sign ("-") indicates no or very little (<4%) expression. Single plus sign ("+") indicates expression in 10 to 50% of transfected larvae. Double plus sign ("++") indicates expression in greater than 50% of transfected larvae. Plus signs without percentage value indicate this expression was visually estimated to be >75% of transfected larvae. Note that non-overlapping fragments (-6240/-5035 and -5034/3950) were capable of driving variable levels of reporter gene expression in ASM precursors. In contrast, ChN and BTN enhancers were found to be restricted to -5034/-3950 and -5915/-5396 fragments, respectively. Expression in other known territories (e.g. palps and oral siphon primordium) of *Islet* expression were not assayed. b) Image of a larva electroporated with *Islet* -7216/-3950 + bpFOG>unc76::GFP, showing expression in ASM precursors (arrowhead) and cholinergic neurons (arrows). c) Image of a larva electroporated with *Islet* -5915/-5396 + bpFOG>unc76::GFP, showing expression in bipolar tail neuron.